



AMERICAN UNIVERSITY OF BEIRUT

ANTITUMOR ACTIVITIES OF NATURAL AND SYNTHETIC  
RETINOIDS IN 2D AND 3D HUMAN BREAST CANCER  
MODELS

by  
PATRICK ANTOINE AOUAD

A thesis  
submitted in partial fulfillment of the requirements  
for the degree of Master of Science  
to the Department of Biology  
of the Faculty of Arts and Sciences  
at the American University of Beirut

Beirut, Lebanon  
April 2016

AMERICAN UNIVERSITY OF BEIRUT

ANTITUMOR ACTIVITIES OF NATURAL AND SYNTHETIC  
RETINOIDS IN 2D AND 3D HUMAN BREAST CANCER  
MODELS

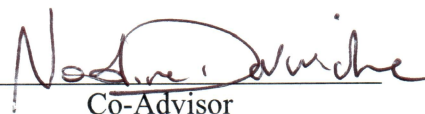
by  
PATRICK ANTOINE AOUAD

Approved by:

Dr. Rabih Talhouk, Professor  
Department of Biology

  
Advisor

Dr. Nadine Darwiche, Professor  
Department of Biochemistry and Molecular Genetics

  
Co-Advisor

Dr. Marwan Sabban, Professor  
Department of Anatomy, Cell Biology  
and Physiological Sciences

  
Member of Committee

Dr. Diana Jaalouk, Assistant Professor  
Department of Biology

  
Member of Committee

Date of thesis defense: April 25, 2016

AMERICAN UNIVERSITY OF BEIRUT

THESIS, DISSERTATION, PROJECT RELEASE FORM

Student Name: ASUAD PATRICK ANTOINETTE  
Last First Middle

☒ Master's Thesis

☐ Master's Project

☐ Doctoral Dissertation

☒ I authorize the American University of Beirut to: (a) reproduce hard or electronic copies of my thesis, dissertation, or project; (b) include such copies in the archives and digital repositories of the University; and (c) make freely available such copies to third parties for research or educational purposes.

☐ I authorize the American University of Beirut, **three years after the date of submitting my thesis, dissertation, or project**, to: (a) reproduce hard or electronic copies of it; (b) include such copies in the archives and digital repositories of the University; and (c) make freely available such copies to third parties for research or educational purposes.

Patrick Asuad May 3, 2016  
Signature Date

## ACKNOWLEDGEMENTS

There are many people who helped me during my Master journey, and for them, I dedicate these words.

I would like to thank my advisor, Dr. Rabih Talhouk, for passing the 3D model wisdom to me. I am very grateful that I got to meet someone as kind-hearted and humble as you. Thank you for all the engaging scientific talks we had during our weekly meetings and for the friendly atmosphere in your laboratory.

My deepest gratitude goes to my co-advisor, Dr. Nadine Darwiche, for believing in my potentials as a cancer researcher, and for giving me the opportunity to pursue my MSc thesis in your laboratory. The journey was indeed tough, but your guidance, whether at the micro- or macro-level, rendered the sleepless nights and disappointing days easier to tolerate. Thank you for letting me design my own experiments and shape the project in a way that meets high standards in the cancer field. Your expertise and knowledge have greatly impacted my graduate experience at AUB.

I would also like to thank Drs. Sabban and Jaalouk for serving on my committee. Dr. Sabban, thank you for your constructive criticism and valuable comments that were of great relevance to my project. Your continuous questions have always triggered me to think outside the box in a very conceptual manner. Dr. Jaalouk, words fail to describe how grateful I am to have been one of your students. Thank you for letting me audit your undergraduate cancer course, and for the valuable outcomes that I learned during the cardiovascular research course. You're truly an inspirational scientist that I will always look up to.

I take the chance to also thank our collaborator, Dr. Claudio Pisano, for generously providing us with the drug and for his insightful advices regarding the direction of my project.

To my dear colleagues in the Blue Lab: Leeanna, Melody, Rana, Zaynab, Berthe, Houda and Zeinab; I am very delighted to have worked with you, you are all unforgettable and I wish you all the best in your future endeavors. Special thanks go to Leeanna, who was not just a colleague of mine, but also a sister whom shoulder and comfort were always present, particularly during my tough days. I wish you all the best at McGill University, and I believe you are going to excel wherever you go.

I would also like to extend my gratitude to Dr. Talhouk's lab members, Sabreen, Dana, Farah N., Farah Y. and Nataly. Thank you Sabreen for the training and all the help in the laboratory. I wish you all the best.

To the inspirational Dr. Rihab Nasr and her team, I am very happy that I had the opportunity to be a member of AMALOUNA, and help raise awareness about cancer

research. Big thanks go to Miss Rabab El Eit for the synergy analysis. To the Woman in Science, Dr. Hiba El Hajj and her wonderful team, I am forever grateful that I had the chance to meet you all; Martin, Nadim and Rita, you are unforgettable and I love you so much. Special thanks go to my best-friend Martin who was always there for me, through thick and thin. I am indebted to you for all your help and guidance during these 3 years. You are a great person and I wish you all the best from the bottom of my heart.

To the great people that I had the chance to meet or work with, particularly Sara Assi who proved to be an exceptional and dear person to my heart, you've been more than nice to me and I enjoyed our mutual support. You deserve nothing but the best. To Dima, Johnny, Layla, Hind and Ahmad from the Biology department, it is an honor to have met you. Thank you for the great times we shared and the memories we made. May your future be as bright as your smiles.

To my former Ecology instructor, and close friend, Mr. Mohammad Al Zein, you've walked with me this path and been there for me all along. You are an inspirational scientist who helped me shape the person I am today. I cannot thank you enough for all the things you've done for me. Your presence in my life will always remain special.

To a very special person in my life who has been with me during my tough and happy days, and never ceased to impress me: Dr. Mariam Karaki, you are a wonderful friend who supported me throughout my journey since BS, and until now. You are the example of an ideal friend, and I am extremely honored and blessed to have you in my life. You are going to make an exceptionally great medical doctor.

Last but not least, my deepest acknowledgements go to the people who made me who I am and who sacrificed a lot so that I could fulfill my dreams. My mother, father, brother, uncles, and cousins; your infinite support has always been there. I love you all dearly and pray that you will always stay proud of me.

# AN ABSTRACT OF THE THESIS OF

Patrick Antoine Aouad

for

Master of Science

Major: Biology

Title: Antitumor Activities of Natural and Synthetic Retinoids in 2D and 3D Human Breast Cancer Models

Breast cancer is the most common malignancy among women and the second cause of cancer-related death worldwide. Despite recent advances in the use of chemotherapy in breast cancer management, achieving complete remission in aggressive and metastatic cancer patients remains a challenge and urges for the development of effective and safer therapies. Retinoids, including vitamin A derivatives and synthetic analogs, regulate cellular proliferation, differentiation, and cell death, and have shown potent chemotherapeutic and chemopreventive properties. However, the use of retinoids in the cancer clinic is often hindered by side effects and resistance to treatment. In fact, all-*trans* retinoic acid (ATRA) is a naturally occurring retinoid that failed phase-II clinical trials in patients with metastatic breast cancer. To overcome retinoids limitations, synthetic retinoids were developed namely, the atypical adamantly retinoid ST1926 which has reduced toxicity and increased specificity. In the present study, we investigated the anti-tumor activities of ATRA, ST1926, and their combinations on the proliferation and cell death of human breast normal and cancer cell lines in 2D and 3D culture models, and the molecular mechanisms involved.

We have shown that in 2D culture models, the breast cancer cells MCF-7 and MDA-MB-231 cells are resistant to ATRA while being sensitive to ST1926 at sub-micromolar ( $\mu\text{M}$ ) concentrations. ST1926-induced growth inhibition persisted after drug removal in breast cancer cells, and spared the ‘normal-like’ MCF-10A and HMT-3522 S1 breast epithelial cells. ST1926 induced massive apoptosis, S-phase arrest, and increased the protein expression levels of the tumor suppressors p53 and p21. ST1926 also caused early DNA damage, downregulated the Wnt/ $\beta$ -catenin pathway, and modulated the expression levels of the different retinoid receptors. ATRA and ST1926 synergized at low sub- $\mu\text{M}$  concentrations to potently inhibit the growth of breast cancer cells, independently of retinoid receptor signaling, while sparing normal breast epithelial cells. Interestingly, nanomolar concentrations of ST1926 reduced the size and number of breast cancer colonies grown in agar matrix and inhibited the sphere-forming ability of breast cancer stem/progenitor cells in the 3D sphere formation assay. Furthermore, ST1926 drastically induced cell death in 3D laminin-rich extracellular matrix-based cell culture of breast cancer cells. Finally, ST1926, ATRA, and their combination treatment did not disrupt the lumen nor affected the diameter of HMT-3522 S1 colonies grown in 3D culture model.

In summary, our studies demonstrate the therapeutic potential of ST1926 alone or in combination with ATRA in breast cancer and call for further testing in animal tumor models.

# CONTENTS

ACKNOWLEDGEMENTS .....	v
ABSTRACT .....	vii
LIST OF ILLUSTRATIONS .....	xii
LIST OF TABLES .....	xv

## Chapter

I. INTRODUCTION .....	1
A. The Mammary Gland .....	1
1. Overview .....	1
2. Development of the Mammary Gland .....	2
B. Breast Cancer: General Background .....	3
1. Overview .....	3
2. Molecular Subtypes of Breast Cancer .....	4
3. Treatment Regimen .....	5
4. Altered Signaling Pathways in Breast Cancer .....	7
5. Breast Cancer Microenvironment .....	7
C. 3D Cell Culture Models .....	10
1. Overview .....	10
2. Types of 3D Cell Culture Models .....	10
3. Advantages of 3D Cell Culture Models .....	12
D. Retinoids .....	13
1. Overview .....	13
2. Mechanisms of Action of Retinoids .....	14



3. Retinoids in the Treatment of Breast Cancer.....	15
4. Understanding ATRA Resistance in Breast Cancer.....	16
E. Overcoming ATRA Drawbacks with Synthetic Retinoids.....	17
1. Overview.....	17
2. ST1926 Mechanism of Action.....	18
3. ST1926 Pharmacokinetic Properties.....	19
F. Aims of the Study.....	21
II. MATERIALS AND METHODS.....	22
A. Cell Culture <i>In Vitro</i> Model.....	22
B. Cell Culture.....	23
C. Cell Passaging.....	23
D. Compounds.....	24
E. Cell Growth Assay.....	24
F. Trypan Blue Exclusion Assay.....	25
G. Cell Cycle Analysis.....	26
H. TUNEL Assay.....	26
I. Immunoblot Analysis.....	27
J. Soft Agar Colony Formation Assay.....	28
K. Three-Dimensional ‘on-top’ Assay.....	28
L. Sphere Formation Assay.....	29
M. Lumen Formation Assay.....	29
N. Image Processing.....	30
O. Synergy Studies and Statistical Analysis.....	31

III. RESULTS.....	32
A. ST1926 Induces Growth Arrest in ATRA-resistant Human Breast Cancer Cells at Pharmacologically Achievable Concentrations.....	32
B. ST1926 Reduces the Viability of Human Breast Cancer Cells and Induces Pronounced Morphological Changes.....	35
C. The Synthetic Retinoid HPR Does Not Affect the MCF-7 Breast Cancer Cells.....	38
D. ST1926 Spares ‘Normal-like’ Human Breast Epithelial Cells.....	39
E. ST1926-induced Growth Inhibition Persists After Drug Removal.....	42
F. ST1926 Induced Pre-G1 Accumulation and S-phase Arrest in Human Breast Cancer Cells.....	44
G. ST1926 Induces Apoptosis in Human Breast Cancer Cells.....	48
H. ST1926 Causes Early DNA Damage and Increases p53 and p21 Protein Levels.....	50
I. ST1926 Downregulates the Wnt/ $\beta$ -catenin Signaling Pathway.....	52
J. ST1926 Modulates Retinoid Receptors Expression.....	54
K. ST1926-growth Inhibitory Effect Is Independent of the Retinoid Receptor Signaling Pathway.....	55
L. Combination Treatments of ATRA and ST1926 Synergistically Inhibit the Proliferation of Human Breast Cancer Cells.....	57
M. Combination Treatments of ATRA and ST1926 Spare the ‘Normal-like’ Breast Epithelial Cells.....	62
N. Combination Treatments of ATRA and ST1926 at Low Concentrations Induce Pre-G1 Cell Accumulation and a Massive S-phase Arrest in MCF-7 cells.....	65
O. ST1926 Treatment at Sub- $\mu$ M Concentrations Inhibit Colony Growth of Breast Cancer Cells in Anchorage-independent 3D Cell Culture Model.....	69
P. ST1926 at Sub- $\mu$ M Concentrations Inhibit the Viability of Breast Cancer Cells in Anchorage-dependent 3D Cell Culture Model.....	72

Q. Single ST1926 Treatment at nM Concentrations in Combination with Sub- $\mu$ M ATRA Concentrations Inhibit the Colony-forming Ability of Breast Cancer Cells.....	76
R. Treatments with ATRA, ST1926, or Their Combination Do Not Disrupt the Lumen and Size of HMT-3522 S1 Acini in 3D Cell Culture Model..	83
IV. DISCUSSION.....	87
REFERENCES.....	99

## ILLUSTRATIONS

Figure	Page
1. Human mammary gland anatomy.....	2
2. Schematic presentation of mammary gland development.....	3
3. The influence of the microenvironment in normal <i>versus</i> tumor breast tissue.....	9
4. 3D cell culture systems.....	11
5. Chemical structures of ATRA and 13- <i>cis</i> RA.....	13
6. Chemical structure of ST1926.....	18
7. Human breast cancer cells are relatively resistant to ATRA.....	33
8. ST1926 at sub- $\mu$ M concentrations inhibit the proliferation of ATRA-resistant human breast cancer cells.....	34
9. Low sub- $\mu$ M concentrations of ST1926 potently reduce the viability of human breast cancer cells.....	36
10. Low sub- $\mu$ M concentrations of ST1926 alter the morphology of human breast cancer cells.....	37
11. MCF-7 cells are resistant to HPR.....	38
12. ST1926 has minimal effects on the growth of ‘normal-like’ breast epithelial cells.....	40
13. ST1926 has minimal effects on the morphology of ‘normal-like’ breast epithelial cells.....	47
14. ST1926-induced growth inhibition of breast cancer cells persists after drug removal.....	43
15. ST1926 treatment induces an accumulation of breast cancer cells in the pre-G <sub>1</sub> region and induces an S-phase arrest.....	45
16. Representative histograms of the cell cycle distribution and progression in ST19126-treated MCF-7 cells.....	46

17.	Representative histograms of the cell cycle distribution and progression in ST1926-treated MDA-MB-231 cells.....	47
18.	ST1926 induces apoptosis in breast cancer cells by TUNEL assay.....	48
19.	ST1926 causes early DNA damage in human breast cancer cells.....	51
20.	ST1926 downregulates the Wnt/ $\beta$ -catenin signaling pathway in human breast cancer cells.....	56
21.	ST1926 upregulates RAR $\beta$ and downregulates RAR $\gamma$ and RXR $\alpha$ .....	54
22.	ST1926-induced growth inhibition is independent of the retinoid receptor signaling pathway.....	56
23.	Combination treatments of ATRA and ST1926 at low concentrations inhibit the proliferation of MCF-7 cells.....	58
24.	Combination treatments of ATRA and ST1926 at low concentrations potentially alter the morphology of MCF-7 cells.....	59
25.	Synergy studies showing Combination Index for combination treatments of ATRA and ST1926 (ST).....	60
26.	Combination treatments of ATRA and ST1926 enhance viability reduction of MDA-MB-231 cells.....	61
27.	Combination treatments of ATRA with low ST1926 concentrations have minimal effects on the proliferation of ‘normal-like’ breast epithelial cells.....	63
28.	Combination treatments of ATRA with high ST1926 concentrations moderately inhibit the proliferation of ‘normal-like’ breast epithelial cells.....	64
29.	Combination treatments with ATRA and ST1926 induce pre-G <sub>1</sub> cell accumulation and a massive S-phase arrest in MCF-7 cells.....	66
30.	Representative histograms of the cell cycle distribution and progression in ATRA and ST1926-treated MCF-7 cells.....	67
31.	ATRA/ST1926-induced growth inhibition in MCF-7 cells is independent of the retinoid receptor signaling pathway.....	68
32.	Effect of ST1926 and ATRA on anchorage-independent growth of breast cancer cells.....	70

33.	ST1926 reduces the growth of breast cancer colonies in agar matrix....	71
34.	Morphology of human breast cancer cells is different in 2D <i>versus</i> 3D cell culture models.....	73
35.	ST1926 decreases the viability of breast cancer cells at low sub- $\mu$ M concentrations.....	74
36.	ST1926 drastically reduced colony formation and stellate structures of breast cancer cells.....	75
37.	Effect of ST1926 and ATRA on the sphere-forming ability of breast cancer cells.....	78
38.	Effect of ST1926 and ATRA on the diameter of mammospheres.....	79
39.	Effect of single or combination treatments with ATRA and ST1926 on the sphere-forming ability and diameter of MCF-7 cells.....	80
40.	Effect of ATRA,ST1926, and their combination on MCF-7 spheres.....	81
41.	Effect of ATRA and ST1926 on MDA-MB-231 spheres.....	82
42.	Morphology of HMT-3522 S1 cells grown in 2D <i>versus</i> 3D cell culture model.....	84
43.	Effect of ATRA, ST1926, and their combination on the lumen of HMT-3522 S1 cells.....	84
44.	Representative photographs showing the effect of ATRA, ST1926, and their combination on the lumen of HMT-3522 S1 cells.....	85
45.	Effect of ATRA, ST1926, and their combination on the size of HMT-3522 S1 cells.....	86

## TABLES

Table		Page
1.	Breast cancer subtypes with their respective gene expression profile...	5
2.	The major molecular subtypes of breast cancer with their clinical features and treatment regimen.....	6
3.	Clinical trials of retinoids in breast cancer.....	16

## ABBREVIATIONS

2D	two-dimensional
3D	three-dimensional
9- <i>cis</i> RA	9- <i>cis</i> retinoic acid
13- <i>cis</i> RA	13- <i>cis</i> retinoic acid
ATL	adult T-cell leukemia/lymphoma
ATRA	all- <i>trans</i> retinoic acid
CAF	cancer-associated fibroblast
CI	combination index
CK5/6	cytokeratin 5/6
CML	chronic myeloid leukemia
CRABP-II	cellular retinoic acid-binding protein II
CSC	cancer stem cell
CYP26	cytochrome-P450-isoform-26
DCIS	ductal carcinoma in situ
DMSO	dimethyl sulfoxide
ECL	enhanced chemiluminescence
ECM	extracellular matrix
EGF	epidermal growth factor
EGFR	epidermal growth factor receptor
EHS	Engelbreth-Holm-Swarm
ER	estrogen receptor
FABP5	fatty-acid binding protein 5



FBS	fetal bovine serum
G1	first generation
HER2	human epidermal growth factor receptor 2
HPR	N-(4-hydroxyphenyl)retinamide
IBC	inflammatory breast cancer
IC <sub>50</sub>	minimum inhibitory concentration
IDC	infiltrating ductal carcinoma
ILC	infiltrating lobular carcinoma
LCIS	lobular carcinoma in situ
LIC	leukemia-initiating cell
lrECM	laminin-rich extracellular matrix
μM	micromolar
MAPK	mitogen-activated protein kinase
MTT	3-(4,5-Dimethylthiazol-2-yl)-2,5-Diphenyltetrazolium Bromide
nM	nanomolar
PARP	poly(ADP-ribose) polymerase
PBS	phosphate-buffered saline
PI	propidium iodide
PI3K	phosphatidylinositol 3-kinase
Poly-HEMA	poly-hydroxyethyl methacrylate
PPAR $\beta/\delta$	peroxisome proliferator-activated receptor $\beta/\delta$
PR	progesterone receptor
RAR	retinoic acid receptor

RARE	retinoic acid response element
RRM	retinoid-related molecules
RXR	retinoid X receptor
SD	standard deviation
SDS	sodium dodecyl sulfate
SEM	standard error of the mean
SFU	sphere-forming unit
ST1926	E-4-(4'-hydroxy-3'-adamantyl biphenyl-4-yl) acrylic acid
TAM	tumor-associated macrophage
TUNEL	dUTP nick end labeling
VEGF	vascular endothelial growth factor

# CHAPTER I

## LITERATURE REVIEW

### **A. The Mammary Gland**

#### ***I. Overview***

The mammary gland is a secretory organ that produces milk during lactation to feed young offspring. The human mammary glands are located in the breasts. Two tissue compartments comprise the mammary glands: the epithelium, which consists of an extensive system of ducts and milk-producing alveolar cells; and the connective tissue also called the stroma or the mammary fat pad, which constitutes the rest of the organ (Figure 1). The majority of epithelial cells in mature mammary glands are luminal, secretory and cuboidal cells, which undergo differentiation during pregnancy to produce milk (Hennighausen 2005). Basal myoepithelial cells with contractility functions surround the luminal cells and participate in the delivery of milk through milk ducts. Altogether, the luminal and basal cells form alveoli with a central lumen (Hennighausen 2005). The epithelium is embedded within the stroma, which consists of adipocytes, fibroblasts, cells of the hematopoietic system, blood vessels, and neurons (Inman 2015). The stroma and the myoepithelial basement membrane constitute the extracellular matrix (ECM) of mammary epithelial cells, and ensure their correct polarized morphology and architecture (Watson 2008).

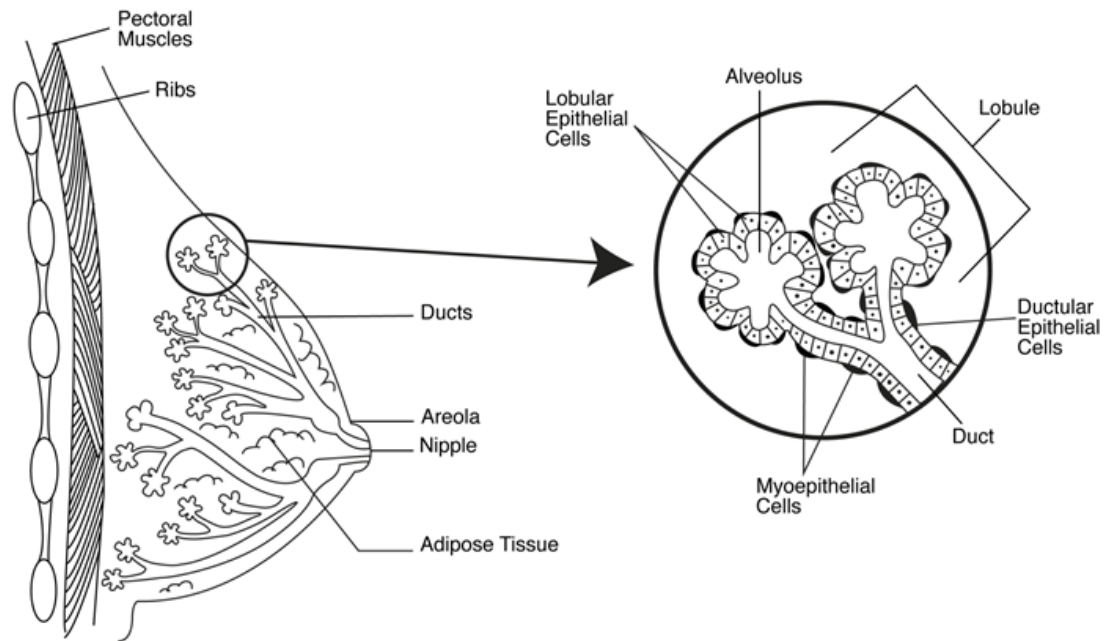


Figure 1. Human mammary gland anatomy. Adopted from (Bazzoun 2014).

## 2. *Development of the mammary gland*

Development of the mammary glands starts in the fetus where small buds form and invade the embryonic stroma, leading to the outgrowth of a primary duct into deeper layers of the stroma and the formation of the nipple (Hennighausen 2005). A small ductal system then forms through the elongation or bifurcation of the primary duct. At birth, the development of the mammary gland pauses, then resumes during puberty. The cyclical production of ovarian oestrogen and progesterone promotes ductal outgrowth into side branches, which form and disappear during each menstrual cycle (Hennighausen 2005; Briskin 2010). Development of the mammary glands into mature, milk-secreting organs occurs during pregnancy, a process that is controlled by prolactin and placental hormones, also termed placental lactogens (Hennighausen 2005; Briskin 2010). At the end of lactation, involution takes place, causing massive cell death and collapse of the alveoli, and thus, the remodeling of the epithelium into a

simple ductal structure again. Expansion and maturation of alveoli are initiated with the next round of pregnancy (Figure 2). The presence of stem cells with self-renewal capacity explains the alveolar renewal in each subsequent pregnancy, and the differentiation of progenitor cells into either basal or luminal cells (Smalley 2003; Smith 2003). Deciphering the molecular events that govern mammary gland development and mammary stem cell biology is an integral step in understanding breast tumorigenesis and ultimately, developing therapies for this disease (Macias 2012).

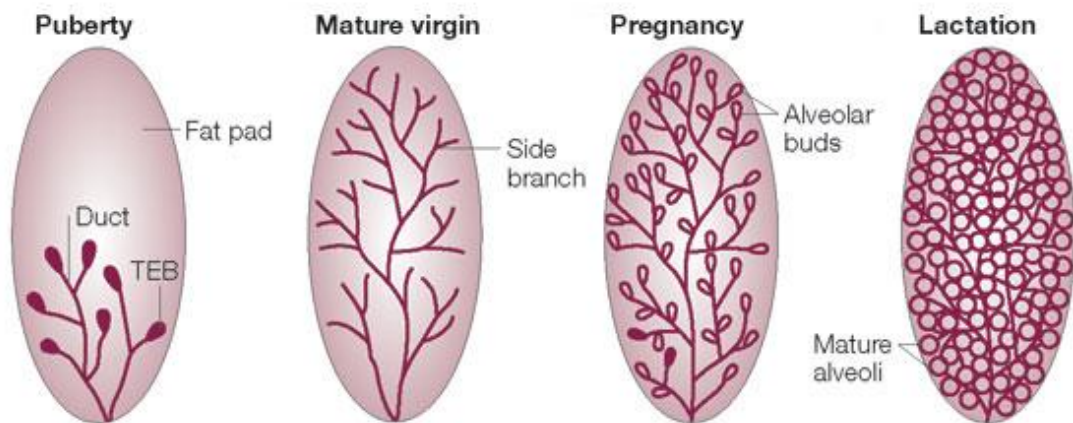


Figure 2. Schematic presentation of mammary gland development

## **B. Breast Cancer: General Background**

### ***1. Overview***

Breast cancer prevalence has been tremendously increasing over the past decades. Being the most common malignancy in females and the second cause of cancer-related death, breast cancer is estimated in 2016 to account for 29% of the total newly estimated cases with an estimate of 40,000 deaths in the United States of America (Siegel 2016). Breast cancer can be classified based on the anatomy of the breast. Sometimes, a breast tumor can be a mixture of these types. In most breast cancer cases, the cancer originates from the epithelial cells lining the ducts and is

referred to as ductal carcinoma in situ (DCIS). When ductal carcinoma breaks through the wall of the ducts and invades the adjacent tissue, it is referred to as invasive or infiltrating ductal carcinoma (IDC). While cancer arising from the alveolar compartment (lobules) is less frequent, it can also be classified into two types: lobular carcinoma in situ (LCIS) or invasive or infiltrating lobular carcinoma (ILC). Finally, inflammatory breast cancer (IBC) is rare and is often mistaken for infection with the absence of a defined lump. IBC has a higher chance of metastasizing and a worse prognosis (American Cancer Society 2016). There are also many other less common types of breast cancer which were not covered here.

## ***2. Molecular subtypes of breast cancer***

Classification of breast cancer mostly relies on molecular markers assessed using gene expression profiles, which includes the absence or presence of receptors displayed by the cells including, estrogen receptor (ER), progesterone receptor (PR), and human epidermal growth factor receptor 2 (HER2). These main biological markers, along with other cellular markers such as Ki67 and cytokeratin 5/6 (CK5/6), have led to four major subtypes underlying the heterogeneity of breast cancer; each with its own signature expression profile that impacts the treatment regimen and the prognosis of breast cancer patients (Perou 2000; Schnitt 2010). Luminal A breast cancer (ER<sup>+</sup> and/or PR<sup>+</sup>, HER2<sup>-</sup>, and low Ki67) tends to have the best prognosis among the four subtypes with fairly high survival rates, whereas luminal B subtype (ER<sup>+</sup> and/or PR<sup>+</sup>, HER2<sup>+</sup>) or (ER<sup>+</sup> and/or PR<sup>+</sup>, HER2<sup>-</sup>, and high Ki67) generally grows faster than luminal A with poor prognosis. Triple negative/basal-like breast cancer (ER<sup>-</sup>, PR<sup>-</sup>, HER2<sup>-</sup>) has been shown to be aggressive, unresponsive to treatment, and thus associated with worst prognosis.

Finally, HER2-positive breast cancer (ER<sup>-</sup>, PR<sup>-</sup>, HER2<sup>+</sup>) are generally responsive to anti-HER2 drugs namely, trastuzumab (Table 1 and 2) (Perou 2000; Schnitt 2010).

Recently, the molecular taxonomy of breast cancer international consortium (METABRIC) identified more than ten different breast cancer subtypes, by incorporating genomic and transcriptomic sequencing (Fadoukhair 2016).

Breast Cancer Molecular Subtype	Gene Expression Profile
<b>Luminal A</b>	ER <sup>+</sup> and/or PR <sup>+</sup> , HER2 <sup>-</sup> , and low Ki67
<b>Luminal B</b>	ER <sup>+</sup> and/or PR <sup>+</sup> , HER2 <sup>+</sup> or ER <sup>+</sup> and/or PR <sup>+</sup> , HER2 <sup>-</sup> , and high Ki67
<b>HER2</b>	ER <sup>-</sup> , PR <sup>-</sup> , HER2 <sup>+</sup>
<b>Triple Negative/Basal-like</b>	ER <sup>-</sup> , PR <sup>-</sup> , HER2 <sup>-</sup>

Table 1. Breast cancer subtypes with their respective gene expression profile.

### 3. *Treatment regimen*

Breast cancer treatment is multidisciplinary and may include surgery, radiation, and systemic therapy (chemotherapy, hormonal, targeted or bone-directed therapies) depending on the type and stage of cancer (American Cancer Society 2016). Luminal A and luminal B breast cancer subtypes are hormone receptor positive and are treated with a number of hormone receptor targeted therapies such as Tamoxifen or aromatase inhibitors. Similarly, luminal B subtype is usually treated with hormone receptor targeted therapies in combination with anti-HER2 drugs such as trastuzumab. HER2-positive breast cancer treatment regimen consists of trastuzumab alone, or in

combination with tyrosine kinase inhibitors such as lapatinib. Combinations of anthracyclines with other drugs, namely, paclitaxel, have been the cornerstone treatment for triple negative breast cancer (PDQ Adult Treatment Editorial Board 2016). However, aggressive and metastatic triple negative/basal-like breast cancer has been shown to develop resistance to current standard treatments, which calls for the development of effective therapies (Brouckaert 2012; Bayraktar 2013; American Cancer Society 2016). Fortunately, recent advances demonstrated that triple negative/basal-like breast cancer was found to be particularly sensitive to poly(ADP-ribose) polymerase (PARP) inhibitors (Crown 2012). However, these drugs are currently being tested in clinical trials for efficacy and safety (Breast Cancer Trials). The major molecular subtypes of breast cancer with their clinical features and treatment regimen are summarized in Table 2.

	<i>Molecular subtype</i>		
	<i>Luminal</i>	<i>HER2</i>	<i>Basal</i>
Gene expression pattern	High expression of hormone receptors and associated genes (luminal A>luminal B)	High expression of HER2 and other genes in amplicon Low expression of ER and associated genes	High expression of basal epithelial genes, basal cytokeratins Low expression of ER and associated genes Low expression of HER2
Clinical features	~70% of invasive breast cancers ER/PR positive Luminal B tend to be higher histological grade than luminal A Some overexpress HER2 (luminal B)	~15% of invasive breast cancers ER/PR negative More likely to be high grade and node positive	~15% of invasive breast cancers Most ER/PR/HER2 negative ('triple negative') BRCA1 dysfunction (germline, sporadic) Particularly common in African-American women
Treatment response and outcome	Respond to endocrine therapy (but response to tamoxifen and aromatase inhibitors may be different for luminal A and luminal B) Response to chemotherapy variable (greater in luminal B than in luminal A) Prognosis better for luminal A than luminal B	Respond to trastuzumab (Herceptin) Respond to anthracycline-based chemotherapy Generally poor prognosis	No response to endocrine therapy or trastuzumab (Herceptin) Appear to be sensitive to platinum-based chemotherapy and PARP inhibitors Generally poor prognosis (but not uniformly poor)

Table 2. The major molecular subtypes of breast cancer with their clinical features and treatment regimen. Adopted from (Schnitt 2010).



#### **4. *Altered signaling pathways in breast cancer***

Next generation sequencing led to the identification of the two most commonly altered signaling pathways in a vast number of breast cancers. The phosphatidylinositol 3-kinase (PI3K) /protein kinase B (PKB or AKT) pathway was shown to be constitutively active whereas the JUN/mitogen-activated protein kinases (MAPK) pathway was shown to be repressed (Guille 2013). In addition, mutations in *p53*, *PIK3CA*, *GATA3*, and *PTEN* genes are among the most frequent mutations in breast cancer (Fadoukhair 2016). For instance, mutations in *p53* occur in more than 30% of breast carcinomas, which are associated with aggressive and therapeutically refractory tumors (Zardavas 2015; Bertheau 2013). Initiation of breast cancer requires a series of genetic and epigenetic perturbations, particularly in tumor suppressor genes such as *p53*, *PTEN*, *BRCA1*, and *BRCA2* (Buchholz 2012). Subsequent mammary tumor progression is driven by the accumulation of more genetic alterations combined with clonal expansion and selection (Fadoukhair 2016). Many studies focused on the identification of driver genes involved in tumor progression, while the potential involvement of breast cancer microenvironment components has not been so far explored in sufficient depth (Polyak 2007).

#### **5. *Breast cancer microenvironment***

Advances in research have paved the way for a better understanding of cancer as a complex disease involving not only the cancerous cells, but also their microenvironment as well which constitutes a dynamic milieu and a critical player in tumor progression (Bissell 2011; Hanahan 2011). In most types of cancer, the structural sites nearby the

tumor are subject to modification. In fact, there are structural, functional, genetic, and epigenetic changes that seem to govern the transformation of normal cells to cancer-associated ones (Patocs 2007). The final outcome can be either suppression or stimulation of cancer growth and development. The impact of the microenvironment on tumor growth has been extensively studied for its positive association as promoter of cancer initiation and progression, invasiveness and metastatic dissemination into the circulation, angiogenesis, and recruitment of immune cells (Bissell 2011). Components of breast cancer microenvironment include myoepithelial basement membrane composed of different types of laminin, collagen, tenascin, and proteoglycans; and various stromal cell types such as macrophages, endothelial cells, adipocytes and fibroblasts (Kessenbrock 2010) (Figure 3). The most crucial components of the tumor microenvironment are the cancer-associated fibroblasts (CAFs), which constitute the majority of cells present in the tumor microenvironment (Hanahan 2012). In breast cancer, CAFs not only promote tumor progression but also induce therapeutic resistance. Accordingly, targeting CAFs provides a novel approach to control tumors with therapeutic resistance (Polyak 2007). Additionally, in invasive breast cancers, the basement membrane of myoepithelial cells is generally lost, which alters the correct polarity of breast epithelial cells and induces an extracellular matrix (ECM) remodeling (Weigelt 2014). Tumor-associated macrophages (TAMs) on the other hand, have been extensively studied for their positive contribution to inflammation, angiogenesis, invasion, and metastatic spread; making them attractive target in breast cancer (Lin 2007). The breast cancer niche suppresses the immune reaction to tumor cells, providing an ideal milieu for cancer cell growth (Vinay 2015). This is due to an interplay between regulatory T-cells, myeloid-derived suppressor cells, and their

derivatives, which sustain an anti-autoimmunity response and tissue inflammation in combination with tumor-secreted cytokines, enzymes, and antigens (Rothschild 2015). Understanding the complexity of breast cancer microenvironment and its critical role in tumor initiation and progression is the key for the development of targeted therapies (Nienhuis 2015; Rothschild 2015).

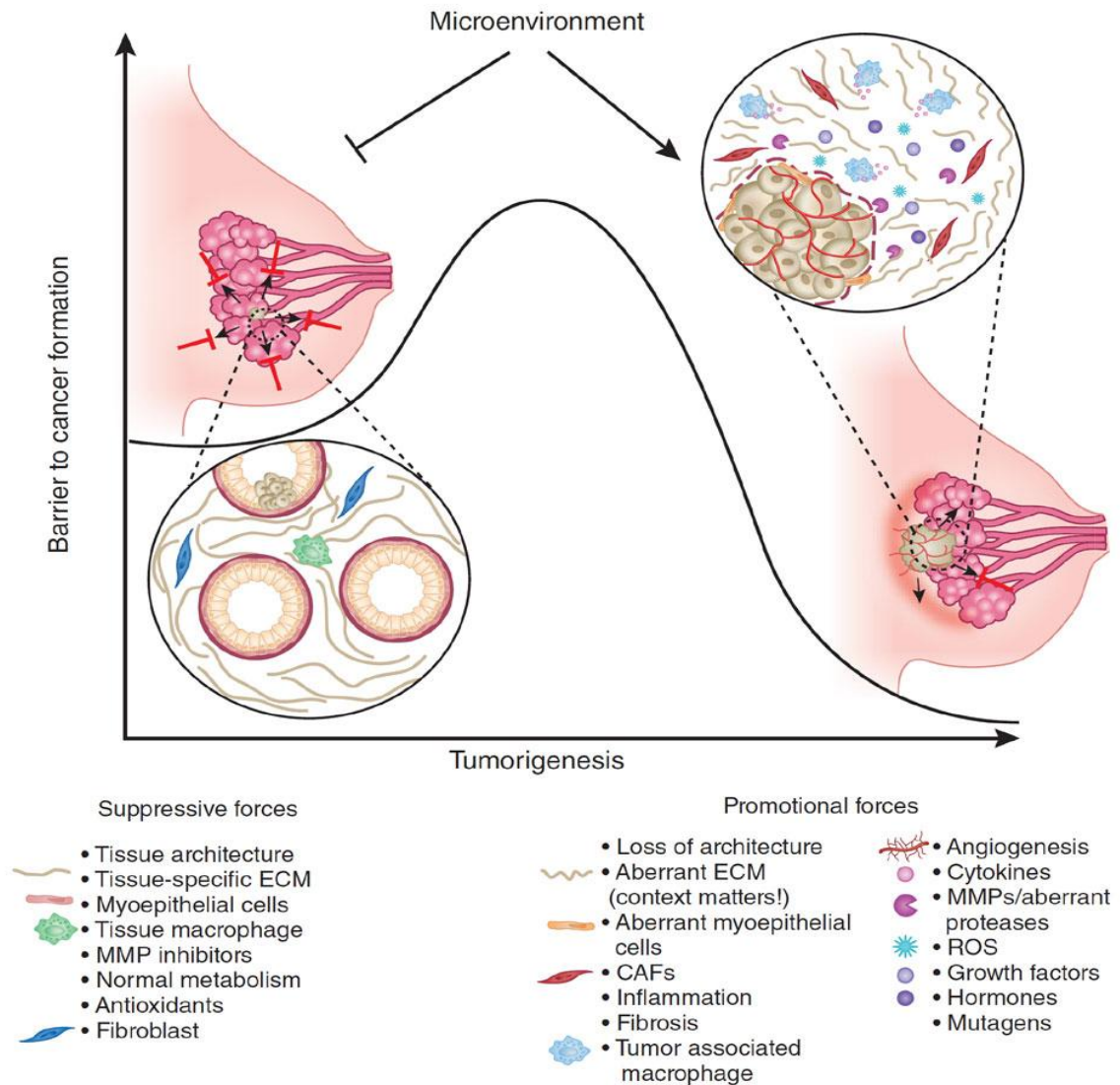


Figure 3. The influence of the microenvironment in normal *versus* tumor breast tissue. Adopted from (Bissell 2011).

## **C. 3D Cell Culture Models**

### ***1. Overview***

For more than four decades, the supporting substrates for cell growth have been made from polystyrene or glass in the form of a flat two-dimensional (2D) surface where cells grow as monolayers, deprived from their interaction with the microenvironment (Kim 2011). How can 2D cell culture models mimic the real and actual physiology of the tissue with respect to all fundamental tissue-specific characteristics? Indeed, it is necessary to create a growth environment that permits cellular differentiation, proliferation, adhesion, and heterotypic interactions. However, a 2D cell culture model fails at providing the representative architecture of a tissue, and precisely the tumor mass embedded in its niche and interacting with the different elements of the microenvironment. Many of these crucial microenvironmental signals, that are initially lost in 2D cell culture models, may be alternatively restored using three-dimensional (3D) cultures (Weigelt 2014).

### ***2. Types of 3D cell culture models***

3D cell culture techniques have been developed and promote two types of cell growth: anchorage-independent and -dependent growth (Lovitt 2014). The former methodology consists of growing the cells as monocultures without the use of substrates to allow the aggregation of cells. Examples of such models include growing cells using low-attachment plates, or plates coated with poly-hydroxyethyl methacrylate (poly-HEMA) or agarose. Anchorage-independent growth can be also achieved by placing the cells in hanging drop culture and incubating them until they form 3D spheroids commonly referred to as multicellular tumor spheroids. Finally, growing cells in soft

agar matrix promotes anchorage-independent growth and 3D spheroids formation (Lovitt 2014). On the contrary, anchorage-dependent growth requires the presence of specific substrates on which cells adhere. The most commonly used substrate for 3D anchorage-dependent growth is basement membrane extracted from the Engelbreth-Holm-Swarm (EHS) murine tumor, which is a form of lamin-rich extracellular matrix (lrECM) capable of restoring functional and morphological properties of malignant and non-malignant cells (Weigelt 2014). 3D lrECM models allow normal cells to form acini with a central lumen that mimic their *in vivo* architecture (Bissell 2011). Cells can be either embedded as 3D ‘embedded’ assay or seeded on top of lrECM gel as 3D ‘on top’ assay. The latter model requires shorter amount of time, less amount of lrECM gel, and hence less money; and facilitates imaging since colonies are in a single plane (Lee 2007). Although collagen I has also been utilized as a biologically relevant matrix, particularly when studying mammary gland branching morphogenesis, lrECM gels promote more of functional and morphological differentiation than do floating collagen gels. 3D Anchorage-dependent and -independent growth methods are summarized in Figure 4.

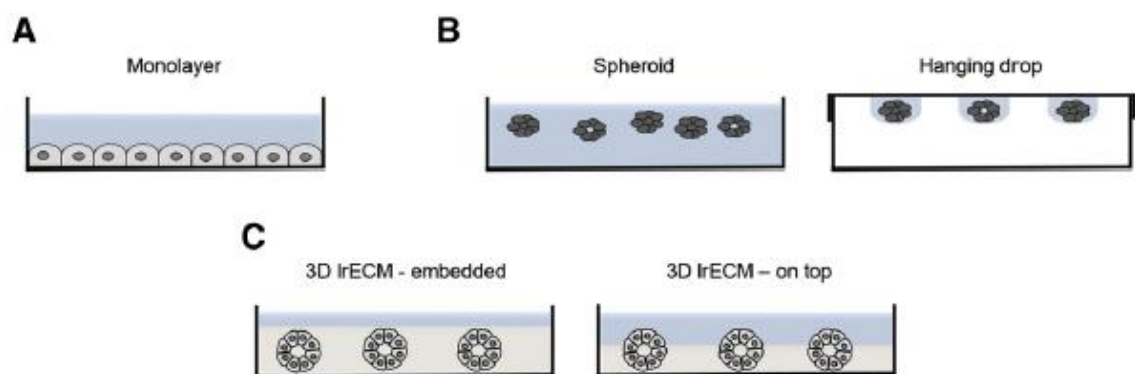


Figure 4. 3D cell culture systems. Adopted from (Weigelt 2014).

### **3. Advantages of 3D cell culture models**

Nowadays, research has been oriented towards the use of 3D cell culture models to answer tissue-specific questions, which offers several advantages over the use of the 2D cell culture model. In fact, cells grown in IrECM tend to have altered morphology and proliferation rate as opposed to the 2D cell culture model (Arai 2013) and have their cellular physiology maintained as observed by the secretion of milk proteins from breast epithelial cells (Lee 1985) and albumin from hepatocytes (Michalopoulos 1997). Furthermore, 2D cell culture models lack inter- and intracellular complexity and fail to represent the true architecture of the microenvironment. Thus, drug screening on such models is often misleading since roughly 90% of preclinical drugs fail to provide expected efficacy in treatment, thereby wasting vast amount of resources and time (Kola 2004). Fortunately, 3D cell culture models can recapitulate part of the microenvironment and restore the *in vivo* architecture of breast tissue, and are hence more valid screening tools for anti-cancer drugs (Weigelt 2014). A recent study showed that leukemic and breast cancer cells embedded within 3D culture matrices are more resistant to doxorubicin than those grown in 2D (Aljitawi 2014; Imamura 2015). Recent advances led to the development of heterotypic 3D culture models by co-culturing malignant cells with stromal and/or endothelial cells to recapitulate tissue architecture and promote heterotypic interactions between different types of cells (Weigelt 2014). These models particularly can be used to study cell-cell and cell-stroma interactions and their modulation of drug response. While animal models remain the ultimate preclinical tool for assessment of drug sensitivity, they remain expensive and time consuming than 3D cell culture models.

## D. Retinoids

### 1. Overview

Retinoids are a class of chemical compounds that have been extensively studied for their role as tumor-suppressive agents due to their implication in several physiologically vital processes such as the regulation of cell proliferation and differentiation in embryonic development and adult life (Altucci 2001; Rhinn 2012). Retinoids comprise both natural and synthetic analogues of vitamin A (retinol). All-*trans* retinoic acid (ATRA) and 13-*cis* retinoic acid (13-*cis*RA) are the active metabolites of retinol or vitamin A (Figure 5) (Garattini 2014). ATRA was shown to display major pleiotropic effects in cellular proliferation, differentiation, and cell death (di Masi 2015). This latter natural retinoid emerged in 1981 as a cyto-differentiating agent and is still being used as a treatment regimen in combination with other drugs for patients with acute promyelocytic leukemia (APL) to date (Breitman 1981; Powell 2010; Liu 2015).

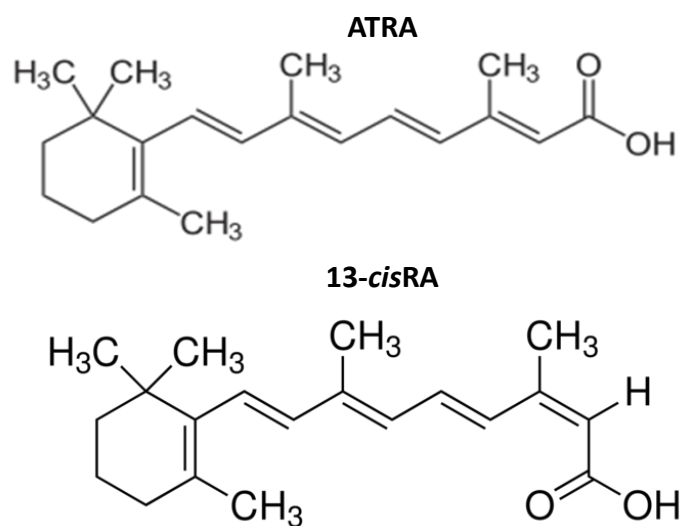


Figure 5. Chemical structures of ATRA and 13-*cis*RA.

## **2. Mechanisms of action of retinoids**

The pharmacological activities of ATRA and 13-*cis*RA are primarily mediated by members of two distinct classes of receptors which belong to the steroid/thyroid hormone nuclear receptors family: retinoic acid receptors (RARs) and retinoid X receptors (RXRs), with each comprising of three different isoforms –  $\alpha$ ,  $\beta$  and  $\gamma$  (Benbrook 2014). Being a nuclear receptor, the ligand-activated complex RAR heterodimerizes with RXR and acts as a transcription factor by binding to retinoic acid responsive elements (RAREs) in retinoid-responsive genes and thus, initiating their transcription (Garattini 2014; di Masi 2015). ATRA and 13-*cis*RA are pan-RAR agonists meaning they can activate all RAR-isoforms with high efficiency (Garattini 2014). Interestingly, RARs and RXRs are not the only nuclear receptors that bind to ATRA, as peroxisome proliferator-activated receptor  $\beta/\delta$  (PPAR $\beta/\delta$ ) can also be bound and activated by ATRA. Partitioning of ATRA between RARs and PPAR $\beta/\delta$  is mediated and controlled by the cytosolic retinoid-binding proteins, cellular retinoic acid-binding protein II (CRABP-II), and fatty-acid binding protein 5 (FABP5) (Schug 2007). FABP5 directs ATRA to PPAR $\beta/\delta$  leading to the activation of PPAR $\beta/\delta$  target genes, namely, vascular endothelial growth factor A (VEGF-A) that promotes tumor growth and angiogenesis (Wang 2006; Schug 2007). CRABP-II directs ATRA to RARs, leading to cytodifferentiating and growth-inhibitory effects (Schug 2007). Finally, ATRA was also shown to display non-genomic effects independent of the classical RAR-mediated action by activating a series of different kinase signaling pathways (Schenk 2014; Garattini 2014). The activation of multiple kinase signaling pathways leads to the transcription of multiple target genes and downstream effectors, independently of the genomic RARs functions (Schenk 2014). Among the activated



kinase signaling pathways by ATRA is MAPK signaling pathway that in turn, activates downstream effectors namely, extracellular signal-regulated kinases (ERKs) and p38 MAPKs (Schenk 2014; Garattini 2014).

### ***3. Retinoids in the Treatment of Breast Cancer***

Recent studies reported that aberrant or de-regulated retinoid signaling pathway may be highly linked to tumorigenesis, particularly in breast cancer cells where there is an altered expression in members of RARs and RXRs (di Masi 2015). In fact, RAR $\alpha$  and RAR $\gamma$  transcript levels were shown to be significantly higher in normal primary cancer samples as compared to normal samples, whereas RAR $\beta$  and RXR $\gamma$  were significantly lower in tumor tissues (Garattini 2014). Hence, retinoids emerged as potential therapeutic agents, displaying potent chemotherapeutic and chemopreventive properties, and were involved in several preclinical studies and few clinical trials for breast cancer (Garattini 2014; di Masi 2015). However, the use of natural retinoids in clinical trials was often hindered by undesirable side effects (Garattini 2014) and resistance to treatment (Connolly 2013; di Masi 2015), and as such they failed to achieve their primary end-point. ATRA failed phase-II clinical trials in patients with metastatic breast cancer (Connolly 2013; di Masi 2015). Other retinoids, such as 9-*cis* retinoic acid (9-*cis*RA), 13-*cis*RA, fenretinide, bexarotene, and retinyl palmitate also failed testing in breast cancer clinical trials. Interestingly, fenretinide is the most studied retinoid in breast cancer chemoprevention clinical trials because of its selective accumulation in breast tissue and favorable pharmacokinetics (Kazaniga 2012). The different clinical trials of retinoids in breast cancer are represented in Table 2.

Compound	End point	Trials (No.)	Clinical Phase
ATRA	BC prevention	0	Ph I/II
	BC treatment	4	
9-cis-RA	BC prevention	0	Ph I
	BC treatment	2	Ph I
13-cis-RA	BC prevention	0	Ph II
	BC treatment	1	
Bexarotene	BC prevention	1	Ph I
	BC treatment	1	Ph II
Retinyl palmitate	BC prevention	0	Ph II
	BC treatment	1	

Table 3. Clinical trials of retinoids in breast cancer. Adopted from (Garattini 2014).

#### 4. *Understanding ATRA resistance in breast cancer*

Current studies are centered on understanding the molecular mechanisms behind the resistance of breast cancer cells to ATRA. Several factors contribute to natural or acquired ATRA resistance. High expression levels of cytochrome-P450-isoform-26 (CYP26) in breast tumors results in the metabolic inactivation of ATRA (Nelson 2013). Recent studies showed that the lack of ATRA responsiveness in breast cancer may be also linked to aberrant epigenetics, which suppress ATRA-regulated gene expression namely of RAR $\beta$  (Sirchia 2000; Sirchia 2002). Furthermore, upregulated PPAR $\beta/\delta$  in breast cancer, particularly in the ER<sup>-</sup> subtype (Garattini 2014), conferred resistance to ATRA, and resulted in pro-oncogenic effect that opposes the RAR-mediated growth inhibition (Schug 2008). This mechanism of action can explain why ATRA enhances the proliferation of certain cancer cell lines. In addition, ATRA resistance may stem from a downregulation of CRABP-II, which represses ATRA-bound RARs and their mediated growth-inhibitory effects (Schug 2008).

## **E. Overcoming ATRA resistance and toxicity with synthetic retinoids**

### ***1. Overview***

To overcome ATRA resistance and toxic side effects, synthetic retinoids were developed to exhibit enhanced specificity and reduced toxicity. A prominent molecule belonging to the family of retinoid-related molecules (RRMs) is the synthetic adamantyl retinoid ST1926 or E-4-(4'-hydroxy-3'-adamantyl biphenyl-4-yl) acrylic acid (Cincinelli 2003), a CD437 analog (Garattini 2004) (Figure 7). ST1926 is synthesized from CD437 through a three-step sequence where the naphthalene ring in CD437 is replaced with a styrene moiety in ST1926 (Cincinelli 2003). ST1926 was shown to be endowed with potent anti-tumor effects in several *in vitro* and *in vivo* cancer models, independently of RAR and *p53* signaling pathways, and displayed a favorable pharmacokinetic profile when compared to HPR and CD437 (Garattini 2004). ST1926 exhibits strong anti-tumor activities in large panel of cancer cell lines, particularly in ATRA-resistant and/or *p53*-mutated cell lines, which offers promise to cancer therapy. ST1926 induced tumor growth inhibition in ovarian carcinoma (Zuco 2004; Zuco 2010), neuroblastoma (Di Francesco 2007; Di Francesco 2012), rhabdomyosarcoma (Basma 2016), and several leukemia animal models (Garattini 2004; El Hajj 2014; Nasr 2015). Furthermore, ST1926 can be administered orally, while achieving effective micromolar ( $\mu\text{M}$ ) concentrations in human and mouse plasma (Sala 2009; Basma 2016).

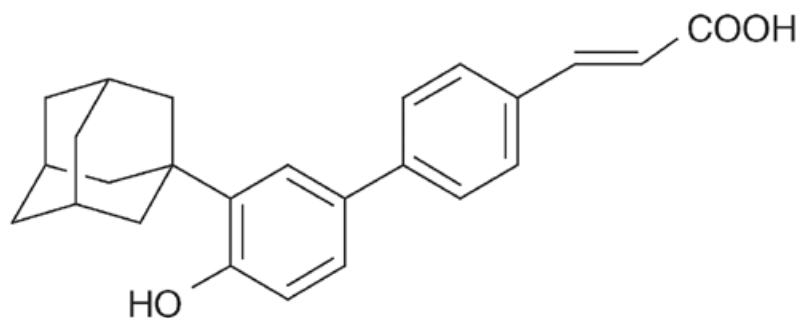


Figure 6. Chemical structure of ST1926.

## 2. *ST1926 mechanism of action*

In *in vitro* ovarian cancer models, ST1926 exhibited growth-inhibitory effects, induced p53-dependent and -independent apoptosis, and activated stress-activated protein kinases (Zuco 2004). Combination treatments of ST1926 with ZD1839, an epidermal growth factor receptor inhibitor (EGFR), enhanced the anti-tumorigenic potentials of ST1926, activated caspase 8, and upregulated the cell death receptor DR5. Interestingly, the histone deacetylase (HDAC) inhibitor (RC307) enhanced the sensitivity of ovarian carcinoma cells to ST1926 by increasing early markers of DNA damage, including ATM and H2AX phosphorylation (Zuco 2009). In addition, ST1926 treatment in teratocarcinoma cell lines resulted in G<sub>2</sub>/M cell cycle arrest, apoptosis, and a perturbation in calcium homeostasis (Parella 2006). In H460 lung carcinoma cell line, ST1926 induced apoptosis through the activation of caspases 3, 8, and 9, alongside with genotoxic stress (Kadara 2006). In a neuroblastoma preclinical study, ST1926 induced potent DNA damage and S/G<sub>2</sub> cell cycle arrest, independent of *p53* and caspases. Oral treatments of ST1926 reduced tumor growth in neuroblastoma xenografts model (Di Francesco 2007). The same research group then tested the effects of ATRA and ST1926 combination treatments on *in vitro* and *in vivo* neuroblastoma models. They

showed that these drug combinations enhanced growth inhibition and apoptosis in both models, clearly indicating the promising use of ST1926 alone, or in combination with ATRA in the treatment of neuroblastoma (Di Francesco 2012). In AML cells, particularly the APL subtype, ST1926 was shown to trans-activate RAR $\gamma$ , phosphorylate p38 and JNK, and increase cytosolic calcium levels that are directly related to apoptosis (Garattini 2004). Combination treatments of ST1926 and ATRA demonstrated enhanced apoptosis without the involvement of cytodifferentiation on transplanted NB4 cells *in vivo*. Additionally, ST1926-induced growth inhibition in AML models was shown to be independent of the retinoid receptor signaling pathway (Valli 2008). Studies from our laboratory demonstrated that ST1926 inhibited the growth of adult T-cell leukemia (ATL) and chronic myeloid leukemia cells (CML) in a partially caspase-dependent mechanism, while sparing resting and activated lymphocytes (El Hajj 2014; Nasr 2015). Oral treatments of ST1926 in ATL and CML animal models potently reduced tumor burden and increased the survival of mice. However, ST1926 did not eradicate the leukemic initiating cells (LICs), evident by the ability of splenocytes isolated from treated primary mice to develop CML in untreated secondary recipients (Nasr 2015). Finally, ST1926 was effective in inhibiting the growth of rhabdomyosarcoma in *in vitro* and *in vivo* models, while inducing early DNA damage that was reversed by caffeine (Basma 2016).

### **3. *ST1926 pharmacokinetic properties***

Although ST1926 showed success in several *in vitro* and *in vivo* cancer models, there are several drawbacks that hinder its promising use in future clinical trials. ST1926 was shown to undergo major glucuronidation, leading to its poor bioavailability

and rapid excretion by the liver, with a half-life of only two hours (Sala 2009; Basma 2016). Hence, ST1926 was halted in Phase 1 clinical trial for patients with ovarian carcinoma. Alternatively, there are ongoing efforts in synthesizing derivatives from ST1926 to overcome glucuronidation. So far, these derivatives were all shown to revert back to their parental drug, ST1926 (Bernasconi 2015).

## **F. Aims of the study**

Given the putative genotoxic and pro-apoptotic effect of ST1926 that was demonstrated on several cancer models from our laboratory including, ATL, CML, colon, rhabdomyosarcoma, prostate, and AML (El Hajj 2014; Nasr 2015; Basma 2016; and unpublished data), we aim in this study to investigate the antitumor activities of ATRA, ST1926, and their combination using 2D and 3D human breast cancer models. First, we aim to determine the effects of ST1926 on the proliferation, viability, cell cycle progression, cell death mechanism, DNA damage, and Wnt/ $\beta$ -catenin and retinoid signaling pathway in two well-characterized breast cancer cell lines, MCF-7 and MDA-MB-231. We will also determine the effects of ATRA/ST1926 combination treatments on the proliferation, viability, and cell cycle progression. Furthermore, given the importance of the microenvironment and its contribution to tumor resistance and drug response, we aim to study the effects of ATRA, ST1926, and combination treatments on the 3D anchorage-independent and -dependent growth of breast cancer cells, and on the colony-forming ability of breast cancer stem/progenitor cells in a 3D cell culture model. Finally, this study will investigate the effect of ATRA, ST1926, and their combination treatments on ‘normal-like’ breast epithelial cells, MCF-10A and HMT-3522 S1, in 2D and 3D culture models.

To date, achieving complete remission in patients with aggressive and metastatic breast cancer remains a daunting task despite major advances in the drug discovery field. This study will hopefully support the potential therapeutic role of ST1926 alone, or in combination with ATRA, in breast cancer, particularly the aggressive and metastatic triple negative subtype.

## CHAPTER II

### MATERIALS AND METHODS

#### A. Cell Culture *In Vitro* Model

MCF-7 and MDA-MB-231 are two human adenocarcinoma cell lines that were first isolated from the pleural effusion of a 69-year old and a 51-year old Caucasian women suffering from metastatic breast cancer, respectively (Soule 1973; Cailleau 1974 ).

MCF-7 cells exhibit several characteristics of differentiated mammary epithelium including their ability to process estradiol and form domes (Levenson 1997). Some of the MCF-7 cells have fusiform shape, and some have polygonal shape. Their doubling time is approximately 29 hours, and may vary according to the source. They express estrogen and progesterone receptors and, therefore, belong to the luminal A subtype (ER<sup>+</sup>, PR<sup>+</sup>, and HER2<sup>-</sup>) (Levenson 1997). They also harbor wild-type *p53* and *p21* genes (Troester 2006).

MDA-MB-231 is a highly aggressive, invasive, and poorly-differentiated human breast cancer cell line that lacks ER, PR, and HER2, and therefore belongs to the triple negative subtype (ER<sup>-</sup>, PR<sup>-</sup>, and HER2<sup>-</sup>) (Lehmann 2011). They are mesenchymal in shape with a doubling time of approximately 27 hours. MDA-MB-231 cells harbor many mutations; of interest to our study is the *p53* mutation which was reported to be heterozygous mutant (Olivier 2002).

MCF-10A and HMT-3522 S1 are two non-tumorigenic epithelial cell lines that were isolated from the breast tissue of Caucasian women (Soule 1990; Briand 1987). They retain several characteristics of differentiated mammary epithelium including



dome formation in confluent cultures and their ability to exhibit 3D growth structures known as acini when grown in lamin-rich extracellular matrix (lrECM) (Petersen 1992; Plachot 2004).

## **B. Cell Culture**

MCF-7 and MDA-MB-231 cells were cultured in RPMI 1640 (Lonza) medium supplemented with 10% Fetal Bovine Serum (FBS) (Sigma-Aldrich) and 50 U/ml penicillin-streptomycin antibiotics (Lonza). MCF-10A cells were cultured in DMEM F-12 medium (Lonza) supplemented with 5% horse serum, 20 ng/ml EGF, 0.5 mg/ml hydrocortisone, 100 ng/ml cholera toxin, 10 mg/ml insulin, and 50 U/ml penicillin-streptomycin. HMT-3522 S1, between passages 52 and 60, were routinely cultured in a 2D culture model as a monolayer in DMEM F12 (Lonza) supplemented with 2 mM glutamine, 250 ng/ml insulin, 10 µg/ml transferrin,  $10^{-8}$  M sodium selenite,  $10^{-10}$  M  $17\beta$ -estradiol, 0.5 µg/ml hydrocortisone, 5 µg/ml ovine prolactin, and 10 ng/ml epidermal growth factor (EGF). The HTLV-1-transformed CD4<sup>+</sup> T-cell line C8166 was grown as previously described (Darwiche 2002, Darwiche 2007). All cells were incubated in a humidified incubator (95% air, 5% CO<sub>2</sub>) at 37°C.

## **C. Cell Passaging**

When cells reached 70 to 80% confluence, they were washed twice with 1X calcium and magnesium-free phosphate buffered saline (PBS) (Lonza), and then were trypsinized with 1X trypsin (Lonza) for two minutes at 37°C. Subsequently, trypsin was neutralized with a ratio of 1:1 complete media (vol/vol). Cells were then centrifuged for 5 minutes at 900 rpm. The supernatant was discarded, while the pellet was resuspended

in fresh new media and transferred into new 75 cm<sup>2</sup> tissue culture flasks for maintenance. Cell number was calculated using a hemocytometer according to the following formula: cells/ml = average number of cells x dilution factor x volume of suspension x 10<sup>4</sup>. Cells were counted by the trypan blue dye exclusion method using 0.4% trypan blue solution (Sigma-Aldrich).

#### **D. Compounds**

ATRA and HPR (fenritinide) were purchased from Sigma, dissolved in 0.1% dimethylsulfoxide (DMSO) under yellow light ( $\lambda > 500$  nm) at a concentration of  $3.3 \times 10^{-2}$  M and  $1 \times 10^{-2}$  M respectively, and stored in amber tubes at -80°C. ST1926 was kindly provided by Dr. Claudio Pisano (Biogem, Research Institute, Ariano Irpino-Martiri, Italy), dissolved in 0.1% DMSO at a concentration of  $1 \times 10^{-2}$  M, and stored in amber tubes at -80°C. The pan-RAR inverse agonist, BMS493, was purchased from Santa Cruz Biotechnology, dissolved in 0.1% DMSO, stored at +4°C, and used at a final concentration of 1  $\mu$ M. Experiments with ATRA and HPR were conducted under yellow light. The final DMSO concentrations never exceeded 0.1% and did not have any effect on the proliferation of all tested cell lines.

#### **E. Cell Growth Assay**

The anti-proliferative effects of ATRA, HPR, and ST1926 were assessed *in vitro* by the MTT ([3-(4, 5-dimethylthiazol-2-yl)-2, 5-diphenyltetrazolium bromide]) assay. MCF-7 and MDA-MB-231 cells were seeded in 96-well plates at the density of 5,000 cells per well whereas MCF-10A and HMT-3522 S1 cells were seeded at the density of 10,000 cells per well: HMT-3522 S1 cells were treated when cell confluence

reached 60% whereas the other cell lines were treated when confluence reached 30-40%. Cells were treated in triplicates with 0.1% DMSO or various drug concentrations for 72 hours. For each time point, 10  $\mu$ l of 5 mg/ml (in 1x PBS) MTT reagent was added to each well and incubated at 37°C for 3-4 hours. Only metabolically active cells can reduce the yellow tetrazolium salt (MTT) into insoluble purple formazan crystals by mitochondrial succinate dehydrogenase. Crystals were then dissolved using 100  $\mu$ l of SDS-based stop solvent. Finally, after overnight incubation, the reduced MTT dye was assessed by measuring the optical density (OD) at 595 nm using an ELISA microplate reader. Cell growth results were expressed as percentage of control (0.1% DMSO) and were derived from triplicate wells, and represent the average of at least three independent experiments  $\pm$  standard error of the mean (SEM).

#### **F. Trypan Blue Exclusion Method**

MCF-7 and MDA-MB-231 cells were seeded in triplicate in 24-well plates at a density of 20,000 cells/well. Cells were incubated overnight and then treated the following day with 0.1% DMSO or various drug concentrations for 72 hours. The supernatant containing floating dead cells was removed, while viable cells were washed with 1X PBS, trypsinized, and collected in the supernatant. Cells were then diluted in trypan blue (1:1) ratio (vol/vol) and counted using a hemocytometer. Viable cells have intact membranes and, therefore, do not take up the impermeable dye while dead cells take up the dye and stain blue. Results were expressed as percentage of control (0.1% DMSO) and represent the average of at least three independent experiments ( $\pm$  SEM).

## **G. Cell Cycle Analysis**

Cell cycle analysis was performed using the propidium iodide (PI) assay. Control and treated cells were washed with 1X PBS, trypsinized, and collected by centrifugation at 1500 rpm for 5 minutes at 4°C. Cells were then fixed with ice-cold 80% ethanol and left at -20°C overnight. Subsequently, samples were first incubated with 50 units RNase A (Roche Diagnostics) for 1 hour, resuspended in 300 ml 1X PBS, and then stained with 50 µg/ml PI and incubated in the dark in flow tubes (BD Falcon). 10,000 cells were collected and analyzed using FACScan flow cytometer (Becton Dickinson) and cell cycle distribution was determined using CellQuest software (Becton Dickinson).

## **H. TUNEL Assay**

Apoptosis was assessed by terminal deoxynucleotidyl transferase-mediated deoxyuridine triphosphate nick endlabeling (TUNEL) assay (Roche Diagnostics) according to manufacturer's instructions. Briefly, control and treated cells were collected, washed with 1% BSA in 1X PBS and then fixed in 4% formaldehyde at room temperature for 30 minutes. Subsequently, cells were incubated in permeabilization solution (10 mg sodium citrate, 100 µL Triton X, in 10 ml 1X PBS) for 2 minutes on ice. Positive control cells were incubated with DNase for 30 minutes at room temperature, and then washed with 1X PBS. Samples were incubated with TUNEL Reagents (labeling solution and enzyme solution) for 1 hour at 37°C. Following incubation, cells were washed with 1X PBS, centrifuged (400 rpm, 5 minutes, 4°C) and then resuspended in 300 µl of 1X PBS. 10,000 cells were collected and analyzed using

FACScan flow cytometry (excitation wavelength set at 470-490 nm and the emission wavelength set at 505 nm).

## **I. Immunoblot Analysis**

Control and treated cells were collected as previously described. Supernatant was then removed and cells were washed once with 1X PBS, centrifuged (1500 rpm, 5 minutes, 4°C), and lysed with 2X Laemmli Lysis Buffer (Bio-Rad) at 95°C to extract total cell lysates. Proteins were then quantified using the NanoDrop-1000 (Thermo Scientific).

5%  $\beta$ -mercaptoethanol was then added to the lysates. Subsequently, proteins were separated by sodium dodecyl sulfate (SDS)-polyacrylamide gel electrophoresis (PAGE), and were then transferred onto nitrocellulose membranes. Membranes were blocked with 5% skimmed milk in TBS (50 mM Tris-HCL and 150 mM NaCl), and were incubated overnight with specific primary antibodies at 4°C. Secondary antibodies were added after mild washing for 2 hours at room temperature while shaking. Proteins were detected by enhanced chemiluminescence (ECL) using the ECL system (Santa Cruz Biotechnology) or by exposing the membranes to X-Ray films using the Xomat machine (Carestream®). The following antibodies were used: p53 (sc-126), p21 (sc-397), cyclin D<sub>1</sub> (sc-83796), c-myc (sc-40), RAR $\alpha$  (sc-551), RAR $\beta$  (sc-552), RAR $\gamma$  (sc-550), RXR $\alpha$  (sc-553), and GAPDH (sc-137) (Santa Cruz Biotechnology), and  $\beta$ -catenin (9562) and  $\gamma$ -H2AX (2577) (Cell Signaling).

## **J. Soft Agar Colony Formation Assay**

Anchorage-independent growth was studied using the CytoSelect™ 96-Well Cell Transformation Assay kit (Cell Biolabs). Briefly, MCF-7 and MDA-MB-231 cells were suspended in 0.4% soft agar at the density of 15,000 cells/well over 0.6% base agar layers. After 48 hours, colonies were treated with either vehicle alone or different doses of ST1926 or ATRA, and were incubated for  $8 \pm 1$  day at 37°C and 5% CO<sub>2</sub>, and replenished with control media or drugs every 2 days. Colonies were photographed using Zeiss axiovert light microscope and then quantified using the CyQuant GR Dye where the fluorescence was measured using a 96-well fluorometer set at a 485/520 nm filter.

## **K. Three-dimensional 'on-top' Assay**

MCF-7 and MDA-MB-231 cells were plated on the growth factor reduced Matrigel™ (60 µl/cm<sup>2</sup>, BD Biosciences) in 24-well tissue-culture plates at a density of  $25 \times 10^3$  cells/well in the presence of culture medium containing 5% Matrigel™ (BD Biosciences). The cells were maintained for 3 days for clusters to form before treatment with selected doses of drugs for 48 hours. Medium was discarded and Matrigel™ was digested using 0.5 ml of dispase solution 1 mg/ml (Invitrogen), dissolved in RPMI-1640 incomplete medium for 60 minutes at 37°C. Spheres were then collected, incubated in 1 ml warm Trypsin at 37°C for 3 minutes, and then passed through a 27 and 20-gauge syringes five times to allow the dissociation of spheres into single cells. Cells were then counted using the trypan blue exclusion method. Results were expressed as percentage of control (0.1% DMSO) and represent the average of at least three independent experiments ( $\pm$  SEM).

## **L. Sphere Formation Assay**

Sphere formation assays have been widely performed to identify cancer stem-like cells, also known as cancer-initiating cells based on their ability to assess self-renewal capability of cells *in vitro* (Pastrana 2011). We sought to determine the potential inhibitory effects of ATRA, ST1926, and ATRA/ST1926 treatments on the colony-forming ability of breast cancer cells. Briefly, 1,000 cells/well were suspended in cold Matrigel<sup>TM</sup>/serum free RPMI-1640 (1:1) in a total volume of 50  $\mu$ l in 24-well plates. Cells were seeded uniformly in a circular manner around the bottom rim of the well and allowed to solidify in the incubator at 37°C for 40 minutes. Subsequently, 0.5 ml of low serum media (2% FBS) media containing ST1926 or control DMSO were added gently in the middle of each well. Spheres were replenished with warm media as in the original seeding every other day. Spheres were counted after 10 to 13 days. The sphere-formation unit (SFU) was calculated for the first generation as follows:  $\text{SFU} = (\text{number of spheres formed} / \text{number of cells plated}) \times 100$ . Results were represented as a percentage of the SFU of the treated spheres compared to the untreated ones. Diameter of spheres was manually recorded using Zeiss axiovert light microscope and the percentage sphere diameter was expressed as percentage growth relative to 0.1% DMSO (control wells) and treated wells with the indicated concentrations.

## **M. Lumen Formation Assay**

We sought to determine whether ATRA, ST1926, or ATRA/ST1926 combination treatments induced lumen disruption of normal epithelial cells. The drip method of 3D cell culture was used to induce the formation of acini. Briefly, HMT-3522 S1 cells were seeded on Matrigel<sup>TM</sup> (60  $\mu$ l/cm<sup>2</sup>, BD Biosciences) at a density of 5

$\times 10^4$  cells/well in the presence of culture medium containing 5% Matrigel<sup>TM</sup> (Plachot 2004). Cells were treated with different concentrations of drugs in media without EGF on day 7. EGF is usually removed from the culture medium after day 7 to allow acinar completion and differentiation (usually observed on day 8 or 9; Plachot 2004; Lelièvre 2005). Cells were permeabilized on day 10 with 0.5% peroxide and carbonyl-free Triton X-100 (Sigma-Aldrich) in cytoskeleton buffer (100 mM NaCl, 300 mM sucrose, 10 mM PIPES, pH 6.8, 5 mM MgCl<sub>2</sub>, 1 mM pefabloc, 10 µg/ml aprotinin, 250 µM NaF) prior to fixation in 4% paraformaldehyde (Sigma-Aldrich). Nuclei were stained with Hoechst 33342 (Sigma-Aldrich) and specimens were mounted in ProLong® Gold antifade reagent (Invitrogen Molecular Probes). A minimum of one hundred acini was analyzed and scored using confocal laser scanning microscope (Zeiss LSM710) for correct lumen formation. Acinar sizes measurements were performed manually on day 10 by recording the diameter of each acinus with respect to the stage micrometer using Zeiss axiovert light microscope. One hundred acini were included in the scoring. The percentage acinar diameter was expressed as percentage growth relative to 0.1% DMSO (control wells) and treated wells with the indicated concentrations.

## **N. Image Processing**

Phase-contrast images of control and treated cells were acquired using Zeiss axiovert light microscope. Images of Hoescht labeling were recorded using confocal laser scanning microscope. Images were processed using *ImageJ* (<http://imagej.nih.gov/ij/>) and assembled using Microsoft Powerpoint 2010.



## **O. Synergy Studies and Statistical Analysis**

Cell growth experiments were conducted at least three times. Data were presented as mean  $\pm$  SEM. Synergy analysis was carried out using Compusyn software that automatically generates the combination index (CI) based on the CI-isobole method of Chou-Talalay (Chou 2010). The CI was used to assess synergistic effect ( $CI < 1$ ), additive effect ( $CI = 1$ ) or antagonistic effect ( $CI > 1$ ). Statistical comparisons were done using Microsoft Excel 2010. Paired t-test was used for comparison of two groups whereas one-way ANOVA was used for three or more groups of treatments. \*, \*\* and \*\*\* indicate p-values  $\leq 0.05$ ; 0.01 and 0.001, respectively; p-values less than 0.05 were considered significant.

## CHAPTER III

### RESULTS

#### **A. ST1926 induces growth arrest in ATRA-resistant human breast cancer cells at pharmacologically achievable concentrations**

We used two well-characterized human breast cancer cell lines, MCF-7 and MDA-MB-231, to test the effects of the natural retinoid ATRA and the synthetic retinoids, HPR and ST1926, on cell growth and viability. While suprapharmacological concentrations of ATRA (10  $\mu$ M) had minimal effects on the cell growth reaching 20% growth inhibition by 72 hours in both cell lines (Figure 7), sub-micromolar ( $\mu$ M) concentrations of ST1926 displayed a time-dependent growth inhibition (Figure 8). Similar growth inhibitory effects were reported in both cell lines where a threshold at 0.5  $\mu$ M ST1926 resulted in approximate 40% and 70% growth inhibition after day 1 and day 3 of treatment, respectively. Additionally, suprapharmacological concentrations of ST1926 (3 and 10  $\mu$ M) displayed similar growth-inhibitory effects to sub- $\mu$ M concentrations (data not shown). The minimum inhibitory concentration ( $IC_{50}$ ) is approximately 0.5  $\mu$ M ST1926 at two days post-treatment in both cell lines (Figure 8). Interestingly, ST1926-induced growth inhibition was independent of *p53* status as shown by its growth suppressive effect on MDA-MB-231 cells that bear a missense *p53* mutation, resulting in a non-functional p53 protein (Olivier 2002).

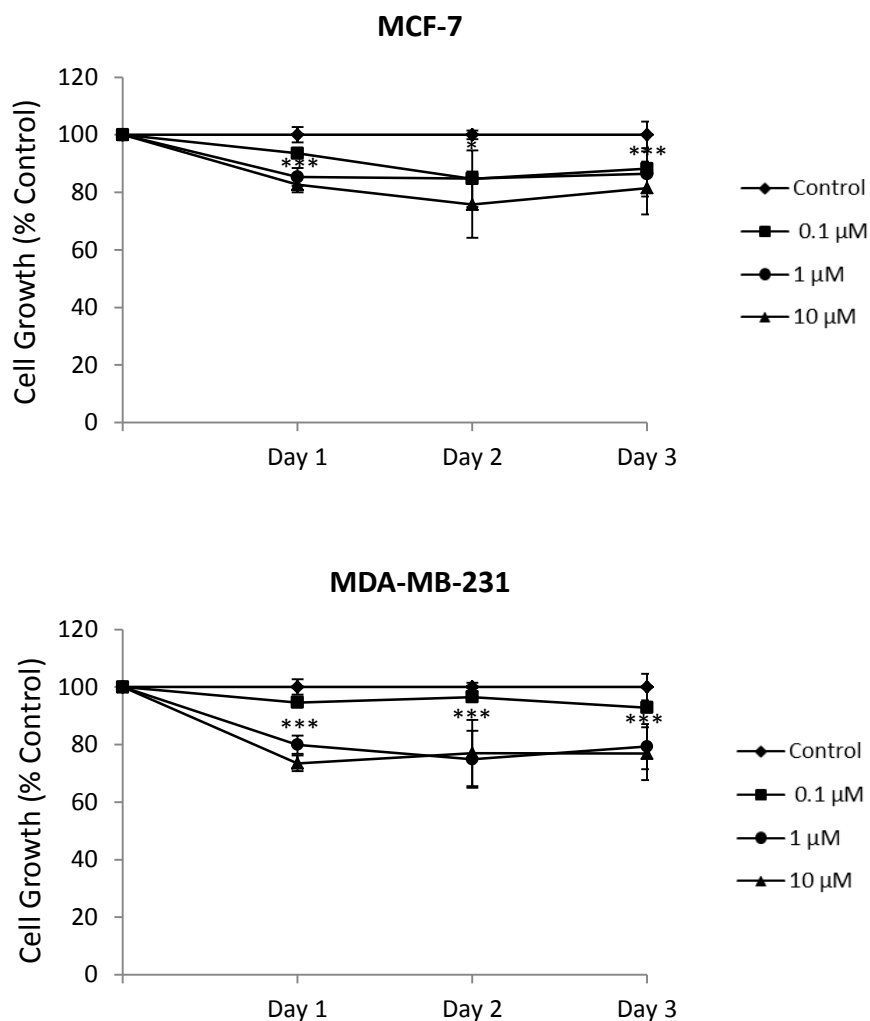


**Figure 7. Human breast cancer cells are relatively resistant to ATRA.** MCF-7 cells and MDA-MB-231 cells were seeded in 96-well plates at a density of  $0.5 \times 10^5$  cells/ml and treated with 0.1% DMSO or the indicated concentrations of ATRA up to 3 days. Cell growth was assayed in triplicate wells using the MTT cell proliferation assay. Cell growth results are expressed as percentage of control (0.1% DMSO) and represent the average of at least three independent experiments ( $\pm$  SEM). Significance from control is indicated by \* at  $P < 0.05$  and \*\*\* at  $P < 0.001$ .

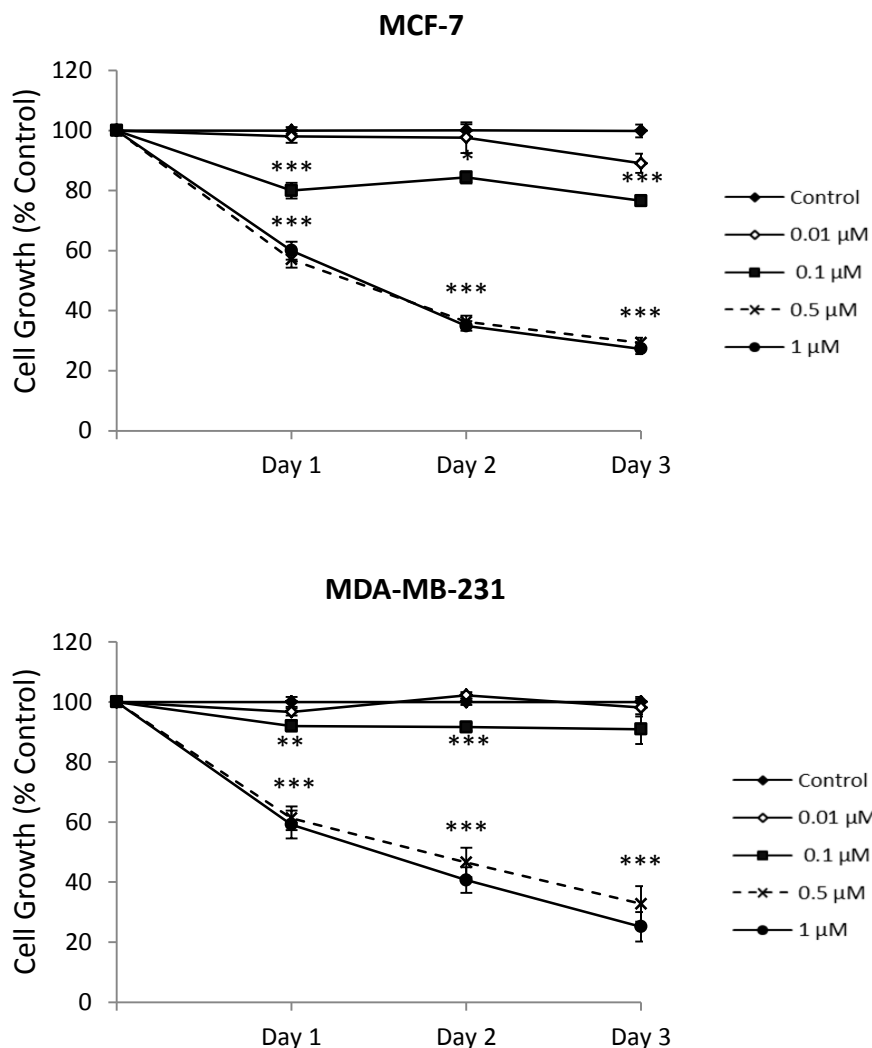


**Figure 8. ST1926 at sub- $\mu$ M concentrations inhibit the proliferation of ATRA-resistant human breast cancer cells.** MCF-7 cells and MDA-MB-231 cells were seeded in 96-well plates at a density of  $0.5 \times 10^5$  cells/ml and treated with 0.1% DMSO or the indicated concentrations of ST1926. Cell growth was assayed in triplicate wells using the MTT cell proliferation assay. Cell growth results are expressed as percentage of control (0.1% DMSO) and represent the average of at least three independent experiments ( $\pm$  SEM). Significance from control is indicated by \* at  $P < 0.05$ ; \*\*  $P < 0.01$ ; \*\*\* at  $P < 0.001$ .

## **B. ST1926 reduces the viability of human breast cancer cells and induces pronounced morphological changes**

We also tested the effect of ST1926 on the viability of MCF-7 and MDA-MB-231 cells using trypan blue exclusion assay. Similar to MTT results, we have shown that ST1926 significantly altered the viability of both tested cell lines at pharmacologically achievable sub- $\mu$ M concentrations (Figure 9), which was even observed at 0.1  $\mu$ M ST1926 concentrations.

The results obtained from the MTT and trypan blue exclusion assays were compatible with confluence changes where ST1926-treated cells showed growth suppression when compared to control cells and displayed drastic morphological changes, as evident in the shrinkage of MCF-7 cells (Figure 10A), and the swelling of MDA-MB-231 cells (Figure 10B).

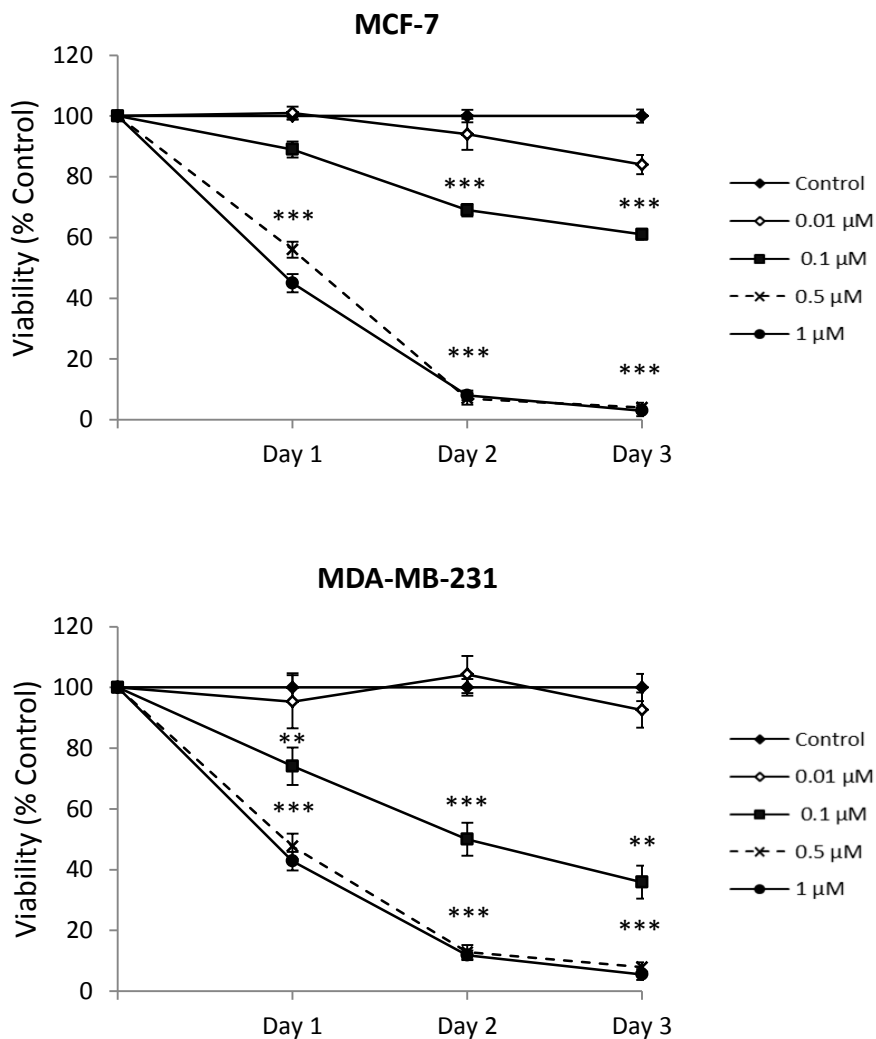


**Figure 9. Low sub- $\mu$ M concentrations of ST1926 potently reduce the viability of human breast cancer cells.** MCF-7 cells and MDA-MB-231 cells were seeded in 24-well plates at a density of  $2 \times 10^4$  cells/well and treated with 0.1% DMSO or the indicated concentrations of ST1926. Cells were counted in triplicate measurements using the trypan blue exclusion method and viability results are expressed as percentage of control (0.1% DMSO). Data represent the average of three independent experiments ( $\pm$  SEM). Significance from control is indicated by \*\*  $P < 0.01$ ; \*\*\* at  $P < 0.001$ .

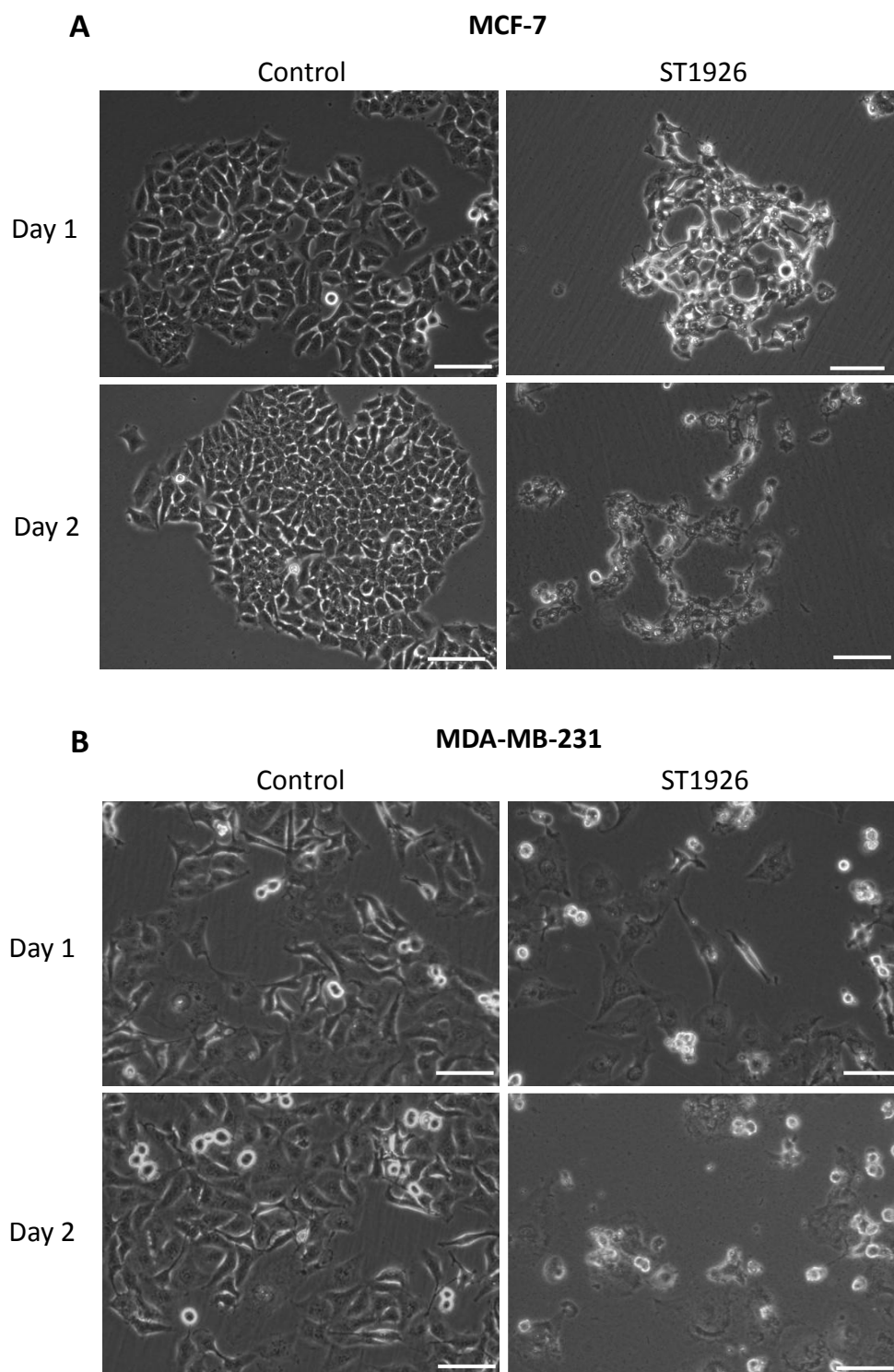


**Figure 10. Low sub- $\mu$ M concentrations of ST1926 alter the morphology of human breast cancer cells.** MCF-7 cells (A) and MDA-MB-231 cells (B) were treated with 0.1% DMSO or 0.5  $\mu$ M ST1926 for 48 hours and representative phase contrast images were acquired using Zeiss axiovert light microscope (x10). Scale bar represents 100  $\mu$ m.

### C. The synthetic retinoid HPR does not affect the MCF-7 breast cancer cells

We then compared the growth-suppressive effects of ST1926 to 4-hydroxy(phenyl)retinamide (HPR, fenretinide), another synthetic retinoid (Sporn 1976). Unlike ST1926, 1  $\mu$ M HPR did not have any effect on the proliferation of MCF-7 cells (Figure 11), highlighting breast cancer cell sensitivity to ST1926 only.

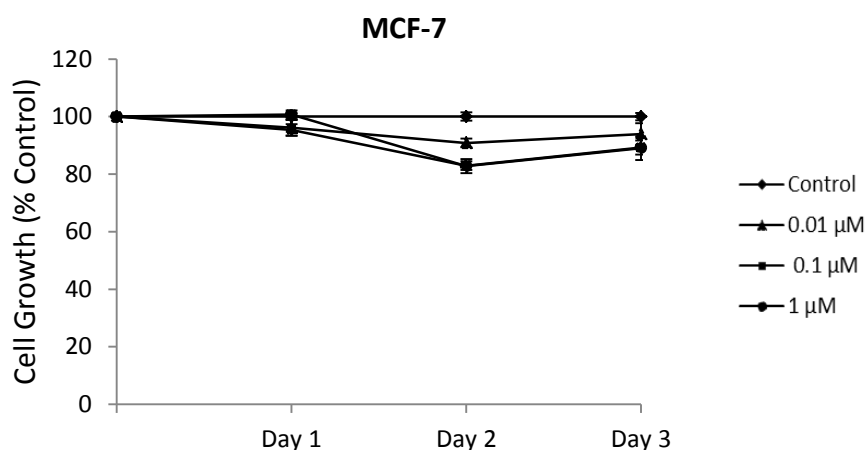
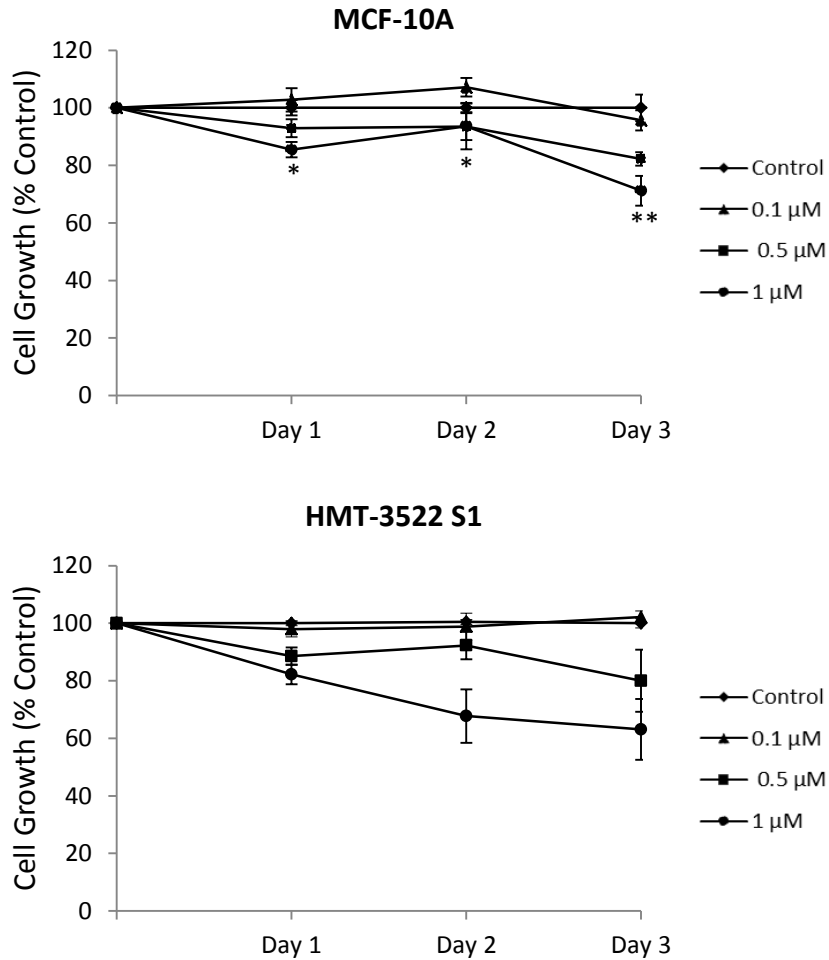


**Figure 11. MCF-7 cells are resistant to HPR.** MCF-7 cells were seeded in 96-well plates at a density of  $0.5 \times 10^5$  cells/ml and treated with 0.1% DMSO or the indicated concentrations of HPR up to 3 days. Cell growth was assayed in triplicate wells using the MTT cell proliferation assay. Cell growth results are expressed as percentage of control (0.1% DMSO) and represent the average of at least three independent experiments ( $\pm$  SEM).

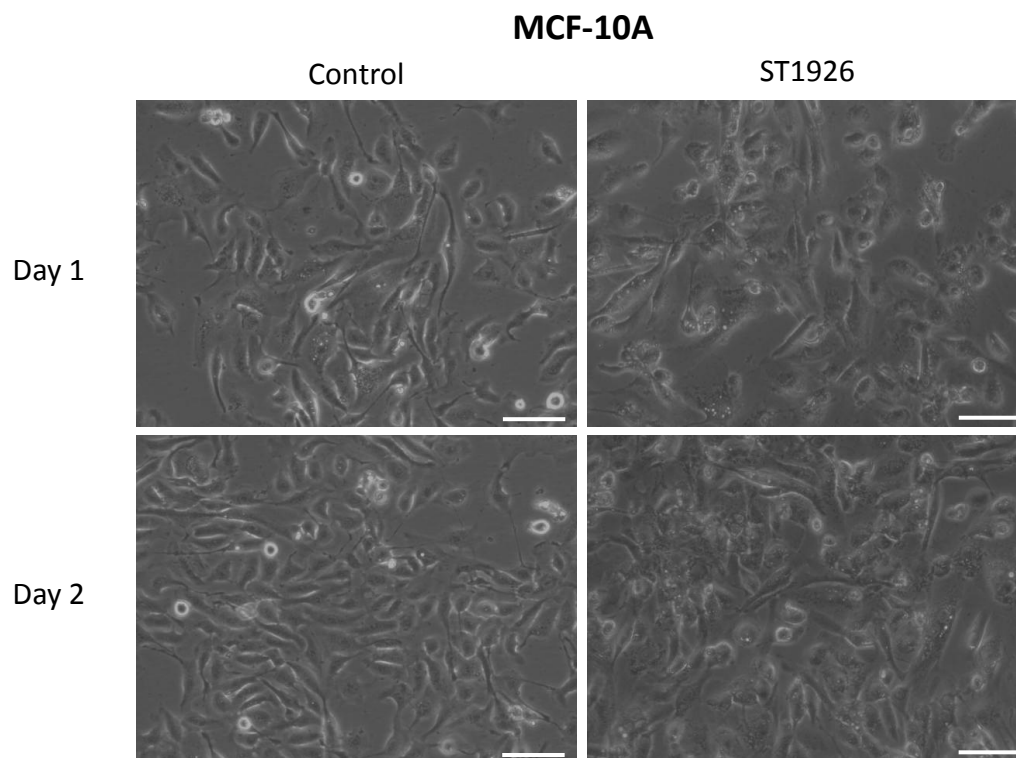


#### **D. ST1926 spares ‘normal-like’ human breast epithelial cells**

We next intended to determine the effect of ST1926 on the two ‘normal-like’ human breast epithelial cell lines, MCF-10A and HMT-3522 S1. Importantly, 0.5  $\mu$ M ST1926 had minimal effects on the growth of both cell lines and resulted in less than 20% growth inhibition 3 days post-treatment (Figure 12). ST1926-treated MCF-10A cells had an outgrowth that was comparable to control cells up to 2 days of treatment at 0.5  $\mu$ M ST1926 (Figure 13). In summary, 0.5  $\mu$ M ST1926 concentrations will be used in all subsequent experiments as they are pharmacologically achievable (Sala 2009; Bassma 2016) and affect breast cancer cells while sparing their normal counterparts.



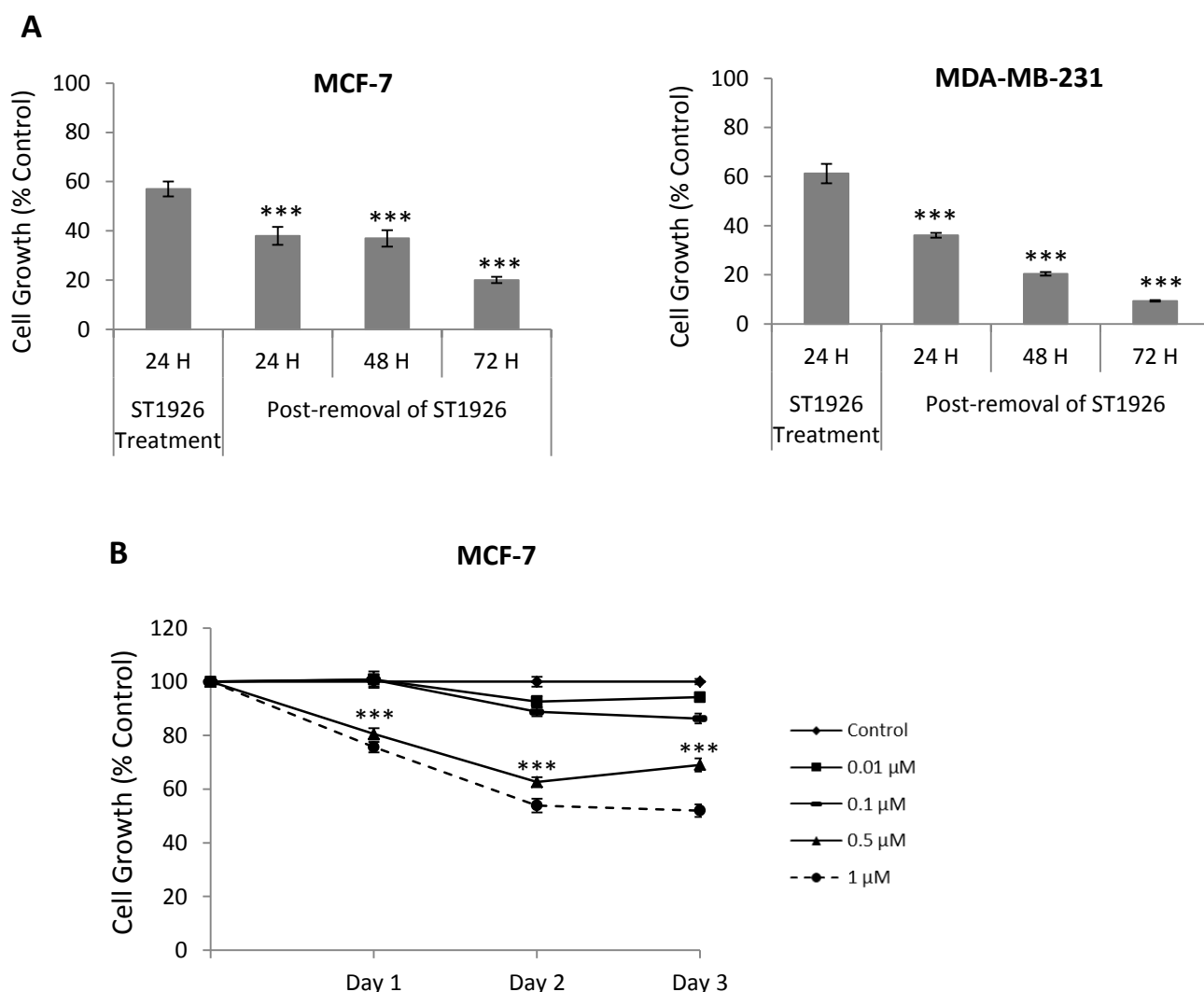
**Figure 12. ST1926 has minimal effects on the growth of ‘normal-like’ breast epithelial cells.** MCF-10A cells and HMT-3522 S1 cells were seeded in 96-well plates at a density of  $1 \times 10^5$  cells/ml and treated with 0.1% DMSO or the indicated concentrations of ST1926 up to 3 days. Cell growth was assessed in triplicate wells using the MTT cell proliferation assay. Cell growth results are expressed as percentage of control (0.1% DMSO) and represent the average of at least three independent experiments ( $\pm$  SEM). Significance from control is indicated by \* at  $P < 0.05$ ; \*\*  $P < 0.01$ .



**Figure 13. ST1926 has minimal effects on the morphology of ‘normal-like’ breast epithelial cells.** MCF-10A cells were treated with 0.1% DMSO or 0.5  $\mu$ M ST1926 up to 48 hours and representative phase contrast images were acquired using Zeiss axiovert light microscope (x10). Scale bar represents 100  $\mu$ m.

#### **E. ST1926-induced growth inhibition persists after drug removal**

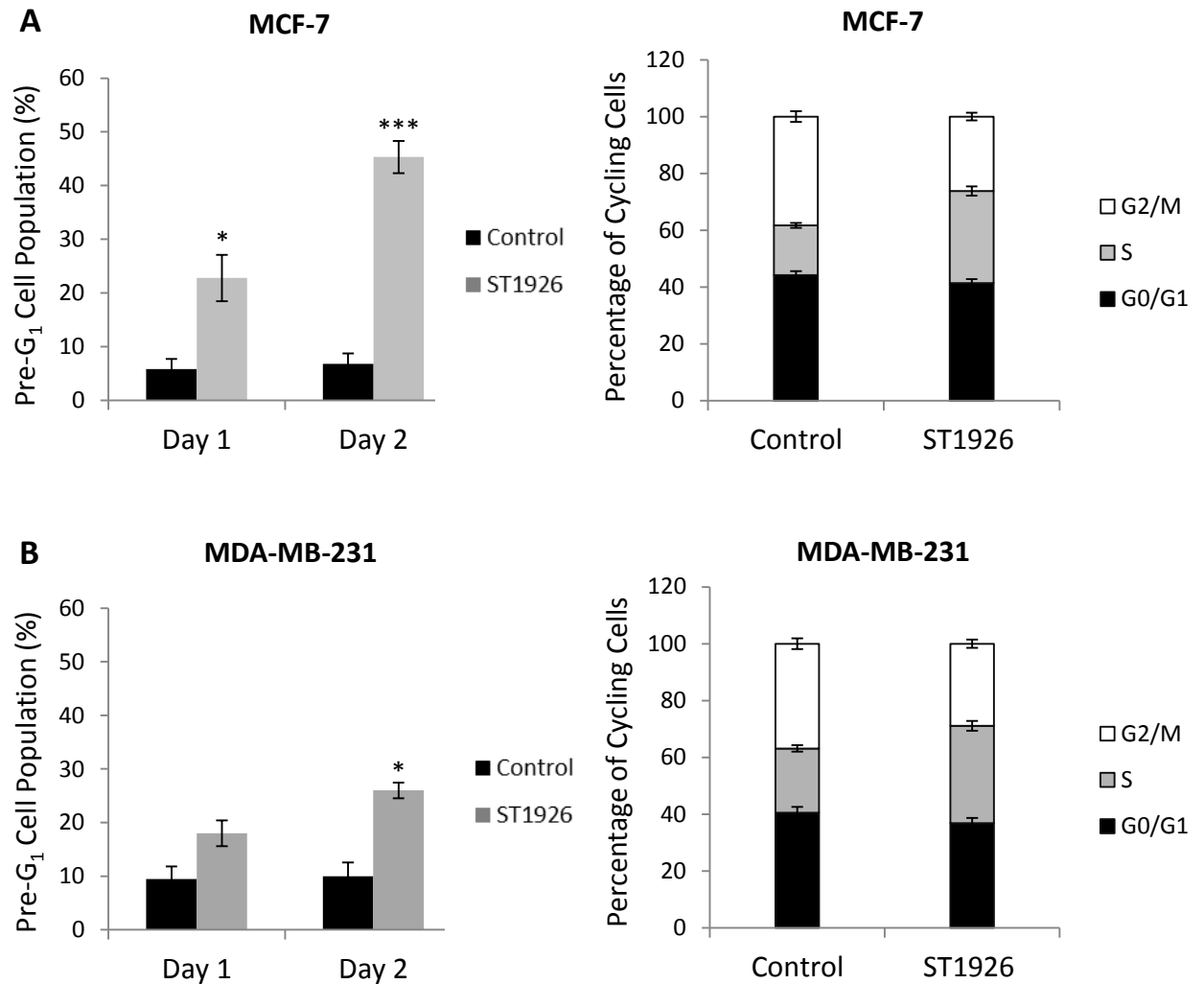
Previous studies have shown that ST1926-induced growth inhibition persists even after drug removal in chronic myeloid leukemia (CML) (Nasr 2015), and acute myeloid leukemia (AML) (El-Houjeiri MS AUB 2015). To assess whether ST1926-induced growth inhibition was prolonged in our *in vitro* breast cancer model, MCF-7 and MDA-MB-231 cells were pre-treated with 0.5  $\mu$ M ST1926 for 24 hours, then drug was removed, and cells were grown up to 3 days in drug-free media. ST1926-induced growth inhibition in 24 hours treated breast cancer cells persisted even after 72 hours of drug removal (Figure 14A). Because of ST1926's poor bioavailability due to a drastic reduction of  $\mu$ M plasma concentration to below sub- $\mu$ M levels by 2 hours in humans (Sala 2009) and mice (Bassma 2016), we were interested in examining the effect of exposing MCF-7 cells to pharmacologically achievable ST1926 concentrations for just one hour. Interestingly, treatment of MCF-7 cells with 0.5  $\mu$ M ST1926 and 1  $\mu$ M ST1926 resulted in 30% and 50% growth inhibition 72 hours post-drug removal, respectively (Figure 14B), further demonstrating the rapid induction and persistent mode of growth suppression by ST1926.



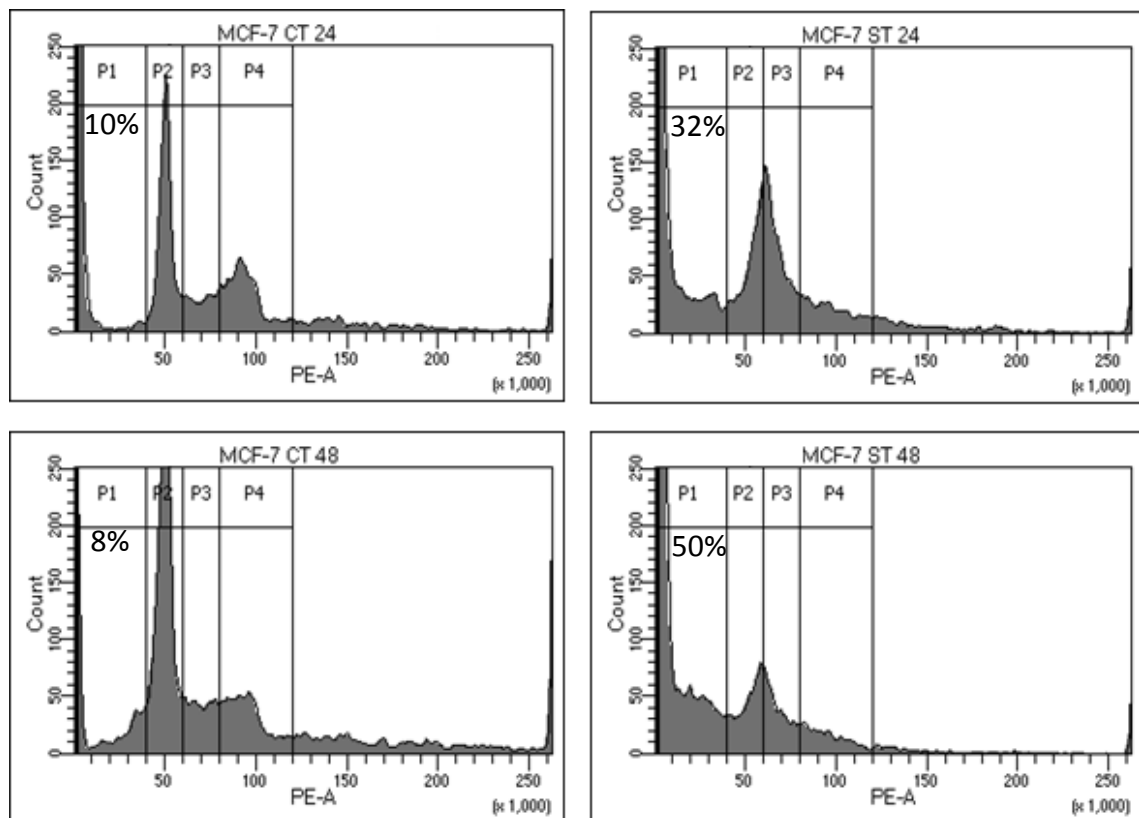
**Figure 14. ST1926-induced growth inhibition of breast cancer cells persists after drug removal.** MCF-7 and MDA-MB-231 cells (A) were seeded in 96-well plates at a density of  $0.5 \times 10^5$  cells/ml and treated with 0.1 % DMSO or 0.5  $\mu$ M ST1926. 24 hours post-treatment, ST1926 was removed, and cells were grown in drug-free media up to 72 hours. MCF-7 cells (B) were seeded in 96-well plates at a density of  $0.5 \times 10^5$  cells/ml and treated with 0.1 % DMSO or the indicated concentrations of ST1926 for one hour then drug was removed and cells were grown in drug-free media up to 72 hours. 1 hour post-treatment, drug-containing media was removed, and the cells were washed with 1X PBS and resuspended in fresh media up to 72 hours. Cell growth was assayed in triplicate wells using the MTT cell proliferation assay. Cell growth results are expressed as percentage of control (0.1% DMSO) and represent the average of at least three independent experiments ( $\pm$  SEM). Significance from control is indicated by \*\*\* at  $P < 0.001$ .

#### **F. ST1926 induced Pre-G<sub>1</sub> accumulation and S-phase arrest in human breast cancer cells**

To investigate the mechanisms involved in ST1926-induced growth inhibition in breast cancer cells, cell cycle analysis was conducted using flow cytometric analysis of DNA content distribution stained with propidium iodide (PI). Treatments of MCF-7 cells with 0.5  $\mu$ M ST1926 resulted in an increase in the pre-G<sub>1</sub> phase from 23% to 45%, 24 and 48 hours post-treatment, respectively (Figure 15A). Similarly, the percentage of cells in the pre-G<sub>1</sub> phase in ST1926-treated MDA-MB-231 cells increased from 18% to 26% 24 and 48 hours post-treatment, respectively (Figure 15B). Pre- G<sub>1</sub> accumulation presumably indicates apoptosis. Furthermore, ST1926 treatment for 24 hours induced an increase in S-phase cells from 18% to 32% in MCF-7 cells, and from 23% to 34% in MDA-MB-231 cells (Figure 15A and 15B). Representative histograms of the cell cycle distribution of ST1926-treated MCF-7 cells and MDA-MB-231 cells compared to their respective controls are shown in figure 16 and 17, respectively. These results indicate that ST1926 treatment of breast cancer cells causes an S-phase cell cycle arrest and an increase in the presumably pro-apoptotic region of the cell cycle (pre-G<sub>1</sub> region).

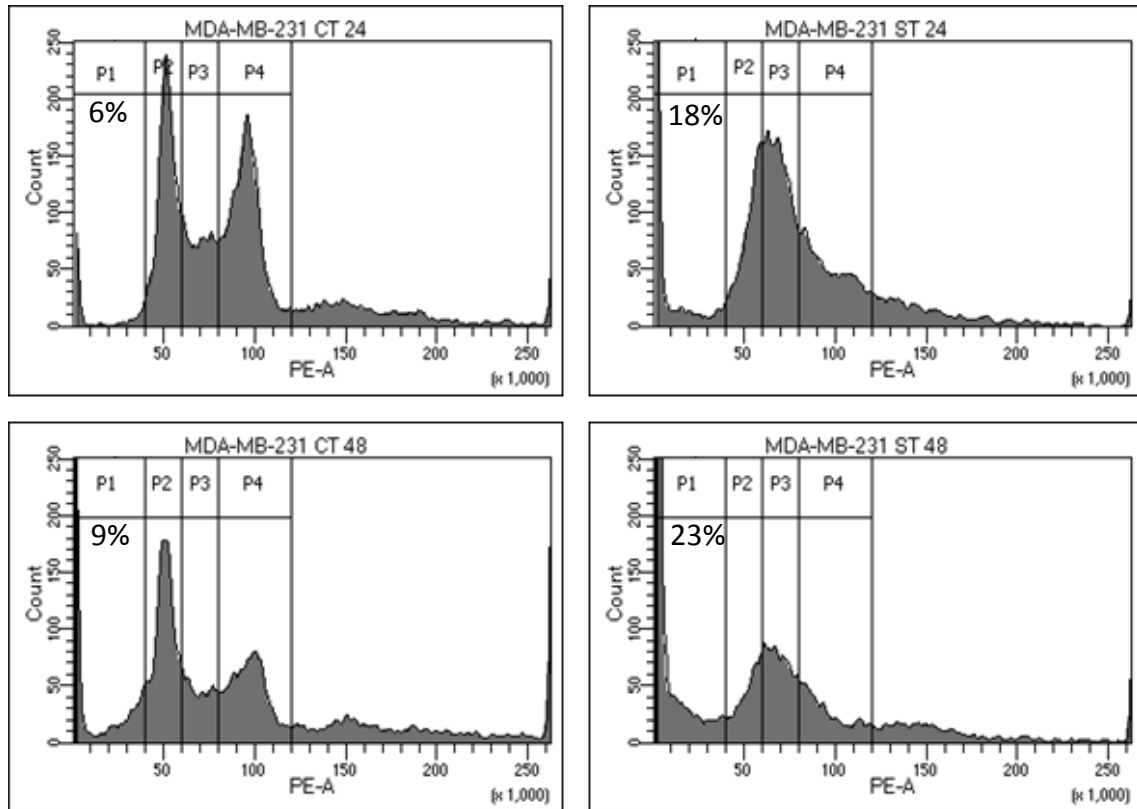


**Figure 15. ST1926 treatment induces an accumulation of breast cancer cells in the pre-G<sub>1</sub> region and induces an S-phase arrest.** MCF-7 and MDA-MB-231 cells were seeded in 100 mm culture plates at a density of  $5 \times 10^5$  cells/plate and treated with 0.1 % DMSO or 0.5  $\mu$ M ST1926. Cell cycle was assessed using propidium iodide-based flow cytometric analysis of DNA content. Cell cycle analysis of MCF-7 cells (A) and MDA-MB-231 cells (B) is represented. Data represent the average of at least three independent experiments ( $\pm$  SEM). Significance from control is indicated by \* at  $P < 0.05$ ; \*\*\*  $P < 0.001$ .



**Figure 16. Representative histograms of the cell cycle distribution and progression in ST1926-treated MCF-7 cells.** MCF-7 cells were seeded in 100 mm culture plates at a density of  $5 \times 10^5$  cells/plate and treated with 0.1 % DMSO (CT) or 0.5  $\mu$ M ST1926 (ST). Cell cycle was assessed using propidium iodide-based flow cytometric analysis of DNA content. P1, P2, P3, and P4 represent the Pre-G<sub>1</sub>, G<sub>0</sub>/G<sub>1</sub>, S, and G<sub>2</sub>/M phases of the cell cycle. Values represent the percentage of cells in the Pre-G<sub>1</sub> region. The shown histograms are representative of three independent experiments.

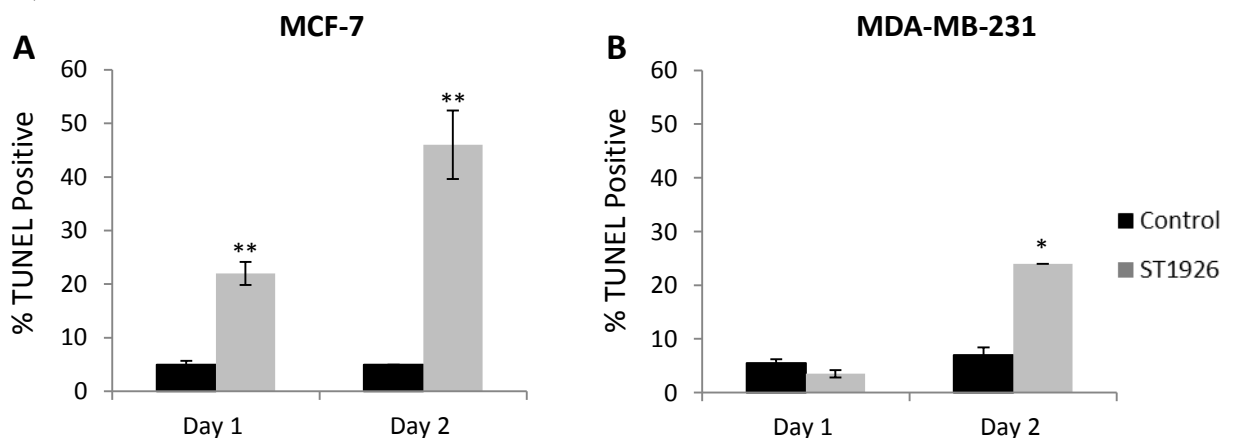




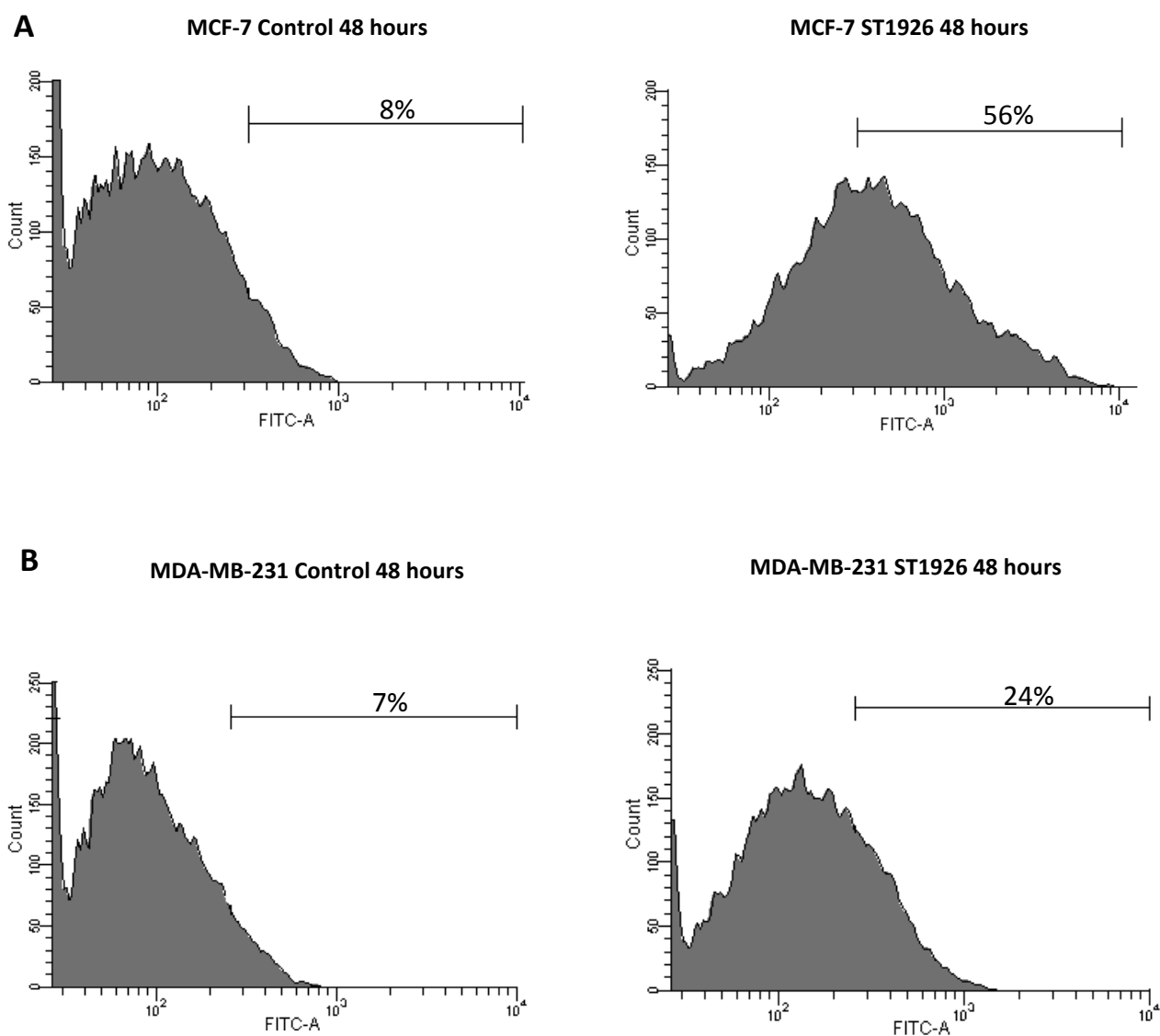
**Figure 17. Representative histograms of the cell cycle distribution and progression in ST1926-treated MDA-MB-231 cells.** MDA-MB-231 cells were seeded in 100 mm culture plates at a density of  $5 \times 10^5$  cells/plate and treated with 0.1 % DMSO (CT) or 0.5  $\mu$ M ST1926 (ST). Cell cycle was assessed using propidium iodide-based flow cytometric analysis of DNA content. P1, P2, P3, and P4 represent the Pre-G<sub>1</sub>, G<sub>0</sub>/G<sub>1</sub>, S, and G<sub>2</sub>/M phases of the cell cycle. Values represent the percentage of cells in the Pre-G<sub>1</sub> region. The shown histograms are representative of three independent experiments.

### G. ST1926 induces apoptosis in human breast cancer cells

We have previously shown that ST1926 resulted in the accumulation of breast cancer cells in the pre-G<sub>1</sub> region which presumably represents apoptotic cells. To confirm apoptosis, TUNEL assay was conducted to assess DNA single and double strand breaks, which is one of the hallmarks of late apoptosis (Darzynkiewicz 2011). Treatments of MCF-7 cells with 0.5  $\mu$ M ST1926 resulted in a substantial increase in the percentage of TUNEL-positive cells from 5% in control to 22% in treated cells by 24 hours of treatment, and from 5% in control to 46% by 48 hours of treatment indicating massive DNA fragmentation, and thus confirming apoptosis induction (Figure 17A). In MDA-MB-231 cells, TUNEL positivity was only detected 48 hours post-treatment. The percentage of TUNEL-positive cells increased from 7% in control to 24% in ST1926-treated cells (Figure 17B), indicating a p53-independent apoptosis in MDA-MB-231 cells. Representative histograms showing DNA fragmentation analysis by TUNEL assay of treated breast cancer cells at 48 hours post-ST1926 treatment (Figure 18A and 18B).



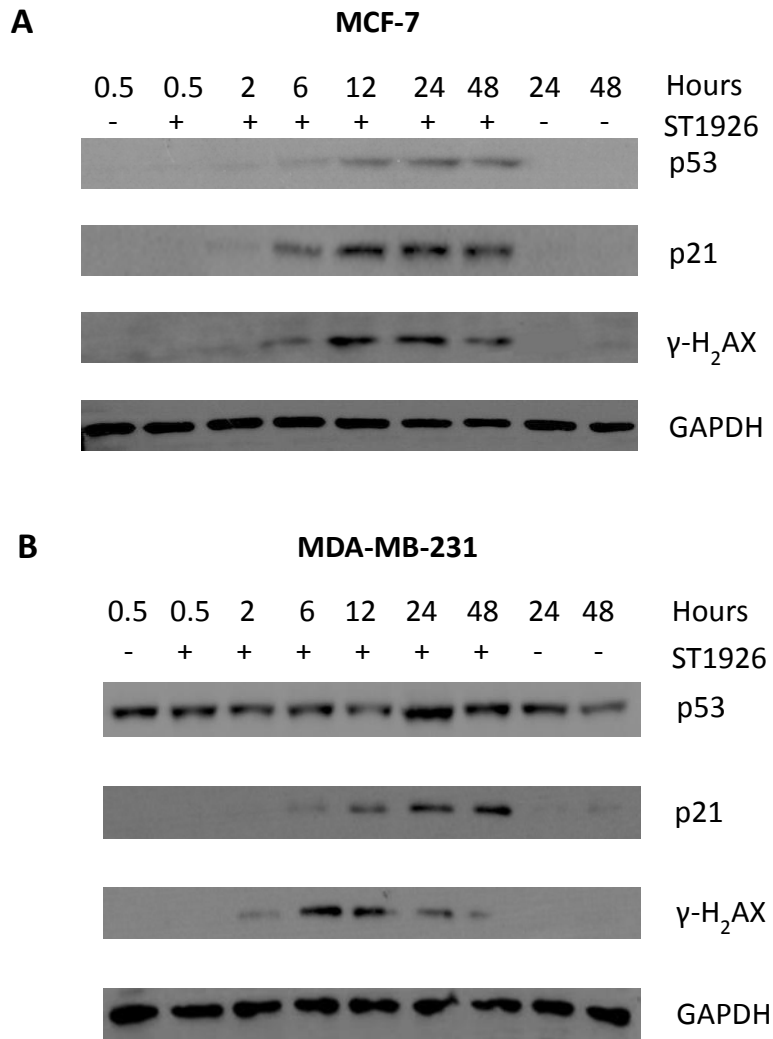
**Figure 17. ST1926 induces apoptosis in breast cancer cells by TUNEL assay.** MCF-7 cells (A) and MDA-MB-231 cells (B) were seeded in 100 mm culture plates at a density of  $5 \times 10^5$  cells/plate and treated with 0.1 % DMSO or 0.5  $\mu$ M ST1926 up to 48 hours. DNA fragmentation was detected by TUNEL assay. Graphs represent the average of two independent experiments  $\pm$  standard deviation (SD). Significance from control is indicated by \* at  $P < 0.05$ ; \*\*  $P < 0.01$ .



**Figure 18. Representative histograms showing TUNEL positivity in ST1926-treated breast cancer cells.** MCF-7 cells (A) and MDA-MB-231 cells (B) were seeded in 100 mm culture plates at a density of  $5 \times 10^5$  cells/plate and treated with 0.1 % DMSO or 0.5  $\mu$ M ST1926 up to 48 hours. DNA fragmentation was detected by TUNEL assay. The histograms are representative of two independent experiments. The percentage of TUNEL-positive cells is indicated.

## **H. ST1926 causes early DNA damage and increases p53 and p21 protein levels**

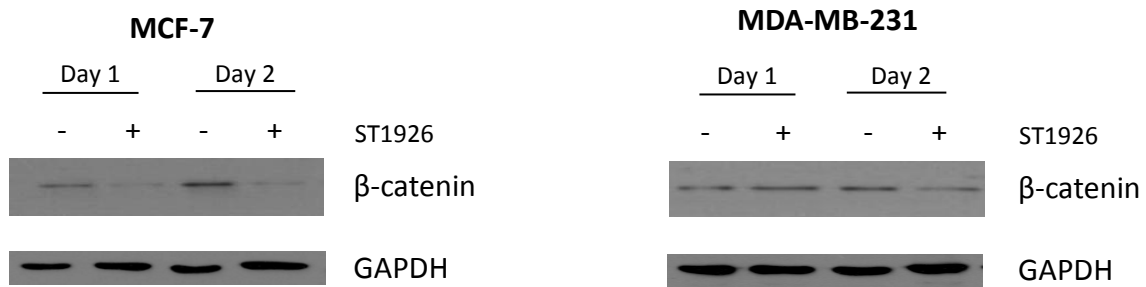
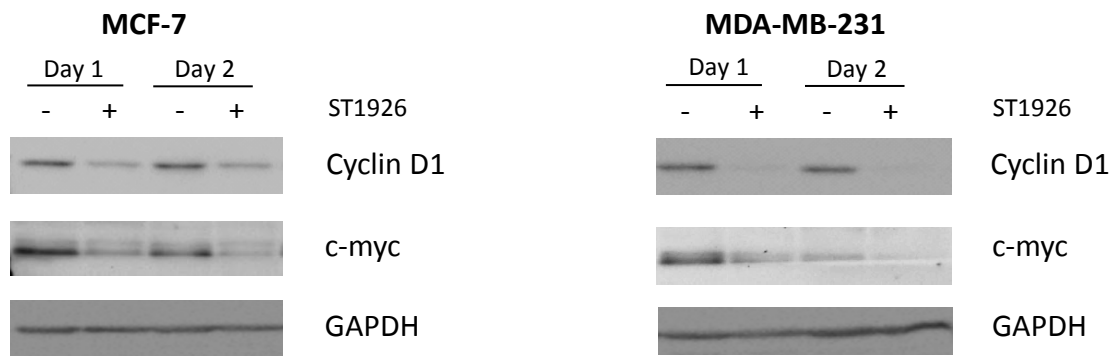
Previous studies have shown that ST1926 induces early DNA damage in various types of tumor cells (Valli 2008; El Hajj 2014; Nasr 2015; Bassma 2016). Upon DNA damage, DNA double strand breaks are generated, followed by a rapid phosphorylation of the histone H2AX to  $\gamma$ -H2AX (Turinetto 2015). Furthermore, recent studies have indicated that ST1926-induced resistance resulted in delayed and lower DNA damage, highlighting the critical role of DNA damage response (DDR) pathways in ST1926-mediated cell death (Di Francesco 2015). To assess the involvement of DDR in MCF-7 and MDA-MB-231 cells upon ST1926 treatment, protein expression levels of  $\gamma$ H<sub>2</sub>AX, p53 and its downstream target p21, were monitored by western blot analysis at 0.5, 2, 6, 12, 24, and 48 hours post-ST1926 treatment at 0.5  $\mu$ M. Interestingly, ST1926 induced an upregulation of  $\gamma$ -H2AX as early as 2 hours, which persisted up to 48 hours in both breast cancer cell lines, indicating an early induction of DDR (Figure 19A and 19B). Similar increases were observed for total p53 and p21 protein levels in both tested breast cancer cells, despite the fact that MDA-MB-231 cells bear mutant *p53* (Figure 19B) (Olivier 2002). This suggests a p53-independent DDR activation and p21 upregulation in ST1926-treated MDA-MB-231 cells.



**Figure 19. ST1926 causes early DNA damage in human breast cancer cells.** MCF-7 cells (A) and MDA-MB-231 cells (B) were seeded in 100 mm culture plates at a density of  $5 \times 10^5$  cells/plate and treated with 0.1 % DMSO or 0.5  $\mu$ M ST1926 up to 48 hours. Whole SDS lysates (50  $\mu$ g/lane) were prepared and immunoblotted against p53, p21, and  $\gamma$ -H<sub>2</sub>AX antibodies. Blots were re-probed with GAPDH antibody to ensure equal protein loading. Similar trends were observed in three independent experiments.

## **I. ST1926 downregulates the Wnt/ $\beta$ -catenin signaling pathway**

Accumulating evidence highlighted the critical role of the Wnt/ $\beta$ -catenin signaling pathway in tumorigenesis, particularly in breast tumors where mammary stem cells with increased activation of Wnt/ $\beta$ -catenin signaling pathway displayed a greater tumorigenic potential compared to their normal counterparts with low signaling activation (Jang 2015). Furthermore, this latter pathway was shown to be a substantial player in the functioning of breast cancer stem cells (CSCs) (Jang 2015). Therefore, we tested for the effects of ST1926 treatment on the protein levels of  $\beta$ -catenin, and its downstream targets, cyclin D1 and c-myc in breast cancer cells. Western blot analysis showed a major downregulation of  $\beta$ -catenin protein levels at 24 hours in MCF-7 treated cells and at 48 hours in MDA-MB-231 treated cells (Figure 20A). Moreover, a prominent downregulation of cyclin D1 and c-myc protein levels was observed as early as 24 hours in ST1926-treated MCF-7 and MDA-MB-231 cells (Figure 20B).

**A****B**

**Figure 20. ST1926 downregulates the Wnt/β-catenin signaling pathway in human breast cancer cells.** MCF-7 cells and MDA-MB-231 cells were seeded in 100 mm culture plates at a density of  $5 \times 10^5$  cells/plate and treated with 0.1 % DMSO or 0.5 μM ST1926 up to 48 hours. Whole SDS lysates (80 μg/lane) were prepared and immunoblotted against β-catenin (A), Cyclin D1 and c-myc (B) antibodies. All blots were re-probed with GAPDH antibody to ensure equal protein loading. Similar trends were observed in two independent experiments.

## J. ST1926 modulates retinoid receptors expression

Although ATRA has been shown to mediate its effect through the retinoid receptors, however, the effect of ST1926 on the retinoid receptors has not been deciphered yet. Knowing that ST1926 is a synthetic derivative of CD437, a RAR $\gamma$  agonist, we sought to study ST1926 effects on the different retinoid receptors protein expression levels, namely RAR $\beta$ , RAR $\gamma$ , and RXR $\alpha$ . In both tested breast cancer cell lines, ST1926 induced a substantial increase in RAR $\beta$  protein levels that was very evident at 24 hours, while a decrease in RAR $\gamma$  and RXR $\alpha$  was observed at 24 and 48 hours post-treatment (Figure 21).

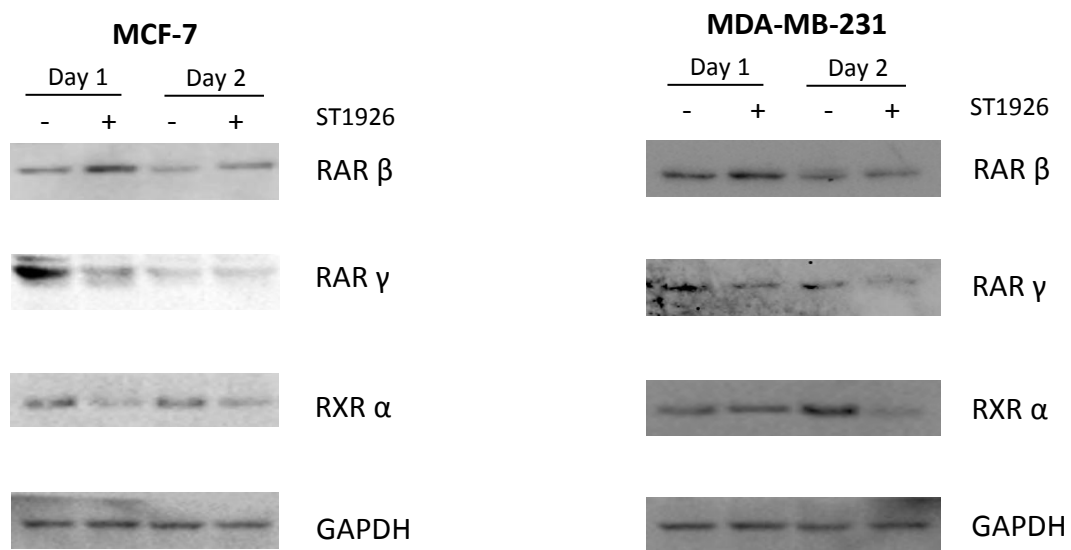


**Figure 21. ST1926 upregulates RAR $\beta$  and downregulates RAR $\gamma$  and RXR $\alpha$  protein levels.** MCF-7 cells and MDA-MB-231 cells were seeded in 100 mm culture plates at a density of  $5 \times 10^5$  cells/plate and treated with 0.1 % DMSO or 0.5  $\mu$ M ST1926 up to 48 hours. Whole SDS lysates (100  $\mu$ g/lane) were prepared and immunoblotted against RAR $\beta$ , RAR $\gamma$ , and RXR $\alpha$ . All blots were re-probed with GAPDH antibody to ensure equal protein loading. Similar trends were observed in two independent experiments.



#### **K. ST1926-growth inhibitory effect is independent of the retinoid receptor signaling pathway**

Since synthetic retinoids can work through retinoid receptor-dependent and -independent pathways, we next assessed whether ST1926-induced growth suppression involved the retinoid receptor signaling pathway by treating MCF-7 cells with the pan-RAR inverse agonist, BMS493. Blocking RARs with BMS493 inhibits the signaling transduction of the retinoid receptor pathway since RXRs can no longer bind to RARs and induce the transcription of target genes. MCF-7 cells were pre-treated with 1  $\mu$ M BMS493 for 20 minutes, then 0.5  $\mu$ M ST1926 was added up to 72 hours. ST1926-induced growth inhibition in MCF-7 cells was not altered in the presence of BMS493 (Figure 22A), indicating a retinoid-receptor independent pathway mode of growth inhibition. To confirm whether BMS493 is actually working, we used C8166 cell line as our positive control. It was previously established that C8166 are the only ATL cells sensitive to ATRA, and that ATRA sensitivity was mediated by retinoid receptor pathway. ATRA at 3  $\mu$ M concentrations induced 65% growth inhibition in C8166 cells after 72 hours of treatment. Interestingly, ATRA-induced growth inhibition was reduced from 65% to 25% of control values in the presence of BMS493 (Figure 22B). These results confirm that ST1926 works through retinoid receptor-independent pathway in MCF-7 breast cancer cells.

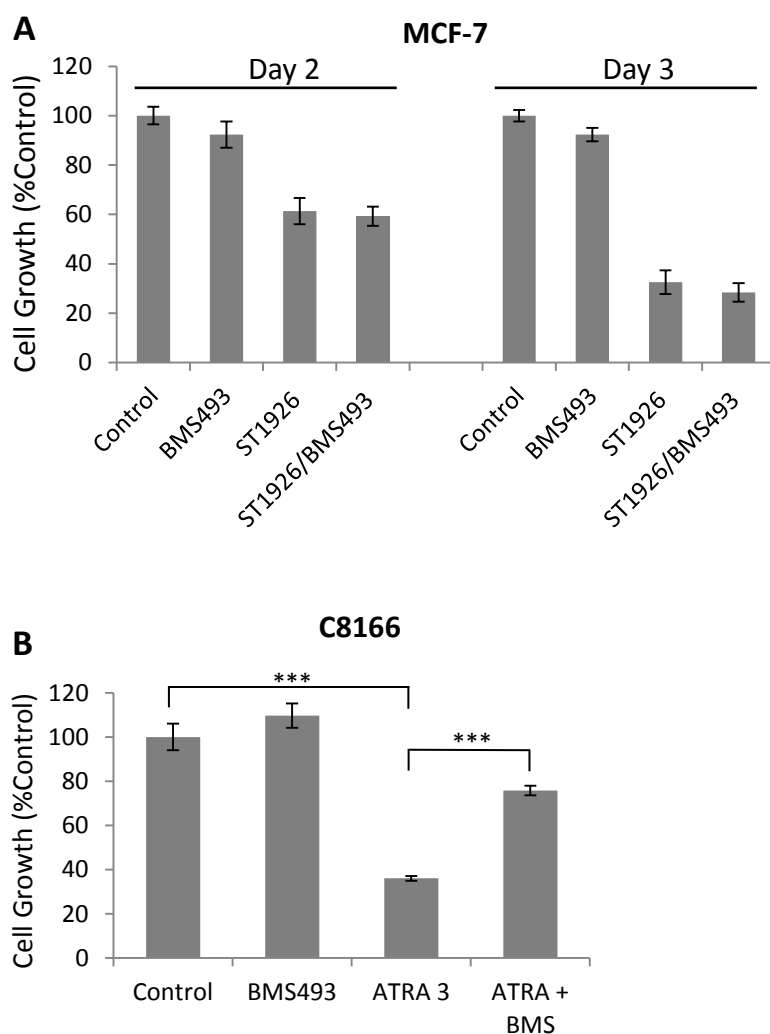


**Figure 22. ST1926-induced growth inhibition is independent of the retinoid receptor signaling pathway.** MCF-7 cells (A) were seeded in 96-well plates at a density of  $0.5 \times 10^5$  cells/ml and treated with 0.1% DMSO or 0.5  $\mu$ M ST1926 or treated with 1  $\mu$ M BMS493 or pretreated with 1  $\mu$ M BMS493 for 20 minutes then treated with 0.5  $\mu$ M ST1926 for 72 hours. Cell growth was assessed in triplicate wells using the MTT cell proliferation assay. Cell growth results are expressed as percentage of control (0.1% DMSO) and represent the average of three independent experiments ( $\pm$  SE). C8166 cells (B) were seeded in 96-well plates at a density of  $2 \times 10^5$  cells/ml and treated with 0.1% DMSO, 1  $\mu$ M BMS493, 3  $\mu$ M ATRA, or pretreated with 1  $\mu$ M BMS493 then treated with 3  $\mu$ M ATRA up to 72 hours. Cell growth was assayed in triplicate wells using the MTT cell proliferation assay. Cell growth results are expressed as percentage of control (0.1% DMSO) and represent the average of two independent experiments ( $\pm$  SEM). Significance from control is indicated by \*\*\* at  $P < 0.001$ .

## **L. Combination treatments of ATRA and ST1926 synergistically inhibit the proliferation of breast cancer cells**

ST1926-induced upregulation of RAR $\beta$ , a substantial determinant of ATRA sensitivity (Connolly 2013), led us to investigate the effects of combination treatments with ATRA and ST1926 on the cell growth of MCF-7 and MDA-MB-231 cells. Our tested breast cancer cells are relatively resistant to ATRA where 1  $\mu$ M concentrations only reduce cell growth by less than 20% after 3 days of treatment. Interestingly, combination treatments of ATRA at 0.5  $\mu$ M with ST1926 concentrations as low as 0.05  $\mu$ M ST1926 significantly inhibited the proliferation of MCF-7 cells by 50% after 3 days of treatment (Figure 23A). Higher concentrations of ST1926 at 0.1 or 0.2  $\mu$ M, in combination with ATRA at 0.5  $\mu$ M or 1  $\mu$ M displayed stronger growth inhibitory activities on MCF-7 cells (Figure 23B and 23C). It is worth noting that combination treatments of 0.1  $\mu$ M ST1926 with 0.5  $\mu$ M ATRA resulted in similar growth inhibitory effects as with 1  $\mu$ M ATRA, both leading to an approximate 80% growth inhibition after 3 days of treatment (Figure 23B). The enhanced growth inhibitory effects of ATRA/ST1926 combination treatments were also evident on cell confluence and morphological changes (Figure 24). Synergy studies were analyzed using different concentrations of ATRA and ST1926. Computerized combination index (CI) analysis indicated synergy (CI < 1) in all tested concentrations. Importantly, 0.5  $\mu$ M ATRA and 0.1  $\mu$ M ST1926 exhibited a moderate synergy (CI=0.41) at 24 and 48 hours, and a strong synergy (CI = 0.17) at 72 hours (Figure 25). Such synergy was observed, but to a lesser extent, in MDA-MB-231 cells where combination treatments of 0.5 or 1  $\mu$ M ATRA with 0.3  $\mu$ M ST1926 synergistically decreased cell viability by 65% *versus* 40% with ST1926 at day 1, and by 85% *versus* 65% at day 2, with ST1926 or ATRA/ST1926, respectively (Figure 26B). Combination of 0.2  $\mu$ M ST1926

concentration with 0.5 or 1  $\mu$ M ATRA had small synergistic effects on the viability of MDA-MB-231 cells, which were observed at all time points (Figure 26A).

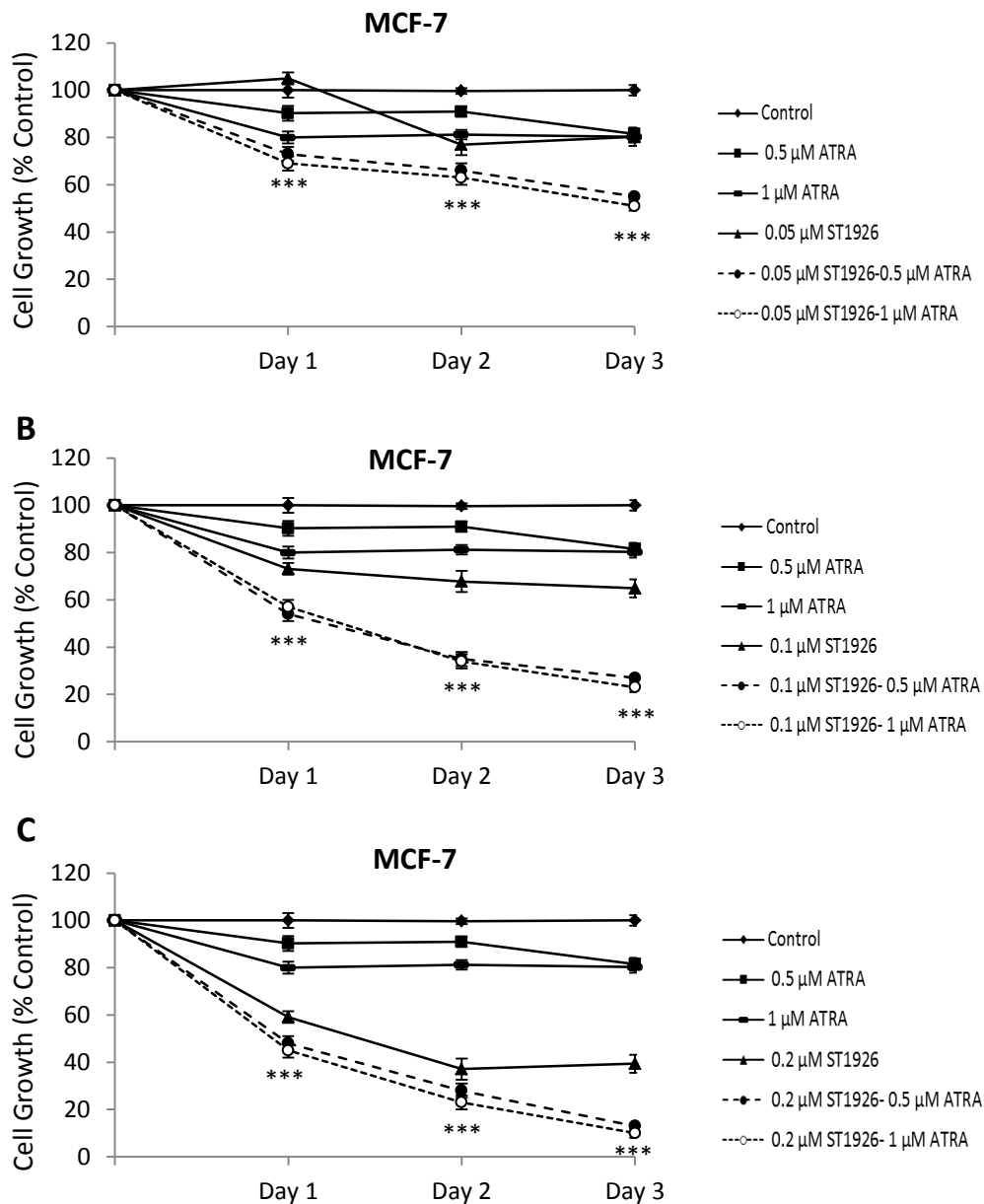


**Figure 23. Combination treatments of ATRA and ST1926 at low concentrations inhibit the proliferation of MCF-7 cells.** MCF-7 cells were seeded in 96-well plates at a density of  $0.5 \times 10^5$  cells/ml and treated with 0.1% DMSO or the indicated concentrations of ATRA and/or ST1926. Cell growth was assayed in triplicate wells using the MTT cell proliferation assay. Cell growth results are expressed as percentage of control (0.1% DMSO) and represent the average of three independent experiments ( $\pm$  SEM). Significance from control is indicated by \*\*\*  $P < 0.001$ .

# MCF-7

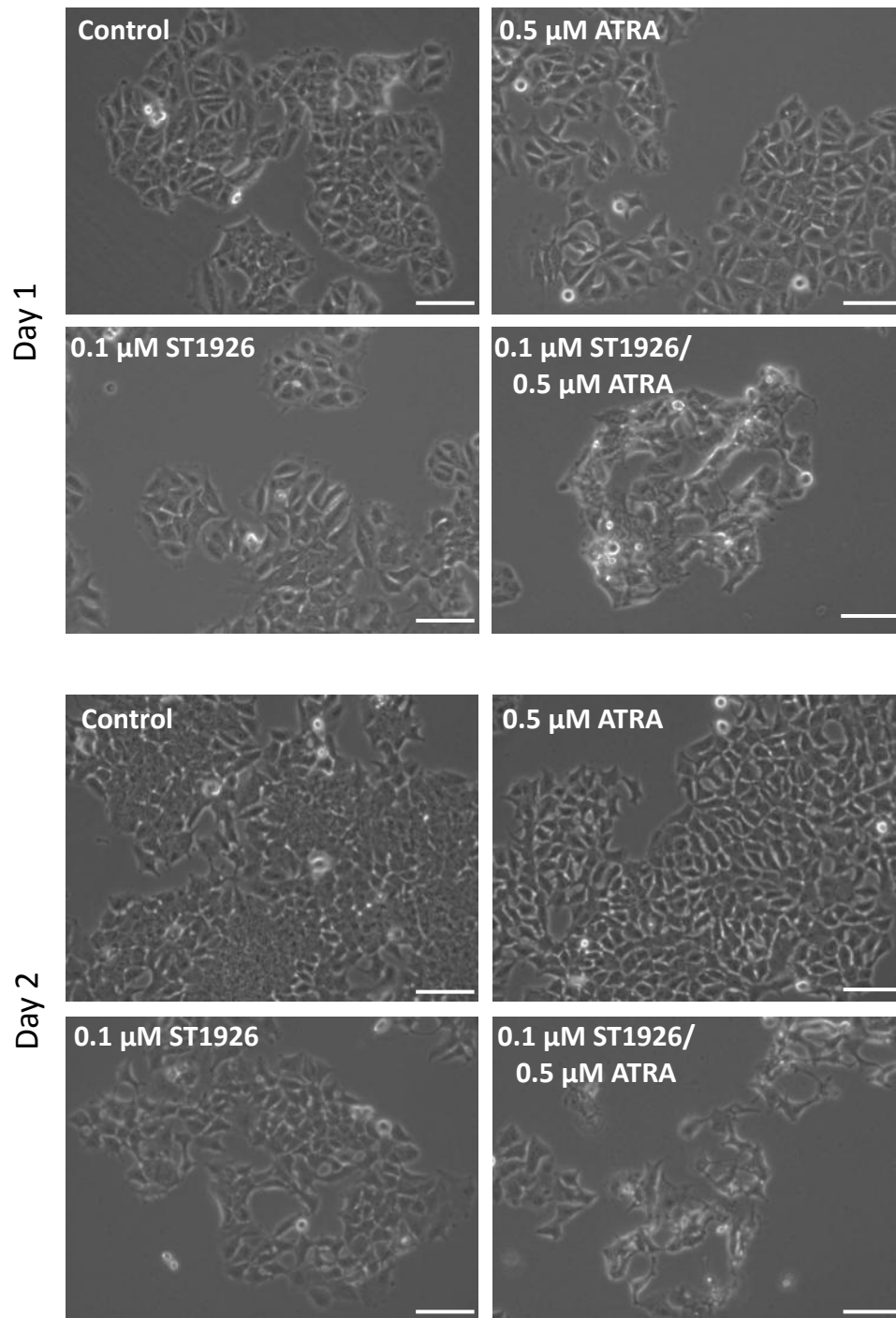


**Figure 24. Combination treatments of ATRA and ST1926 at low concentrations potentially alter the morphology of MCF-7 cells.** MCF-7 cells were seeded in 100 mm plates at a density of  $5 \times 10^5$  cells/plate and treated with 0.1% DMSO or the indicated concentrations of ATRA and/or ST1926. Representative phase contrast images were acquired using Zeiss axiovert light microscope (x10). Scale bar represents 100  $\mu\text{m}$ .

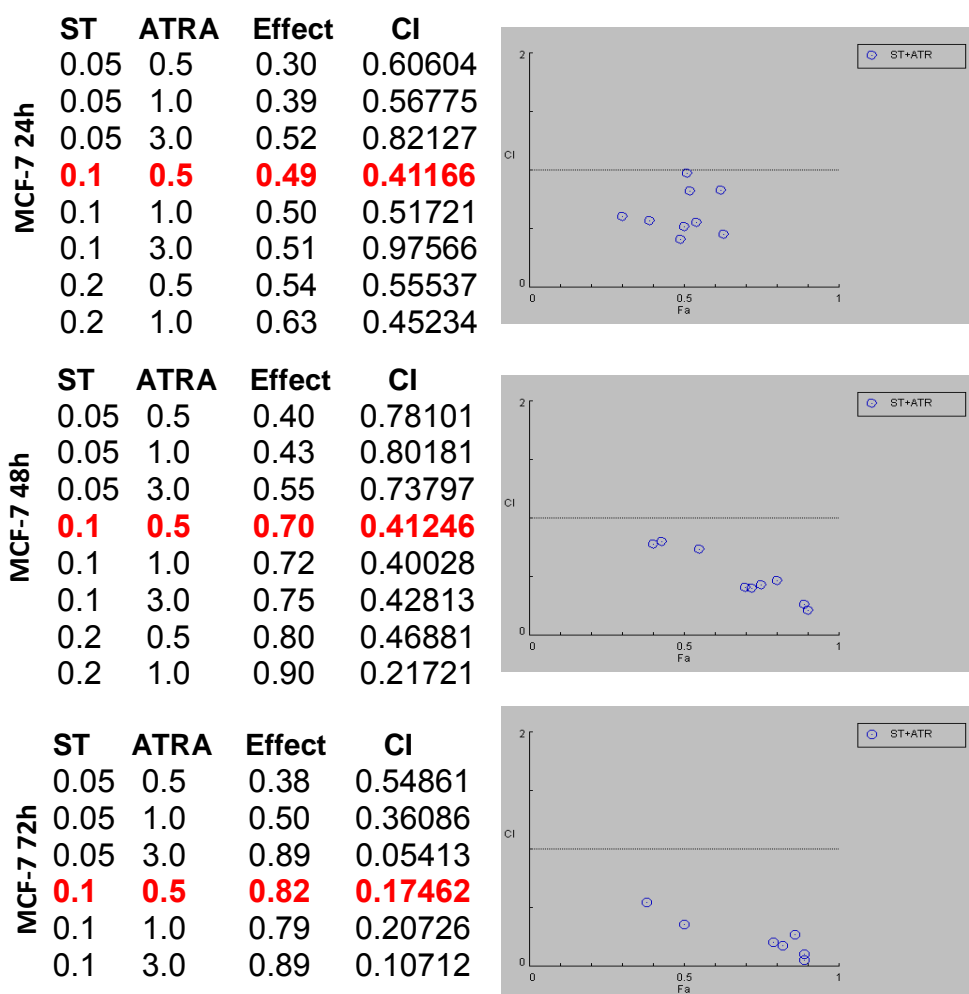


**Figure 25. Synergy studies showing Combination Index for combination treatments of ATRA and ST1926 (ST).** The combination index (CI) (B) was generated automatically using CompuSyn software based on the CI-isobol method of Chou–Talalay. The CI was used to assess synergistic effect ( $CI < 1$ ), additive effect ( $CI = 1$ ) or antagonistic effect ( $CI > 1$ ). Synergy analysis was carried out using Compusyn software that automatically generates the combination index (CI) based on the CI-isobole method of Chou-Talalay.

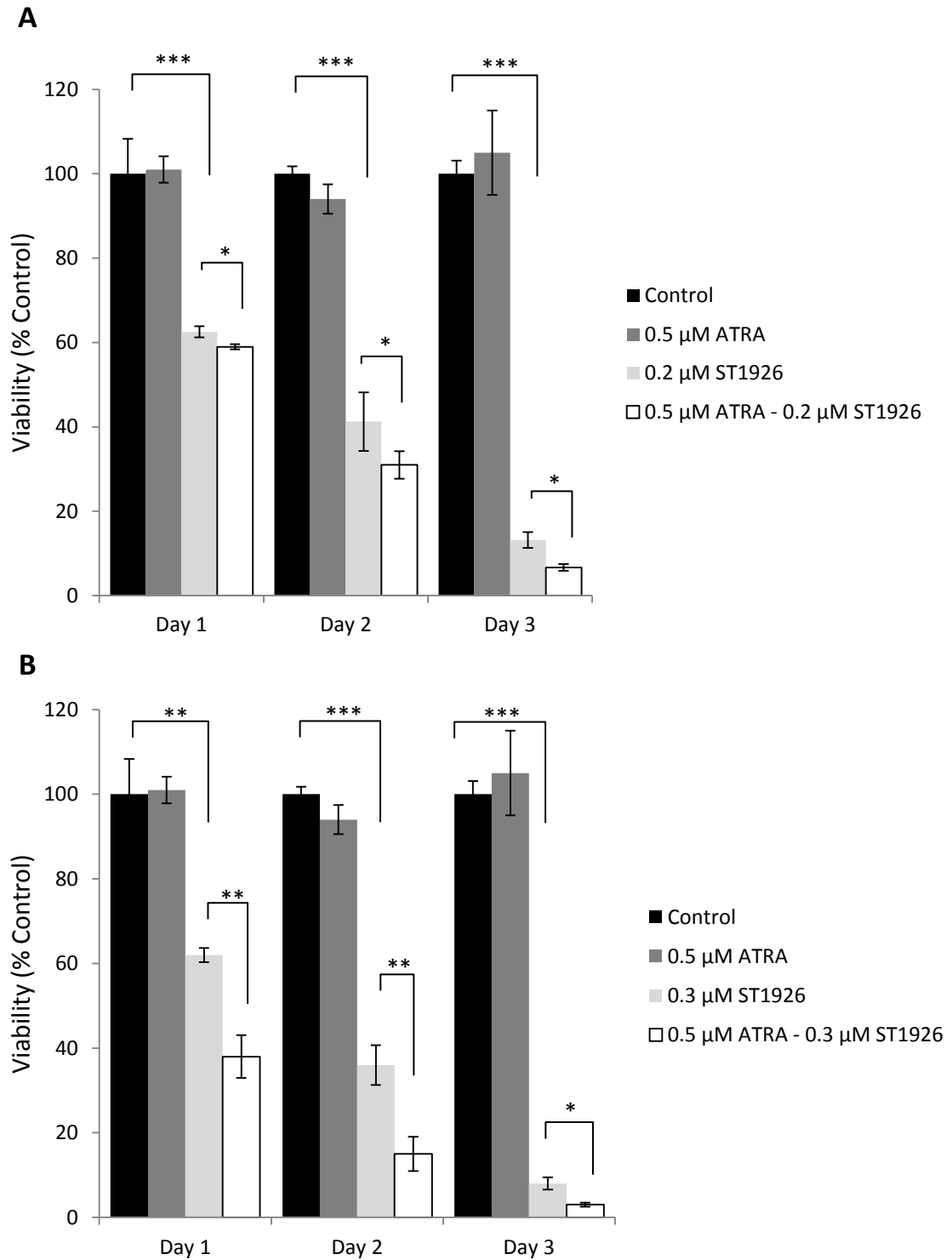


**Figure 26. Combination treatments of ATRA and ST1926 enhance viability reduction of MDA-MB-231 cells.** Cells were seeded in 24-well plates at a density of  $2 \times 10^4$  cells/well and treated with 0.5  $\mu$ M ATRA and indicated treatments with ST1926 (0.2  $\mu$ M) (A) or (0.3  $\mu$ M) (B) with or without 0.5  $\mu$ M ATRA (B). Cells were counted in triplicate measurements using the trypan blue exclusion method and viability results are expressed as percentage of control (0.1% DMSO). Data represent the average of three independent experiments ( $\pm$  SEM). (\*,  $P < 0.05$ ; \*\*,  $P < 0.01$ ; \*\*\*,  $P < 0.001$ ).

### **M. Combination treatments of ATRA and ST1926 spare the ‘normal-like’ breast epithelial cells**

Combination treatments of ATRA at 0.5  $\mu$ M with ST1926 at 0.1  $\mu$ M did not have any effect on the growth of MCF-10A cells (Figure 27A), while it resulted in approximate 20% growth inhibition in HMT-3522 S1 cells 72 hours after treatment (Figure 27B). Because a synergy was observed at higher concentrations in MDA-MB-231 cells, we next assessed whether combination treatments of ST1926 at 0.5  $\mu$ M with ATRA at 0.5  $\mu$ M had an effect on the growth of MCF-10A and HMT-3522 S1 cells. Combination treatments at these latter concentrations resulted in approximate 20% growth inhibition in MCF-10A cells 72 hours after treatment (Figure 28A), while a more pronounced effect was observed in treated HMT-3522 S1 cells where 30% and 40% growth inhibition was noted 48 and 72 hours after treatments respectively (Figure 28B). In summary, to investigate the mechanism of action of combination treatments on breast cancer cells, we chose concentrations of ATRA at 0.5  $\mu$ M and ST1926 at 0.1  $\mu$ M, as these concentrations were highly effective to suppress growth of cancer cells while spare their normal counterparts. Importantly, these sub- $\mu$ M concentrations of retinoids are pharmacologically achievable in plasma of patients for prolonged periods.



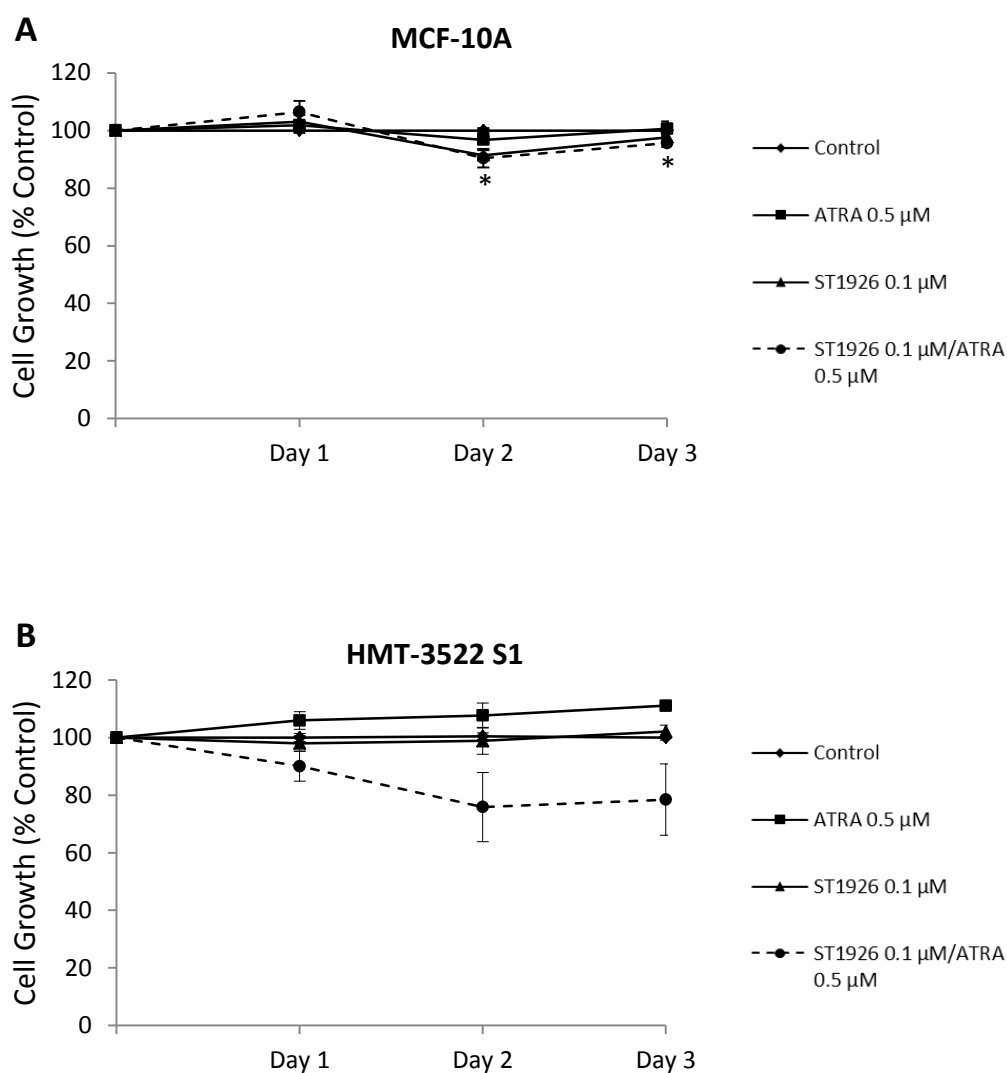


**Figure 27. Combination treatments of ATRA with low ST1926 concentrations have minimal effects on the proliferation of ‘normal-like’ breast epithelial cells.** MCF-10A cells (A) and HMT-3522 S1 cells (B) were seeded in 96-well plates at a density of  $1 \times 10^5$  cells/ml and treated with 0.1% DMSO or the indicated concentrations of ATRA and/or ST1926. Cell growth was assayed in triplicate wells using the MTT cell proliferation assay. Cell growth results are expressed as percentage of control (0.1% DMSO) and represent the average of at least three independent experiments ( $\pm$  SEM). Significance from control is indicated by \*  $P < 0.05$ .

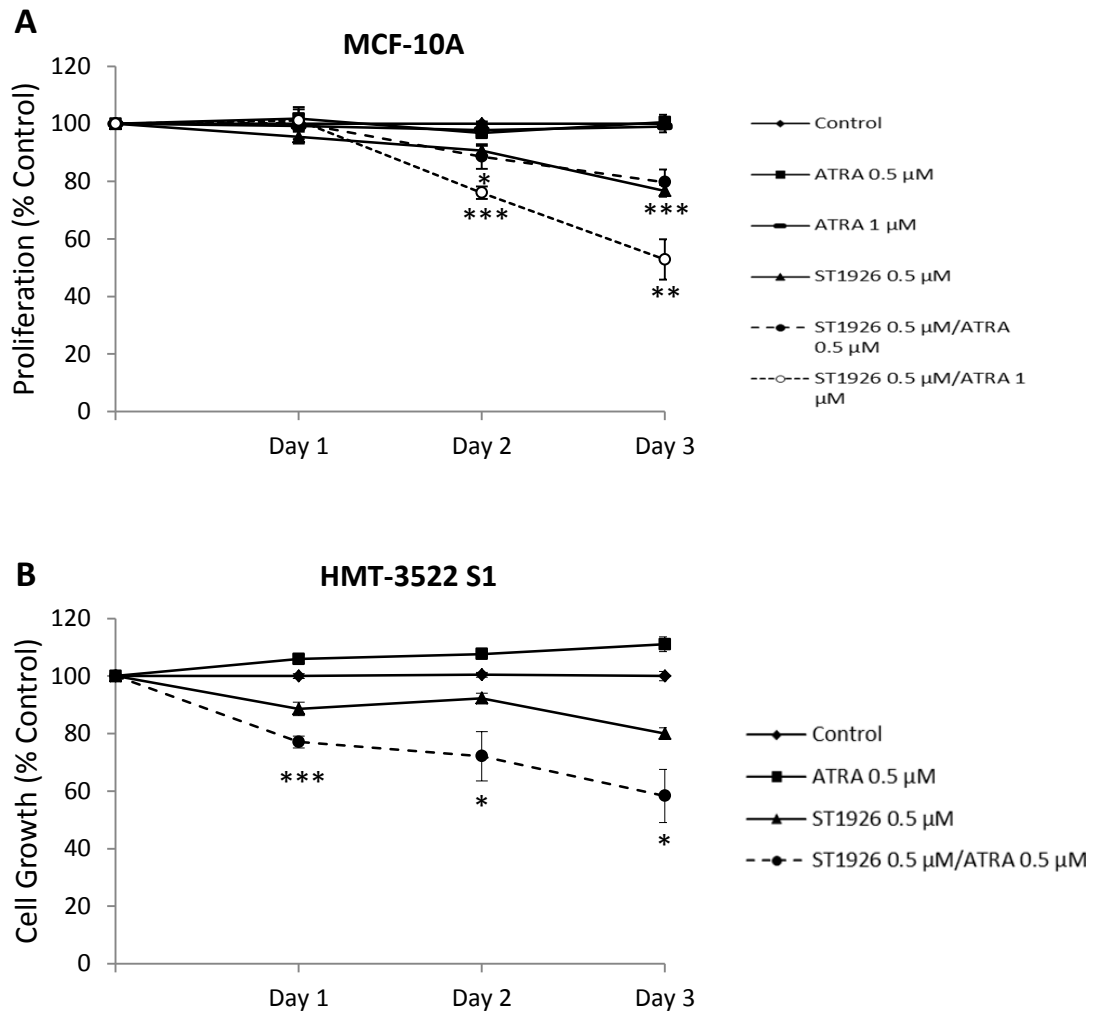


**Figure 28. Combination treatments of ATRA with higher ST1926 concentrations moderately inhibit the proliferation of ‘normal-like’ breast epithelial cells.** MCF-10A cells (A) and HMT-3522 S1 cells (B) were seeded in 96-well plates at a density of  $1 \times 10^5$  cells/ml and treated with 0.1% DMSO or the indicated concentrations of ATRA and/or ST1926. HMT-3522 S1 cells were treated when cell confluence reached 60%. Cell growth was assayed in triplicate wells using the MTT cell proliferation assay. Cell growth results are expressed as percentage of control (0.1% DMSO) and represent the average of at least three independent experiments ( $\pm$  SEM). Significance from control is indicated by \*  $P < 0.05$ ; \*\*  $P < 0.01$ ; \*\*\*  $P < 0.001$ .

#### **N. Combination treatments of ATRA and ST1926 at low concentrations induce pre-G<sub>1</sub> cell accumulation and a massive S-phase arrest in MCF-7 cells**

To investigate the mechanisms involved in ATRA/ST1926-induced growth arrest, cell cycle analysis was conducted using flow cytometric analysis of DNA content. Treatments of MCF-7 cells with 0.1  $\mu$ M ST1926 in combination with 0.5 or 1  $\mu$ M ATRA resulted in a 15% and 17% increase in the pre-G<sub>1</sub> phase respectively after 48 hours of treatment, while no change was observed in control cells (Figure 29A). Furthermore, a massive S-phase arrest was observed in ATRA/ST1926-treated MCF-7 cells after 24 and 48 hours of treatment, where approximately 50% of cycling cells were arrested in the S-phase, while only 18% control, 26% 0.5  $\mu$ M ATRA, 25% 1  $\mu$ M ATRA, and 29% 0.1  $\mu$ M ST1926 24 hours after treatment (Figure 29B). Similar results were obtained at 48 hours, clearly supporting the synergistic results reported previously. Representative histograms of the cell cycle distribution of treated MCF-7 cells compared to their respective controls for 48 hours post-treatments are shown in (Figure 30). The massive S-phase arrest, along with the observed accumulation of treated cells in the Pre-G<sub>1</sub> region of the cell cycle 48 hours post-treatments might explain the synergistic results obtained in the MTT assay. ATRA/ST1926-induced growth inhibition in MCF-7 cells was not altered in the presence of BMS493 (Figure 31), indicating a retinoid-receptor independent pathway mode of growth inhibition.

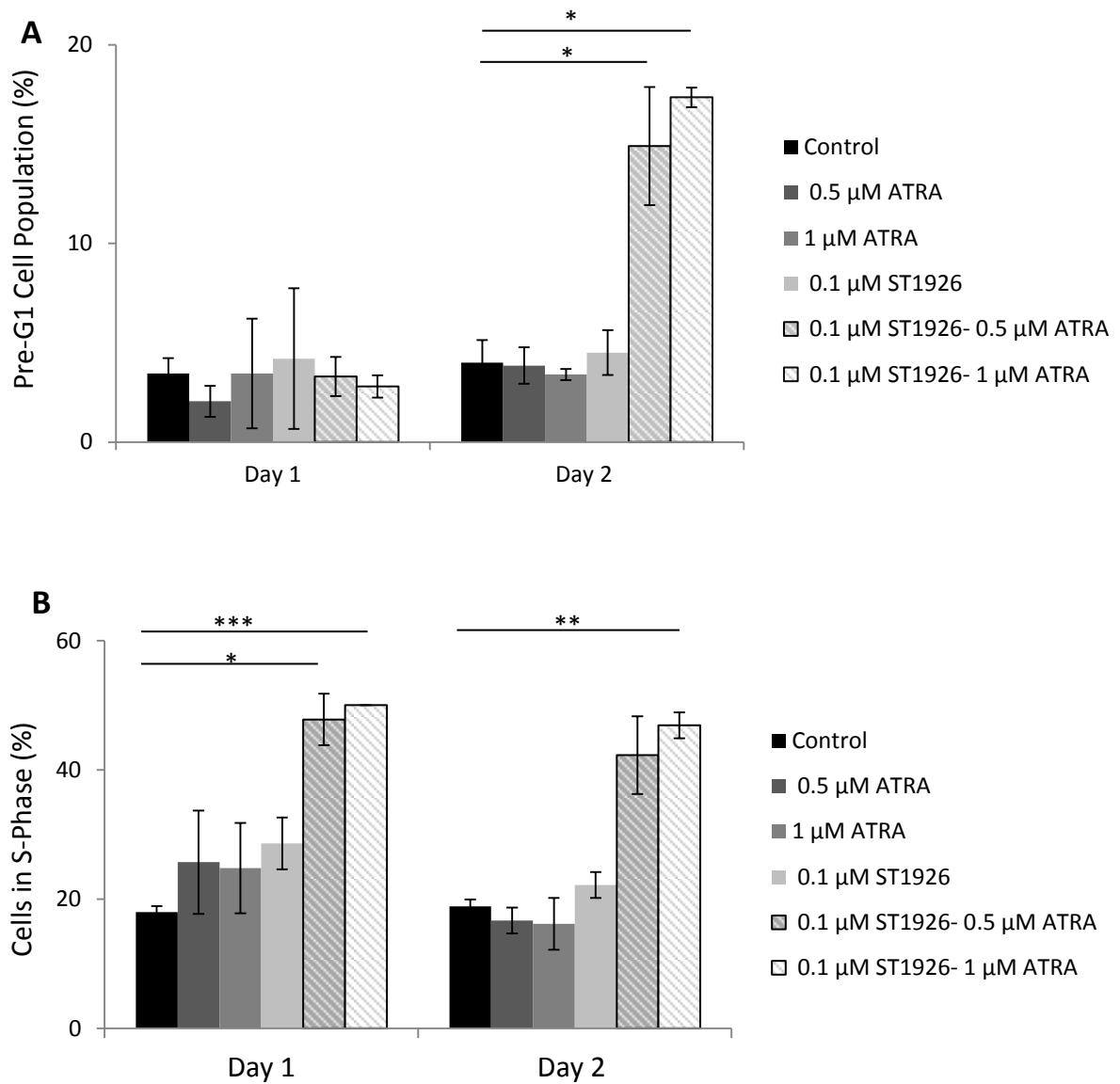


**Figure 29. Combination treatments with ATRA and ST1926 induce pre-G<sub>1</sub> cell accumulation and a massive S-phase arrest in MCF-7 cells.** MCF-7 cells were seeded in 100 mm culture plates at a density of  $5 \times 10^5$  cells/plate and treated with 0.1 % DMSO (Control) or the indicated concentrations of ATRA and/or ST1926. Cell cycle was assayed using propidium iodide-based flow cytometric analysis of DNA content. (A) represents the percentage of cells in the pre-G<sub>1</sub> phase of the cell cycle, while (B) represents the percentage of cells in the S-phase of the cell cycle. Data represent the average of at least two independent experiments ( $\pm$  SD). Significance from control is indicated by \*  $P < 0.05$ ; \*\*  $P < 0.01$ ; \*\*\*  $P < 0.001$ .

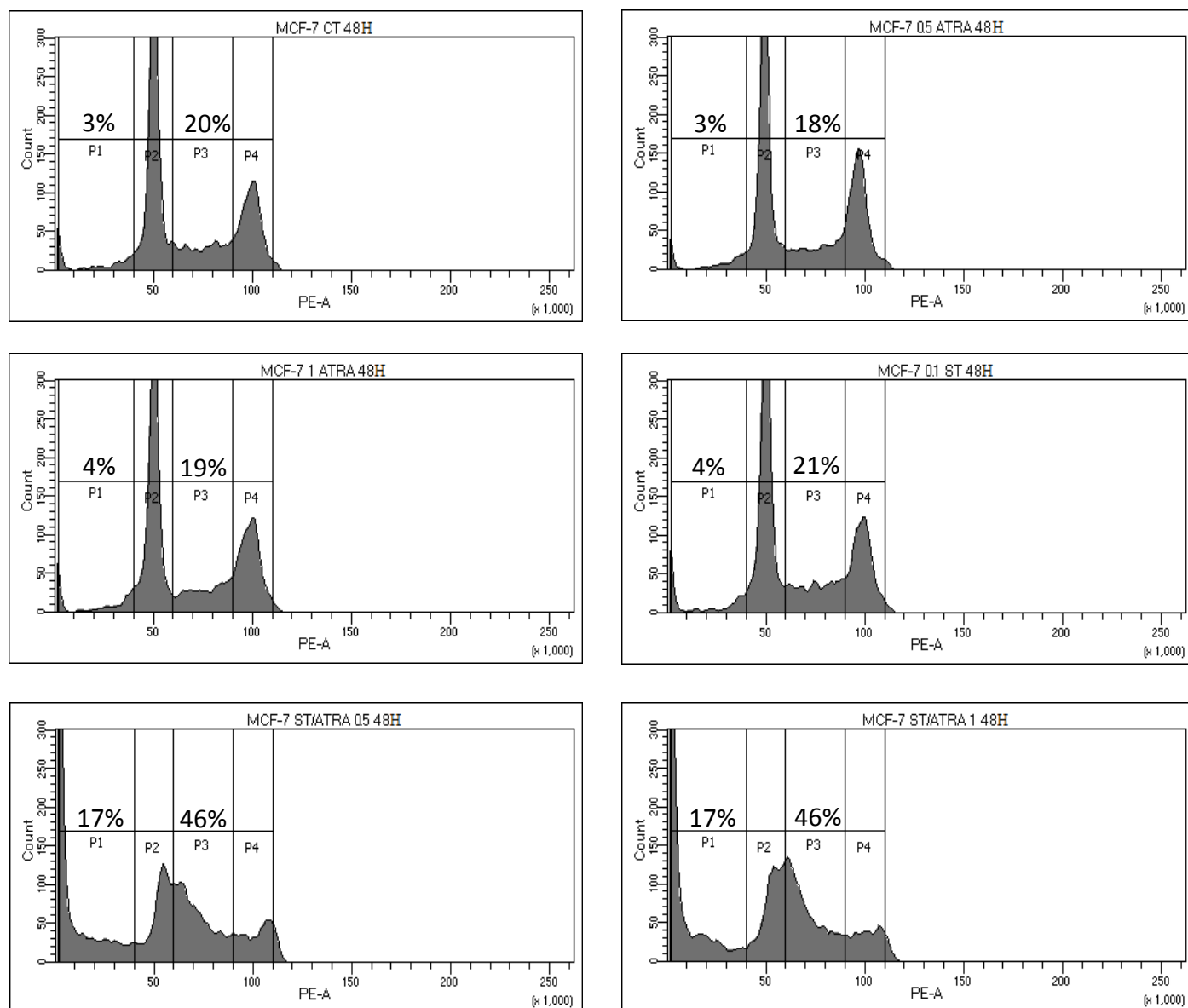


**Figure 30. Representative histograms of the cell cycle distribution and progression in ATRA and ST1926-treated MCF-7 cells.** MCF-7 cells were seeded in 100 mm culture plates at a density of  $5 \times 10^5$  cells/plate and treated with 0.1 % DMSO (CT) or the indicated concentrations of ATRA and/or ST1926 (ST). Cell cycle was assayed using propidium iodide-based flow cytometric analysis of DNA content. P1, P2, P3, and P4 represent the pre-G<sub>1</sub>, G<sub>0</sub>/G<sub>1</sub>, S, and G<sub>2</sub>/M phases of the cell cycle. Values represent the percentage of cells in the pre-G<sub>1</sub> (P1) and S-Phase (P3) regions of the cell cycle. The shown histograms are representative of two independent experiments.

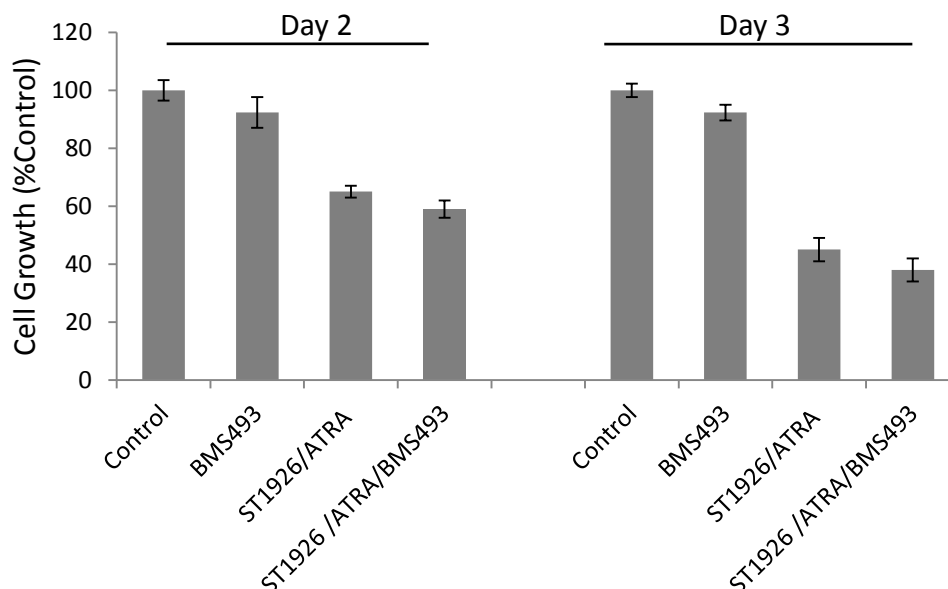


**Figure 31. ATRA/ST1926-induced growth inhibition is independent of the retinoid receptor signaling pathway.** MCF-7 cells were seeded in 96-well plates at a density of  $0.5 \times 10^5$  cells/ml and treated with 0.1% DMSO or treated with 1  $\mu$ M BMS493 or 0.1  $\mu$ M ST1926 in combination with 0.5  $\mu$ M ATRA or pretreated with 1  $\mu$ M BMS493 for 20 minutes then treated with 0.1  $\mu$ M ST1926 in combination with 0.5  $\mu$ M ATRA for 72 hours. Cell growth was assayed in triplicate wells using the MTT cell proliferation assay. Cell growth results are expressed as percentage of control (0.1% DMSO) and represent the average of three independent experiments ( $\pm$  SEM).

#### **O. ST1926 treatment at sub- $\mu$ M concentrations inhibit colony growth of breast cancer cells in anchorage-independent 3D cell culture model**

Nowadays, there is increasing interest in developing 3D *in vitro* cell culture models for evaluating pre-clinical efficacy of anticancer drugs (Edmondson 2014). This is because 2D cell culture models lack inter- and intracellular complexities and fail to represent the true architecture of the tissue microenvironment. Drug screening in 2D cell culture models remains misleading since roughly 90% of preclinical drugs fail to provide expected efficacy in patients. Thus, we evaluated the influence of the microenvironment on the response of human breast cancer cells to ST1926 and ATRA using anchorage-independent and -dependent cell culture models.

Anchorage-independent growth of MCF-7 and MDA-MB-231 cells was examined using the soft-agar colony formation assay, which is reported in the literature as a 3D cell culture model (Edmondson 2014). Similar colony growth inhibitory effects were observed in both tested cell lines where long-term exposure of ST1926 as low as 10 nM significantly reduced the size of breast cancer colonies (data not shown) and decreased their numbers by approximately 30% (Figure 32B). Furthermore, 0.5  $\mu$ M ST1926 reduced the size of both breast cancer colonies (Figure 33) and significantly decreased colony growth by 60% and 75% in MCF-7 and MDA-MB-231 cells, respectively. Interestingly, long-term exposure to ATRA resulted in colony growth inhibitory effects of MCF-7 cells at all tested concentrations except for 0.01  $\mu$ M with 3  $\mu$ M ATRA reducing the number by 60% (Figure 32A). MDA-MB-231 colonies were resistant to ATRA treatment in anchorage-independent cell culture model where only 3  $\mu$ M ATRA was shown to decrease colony growth by 35% (Figure 32A). In summary, unlike in 2D cell culture model, MCF-7 and MDA-MB-231 are sensitive to pharmacologically achievable  $\mu$ M ATRA concentrations in anchorage-independent cell

culture model. Furthermore, this latter model enhances the sensitivity of breast cancer cells to nM concentrations of ST1926.

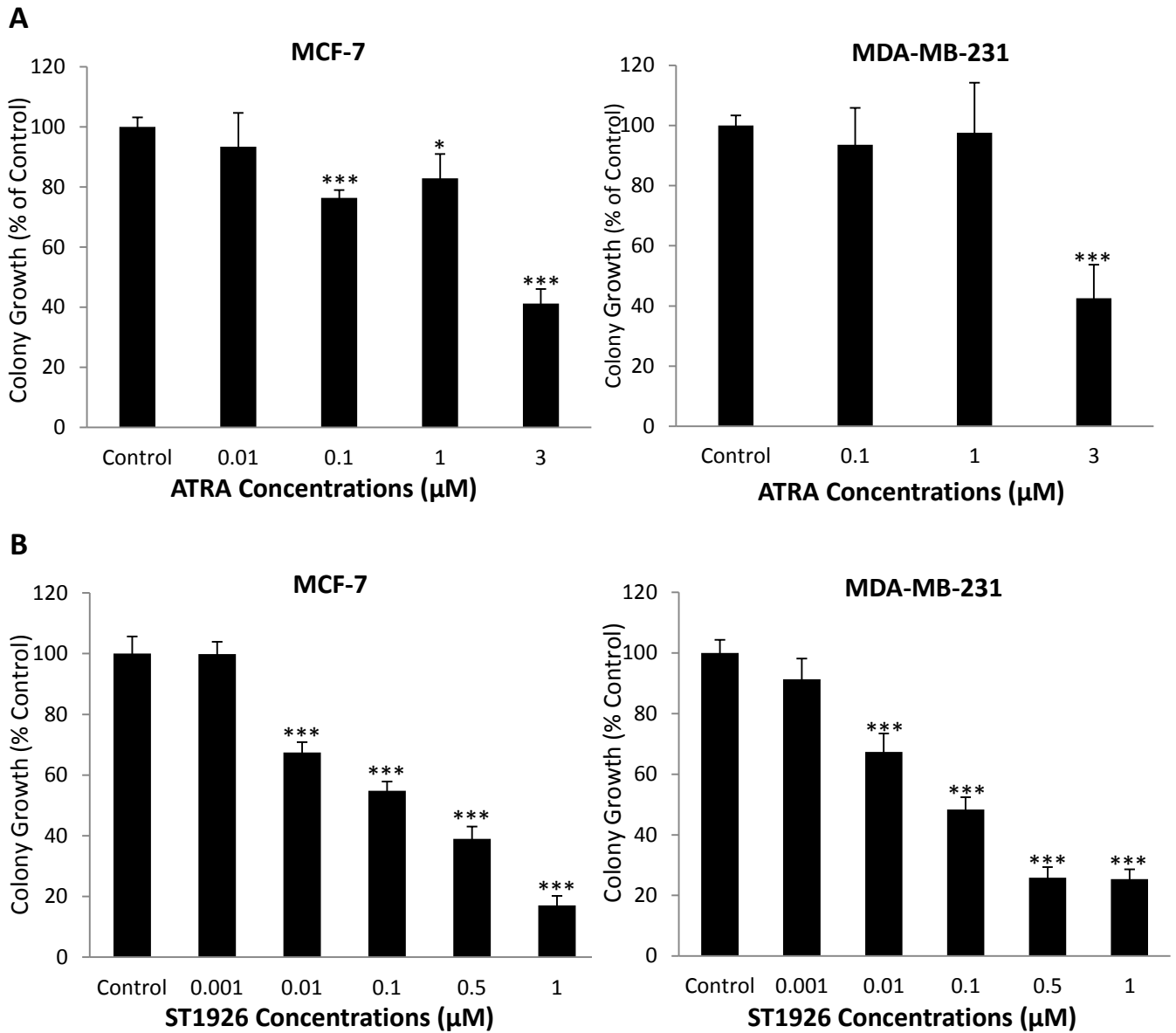


**Figure 32. Effect of ST1926 and ATRA on anchorage-independent growth of breast cancer cells.** Dose-response bar graphs showing the effect of ATRA (A) and ST1926 (B) on anchorage-independent growth of MCF-7 and MDA-MB-231 cells. Cells were suspended in 0.4 % soft agar over 0.6 % base agar layers with or without the indicated ATRA or ST1926 concentrations. Treatments were replenished every two days, and colony growth was quantified  $8 \pm 1$  day post-seeding using the CytoSelect™ 96-Well Cell Transformation Assay kit. Colony growth is expressed as percentage of DMSO-treated cells and plotted as colony growth ( $\pm$  SEM) of three independent experiments done in triplicate wells. Significance from control is indicated by \*  $P < 0.05$ ; \*\*  $P < 0.01$ ; \*\*\*  $P < 0.001$ .



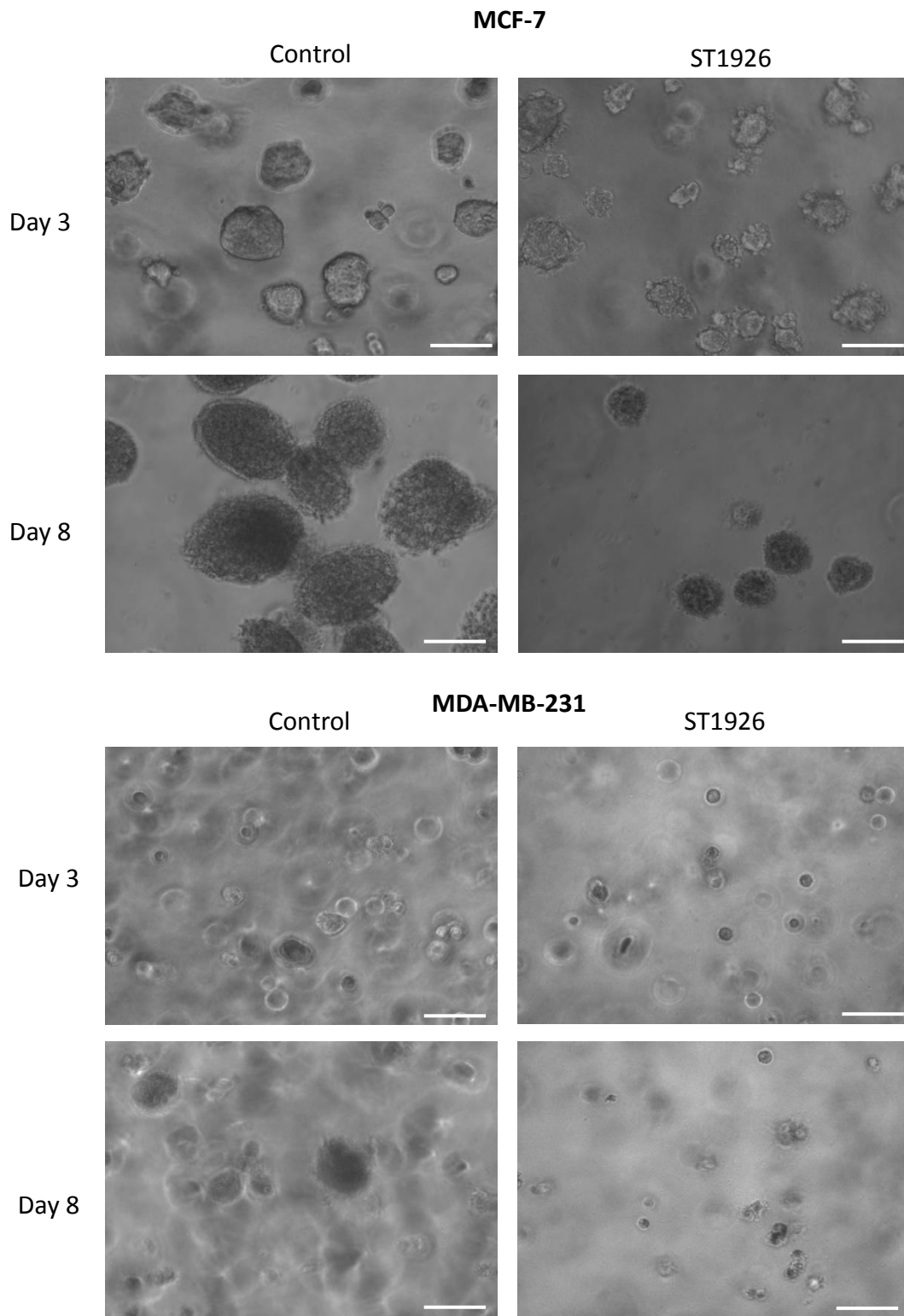


**Figure 33. ST1926 reduces the growth of breast cancer colonies in agar matrix.** MCF-7 cells and MDA-MB-231 cells were suspended in 0.4 % soft agar over 0.6 % base agar layers with 0.1% DMSO or 0.5  $\mu$ M ST1926 for 8 days. Treatments were replenished every two days. Representative phase contrast images were acquired using Zeiss axiovert light microscope (x10). Scale bar represents 100  $\mu$ m.

**P. ST1926 at sub- $\mu$ M concentrations inhibit the viability of breast cancer cells in anchorage-dependent 3D cell culture model**

We next examined the effects of ST1926 on anchorage-dependent growth of MCF-7 and MDA-MB-231 cells using 3D ‘on-top’ assay. When maintained in a 3D context (on top of growth factor-reduced basement membrane), both cancer cell lines showed morphological differences; as viewed by phase contrast microscopy. MCF-7 cells formed round colonies referred to as ‘spheres’ (Figure 34A) and MDA-MB-231 cells formed large branching, stellate structures (Figure 34B). Treatments of MCF-7 and MDA-MB-231 cells with different concentrations of ST1926 (0.01-1  $\mu$ M) decreased the viability in a time and dose-dependent manner (Figure 35A and 35B). ST1926 treatment at 0.5 or 1  $\mu$ M for 2 days reduced the viability of MCF-7 and MDA-MB-231 by 90% and 80%, respectively (Figure 35A and 35B). Interestingly, 0.5  $\mu$ M ST1926 drastically reduced MCF-7 colonies (Figure 36A) and decreased the branching, stellate structures of MDA-MB-231 (figure 36B). Interestingly, 3D cell cultures did not reduce the sensitivity of breast cancer cells to drug treatments, although previous studies have reported that 3D cell cultures might render cancer cells more resistant to anti-cancer drugs (Imamura 2015). Our data suggest that ST1926-induced growth inhibition was more prominent in 3D compared to 2D cell cultures, highlighting ST1926 potential as an anti-cancer agent.

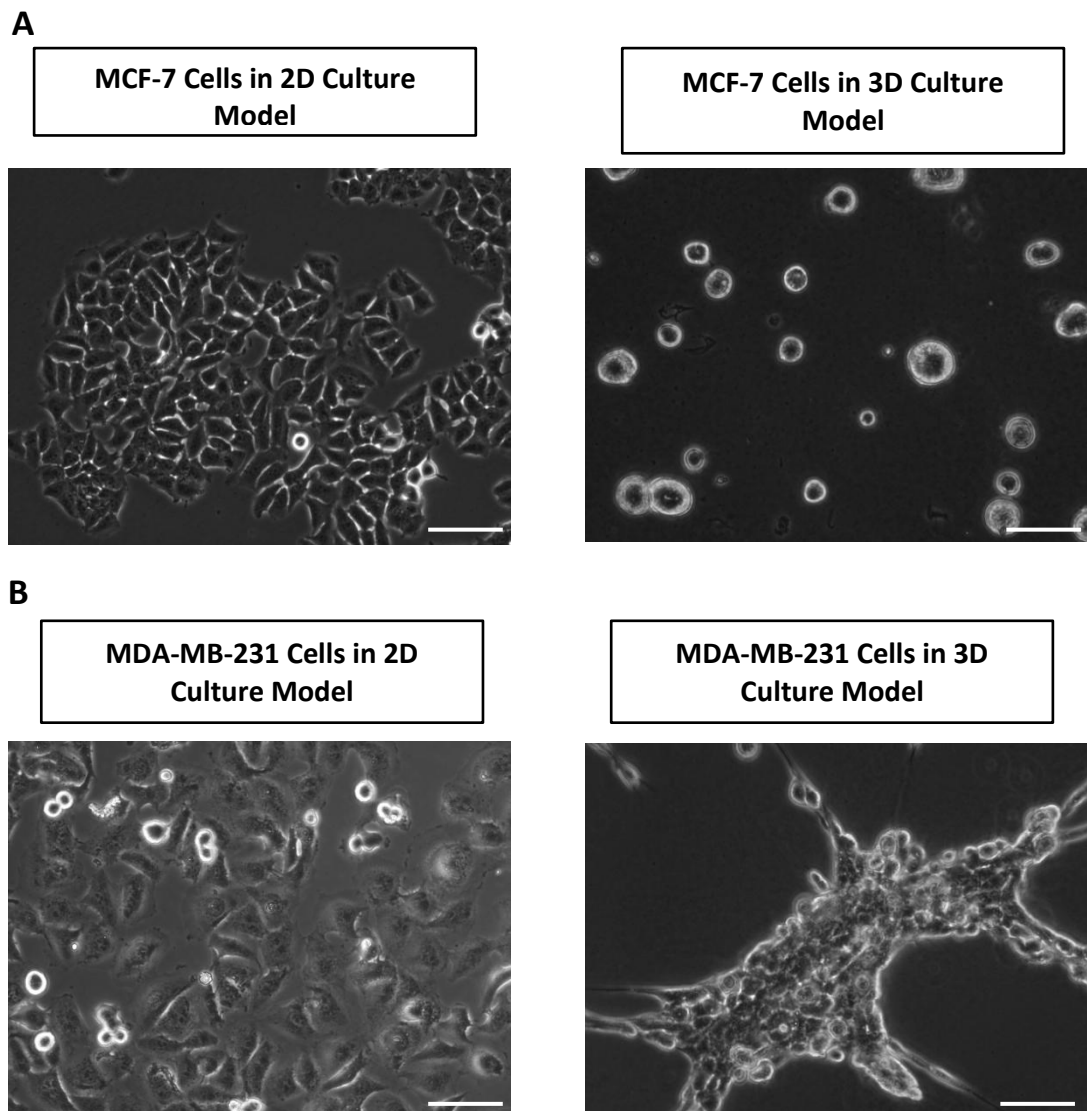


**Figure 34. Morphology of human breast cancer cells is different in 2D versus 3D cell culture models.** MCF-7 Cells (A) and MDA-MB-231 cells (B) were plated on the growth factor reduced Matrigel in 24-well tissue culture plates at a density of  $25 \times 10^3$  cells/well. Representative phase contrast images were acquired 48 hours after seeding using Zeiss axiovert light microscope (x10). Scale bar represents 100  $\mu\text{m}$ .

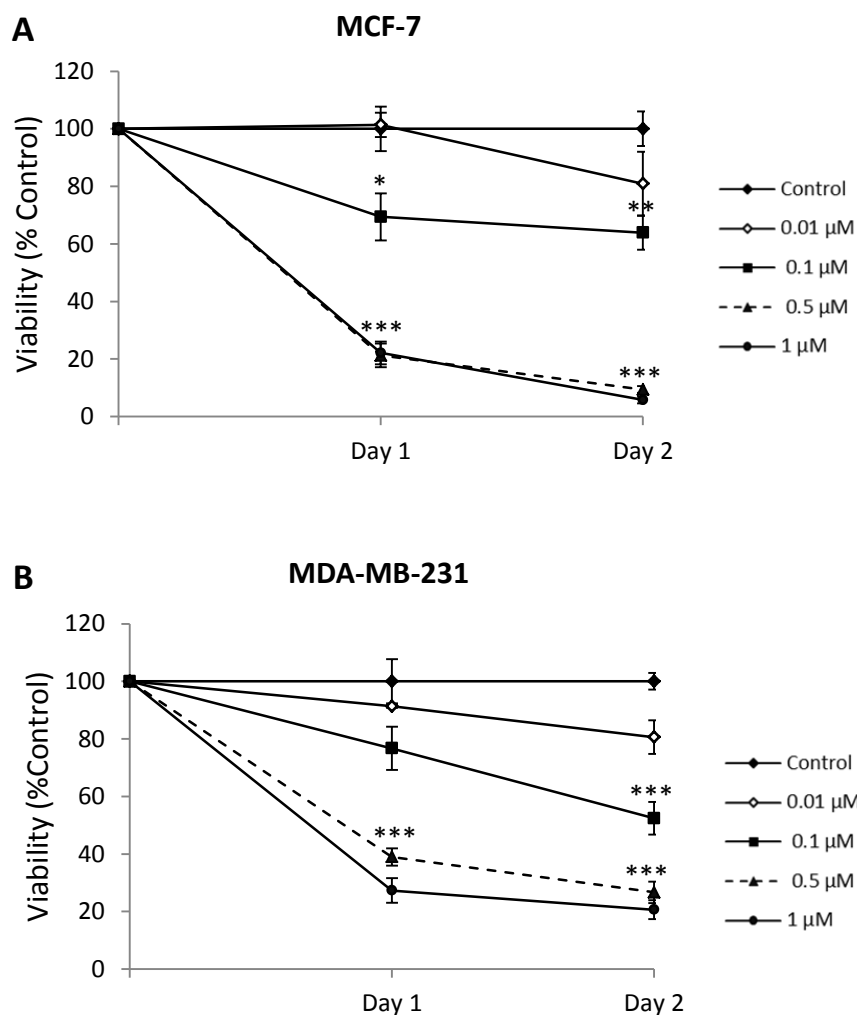


**Figure 35. ST1926 decreases the viability of breast cancer cells at low sub- $\mu$ M concentrations.** MCF-7 (A) and MDA-MB-231 cells (B) were plated on the growth factor reduced Matrigel in 24-well tissue culture plates at a density of  $25 \times 10^3$  cells/well and treated with 0.1% DMSO or the indicated concentrations of ST1926. Cells were counted in duplicate measurements using the trypan blue exclusion method and viability results are expressed as percentage of control (0.1% DMSO). Data represent the average of three independent experiments ( $\pm$  SEM). Significance from control is indicated by \*  $P < 0.05$ ; \*\*  $P < 0.01$ ; \*\*\*  $P < 0.001$ .

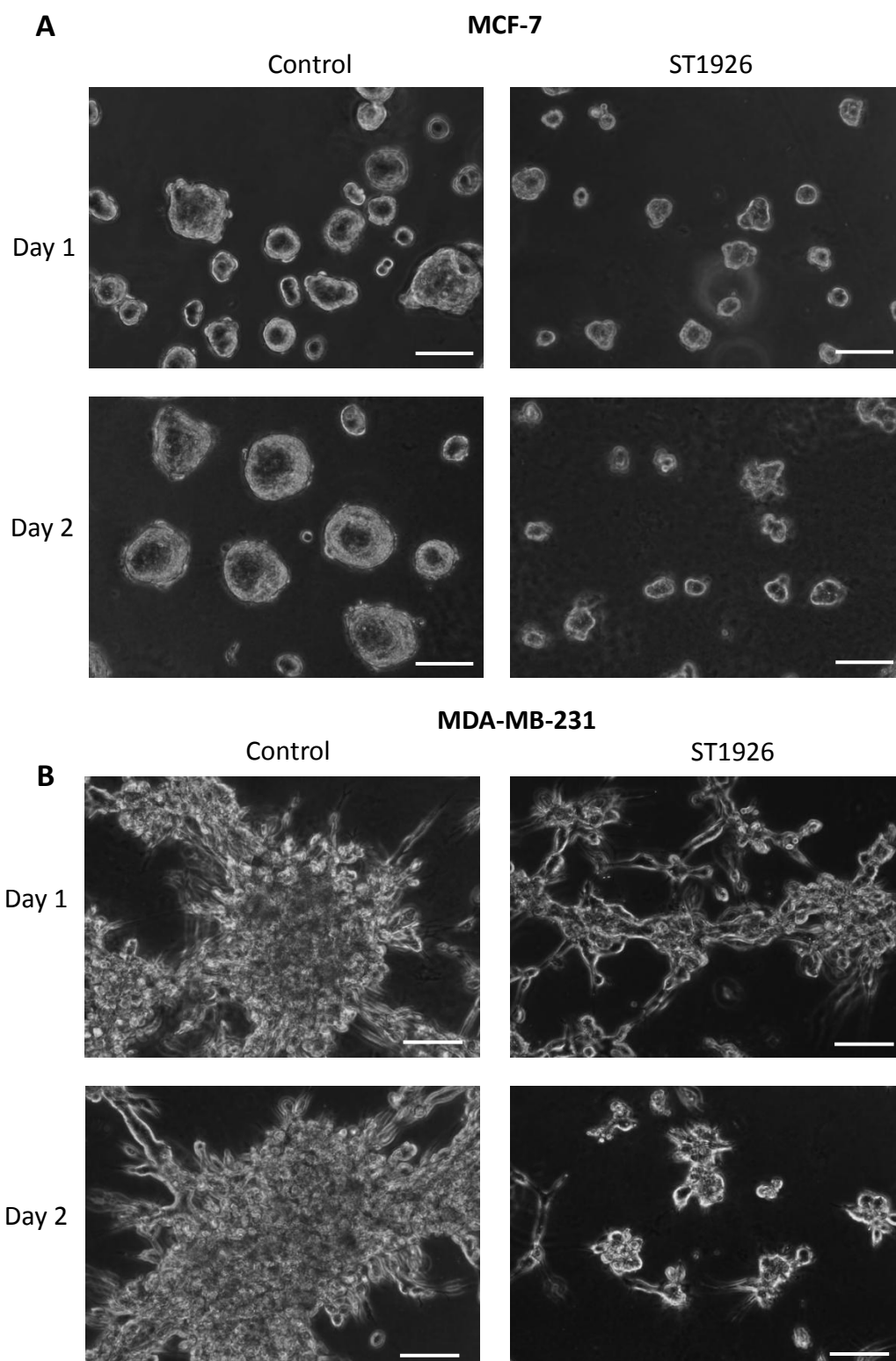


**Figure 36. ST1926 drastically reduced colony formation and stellate structures of breast cancer cells.** MCF-7 cells (A) and MDA-MB-231 cells (B) were plated on the growth factor reduced Matrigel in 24-well tissue culture plates at a density of  $25 \times 10^3$  cells/well and were treated with 0.1% DMSO or 0.5  $\mu$ M ST1926 for two days. Representative phase contrast images were acquired using Zeiss axiovert light microscope (x10). Scale bar represents 100  $\mu$ m.

**Q. Single ST1926 treatment at nM concentrations in combination with sub- $\mu$ M ATRA concentrations inhibit the colony-forming ability of breast cancer cells**

We sought to determine the effects of ATRA, ST1926, and their combination on the sphere-forming ability of breast cancer cells- a key characteristic of breast CSC. Mammospheres were generated from 1,000 single cells of MCF-7 and MDA-MB-231 cells, embedded in Matrigel™ and were treated with or without ATRA, ST1926, or their combination. After culturing MCF-7 and MDA-MB-231 spheres for 13 days, we obtained a sphere-forming unit (SFU) of around 12% and 14% respectively in control cells. Interestingly, nM concentrations of ST1926, as low as 10 nM, decreased mammosphere formation of MCF-7 and MDA-MB-231 spheres by approximately 45%, while 0.1  $\mu$ M and 0.5  $\mu$ M ST1926 completely abrogated the SFU of breast cancer cells up to 13 days (Figure 37A). Such decrease in the number of spheres was also associated with a reduction in their size and diameter, whereby treatment with 10 nM ST1926 significantly decreased the diameter by 30% in both cell lines (Figure 38A, 40A and 41A). Furthermore, the number of cultured mammospheres decreased in a dose-dependent manner when treated with ATRA. In fact, 0.5  $\mu$ M ATRA decreased mammosphere formation in MCF-7 and MDA-MB-231 cells by 30% and 40%, respectively (Figure 37B), and reduced the sphere diameter by 55% and 30%, respectively (Figure 38B). We noticed a distinct morphological change that was very evident at 0.1 and 0.5  $\mu$ M ATRA concentrations, whereby MCF-7 mammospheres had a ‘flower-like’ shape and a rough texture when compared to the smooth-textured control spheres (Figure 40B). Also, there was a halo extending from treated spheres that was absent in control cultures (Figure 40B). Given the synergy between ST1926 and ATRA that was previously established in 2D culture models, we aimed to determine the effects of ATRA/ST1926 combination treatments on the sphere-forming abilities of MCF-7

cells. Interestingly, combination treatments of 1 nM ST1926 with 0.1  $\mu$ M ATRA decreased the SFU from 12% in control to 7% in treated mammospheres (data not shown) while combination treatments of 10 nM ST1926 with 0.5  $\mu$ M ATRA synergized to decrease the SFU from 12% in control to only 3% in treated mammospheres (Figure 39A), indicating a more pronounced effect on the sphere-forming ability of combination *versus* single treatments. We also observed a decrease in the size and diameter of ATRA/ST1926-treated MCF-7 spheres (Figure 39B and 40C); however, this decrease was similar to the decrease in diameter of ATRA-treated spheres, indicating that ATRA/ST1926 synergized to drastically decrease the SFU but not the sphere diameter. In summary, the effect of ST1926, ATRA, and specifically their combination treatments was more pronounced on 3D compared to 2D cell culture models, whereby a lower concentration of each drug, had major effects on the stem-like breast cancer population.

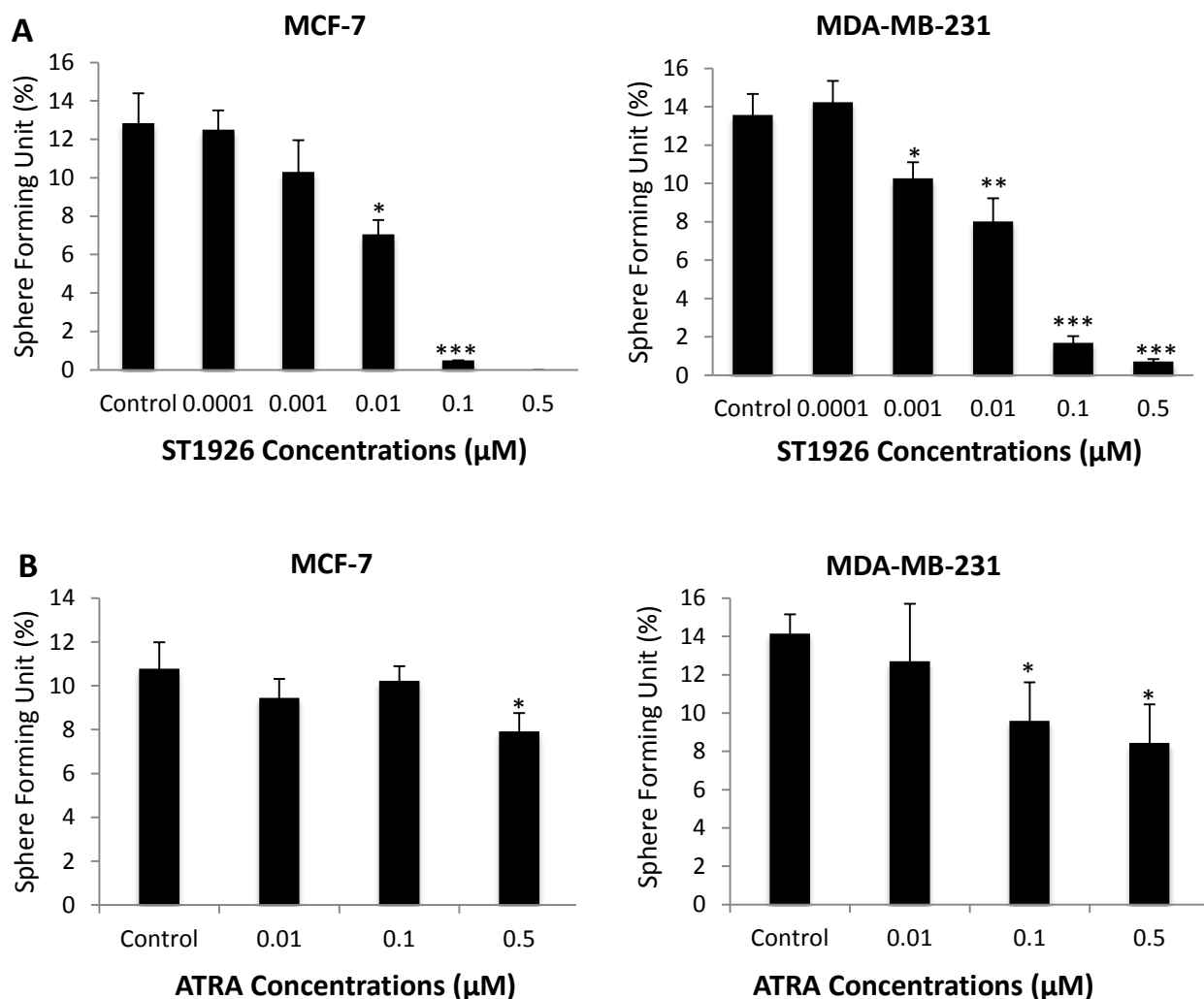


**Figure 37. Effect of ST1926 and ATRA on the sphere-forming ability of breast cancer cells.** Dose-response bar graphs showing the effect of ATRA (A) and ST1926 (B) for 13 days on the sphere-forming ability of MCF-7 and MDA-MB-231 cells. Generated spheres are referred to as G1 (Generation 1) spheres. Sphere-forming unit (SFU) is calculated according to the following formula:  $SFU = (\text{number of spheres counted} / \text{number of input cells}) \times 100$ . Data represent an average of two independent experiments ( $\pm$  SEM). Significance from control is indicated by \*  $P < 0.05$ ; \*\*  $P < 0.01$ ; \*\*\*  $P < 0.001$ .



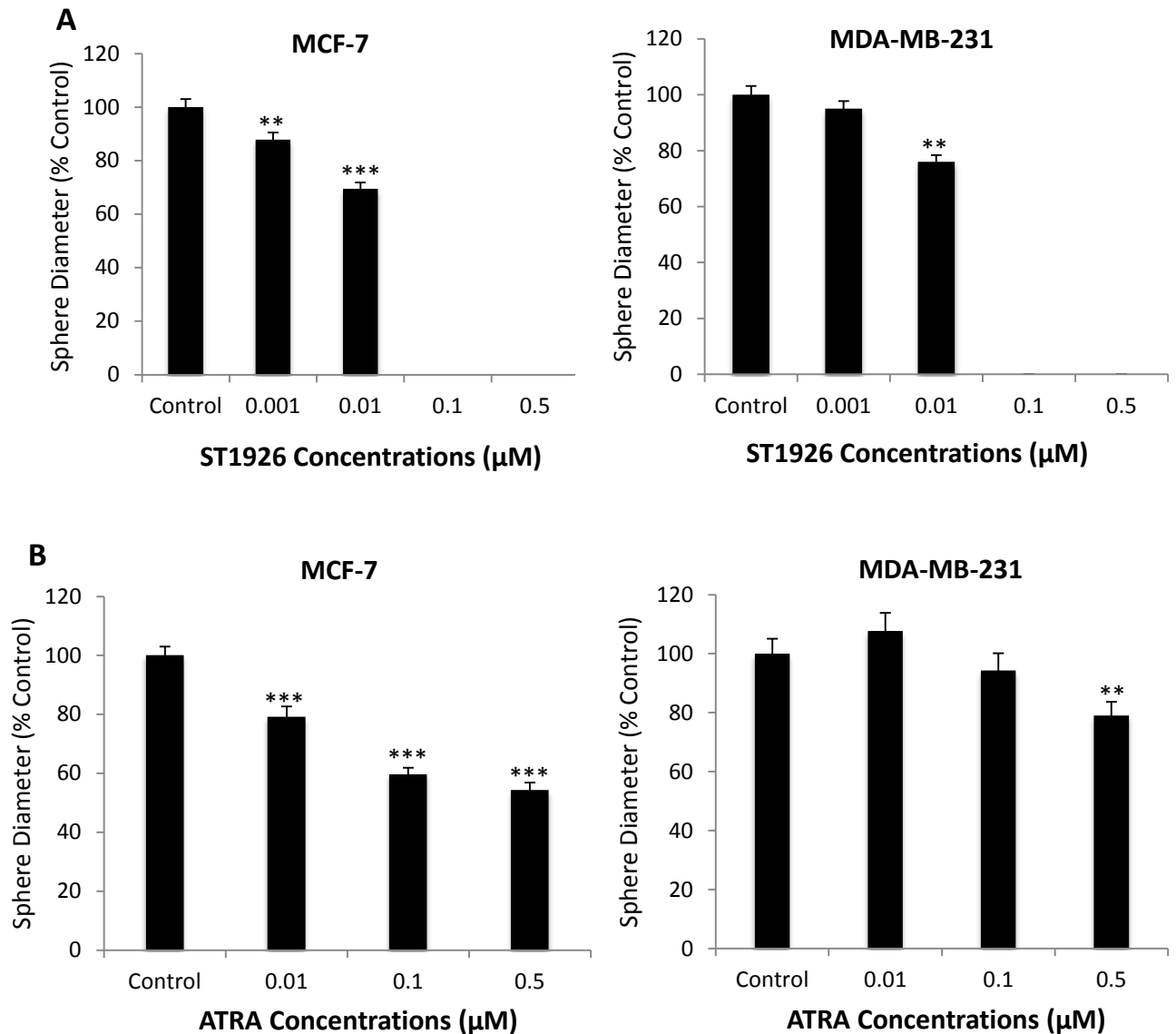


**Figure 38. Effect of ST1926 and ATRA on the diameter of mamospheres.** Dose-response bar graphs showing the effect of ATRA (A) and ST1926 (B) for 13 days on the diameter of MCF-7 and MDA-MB-231 colonies. Generated spheres are referred to as G1 (Generation 1) spheres. The percentage sphere diameter was expressed as percentage relative to 0.1% DMSO (control wells) and treated wells with the indicated concentrations. Data represent the average of two independent experiments ( $\pm$  SEM). Data represent an average diameter of 20 measured MCF-7 spheres and 20 measured MDA-MB-231 spheres. Significance from control is indicated by \*  $P < 0.05$ ; \*\*  $P < 0.01$ ; \*\*\*  $P < 0.001$ .

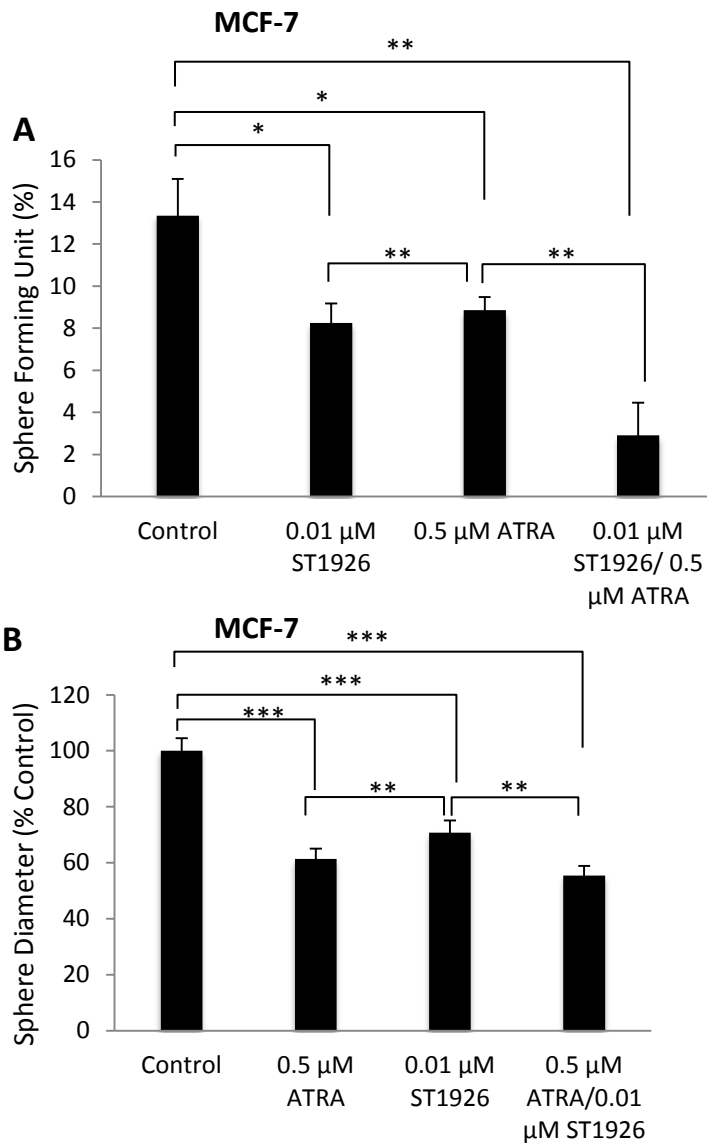


**Figure 39. Effect of single or combination treatments with ATRA and ST1926 on the sphere-forming ability and diameter of MCF-7 cells.** (A) Dose-response bar graphs showing the effect of ATRA, ST1926, and their combination for 13 days on the sphere-forming ability of MCF-7 cells. Generated spheres are referred to as G1 (Generation 1) spheres. Sphere-forming unit (SFU) is calculated according to the following formula:  $SFU = (\text{number of spheres counted} / \text{number of input cells}) \times 100$ . Data represent an average of one independent experiments ( $\pm$  SD). (B) Dose-response bar graphs showing the effect of ATRA, ST1926, and their combination for 13 days on the diameter of MCF-7 spheres. The percentage sphere diameter was expressed as percentage relative to 0.1% DMSO (control) and treated wells with the indicated concentrations. Data represent an average diameter of 20 measured MCF-7 spheres ( $\pm$  SD). Significance from control is indicated by \*  $P < 0.05$ ; \*\*  $P < 0.01$ ; \*\*\*  $P < 0.001$ .

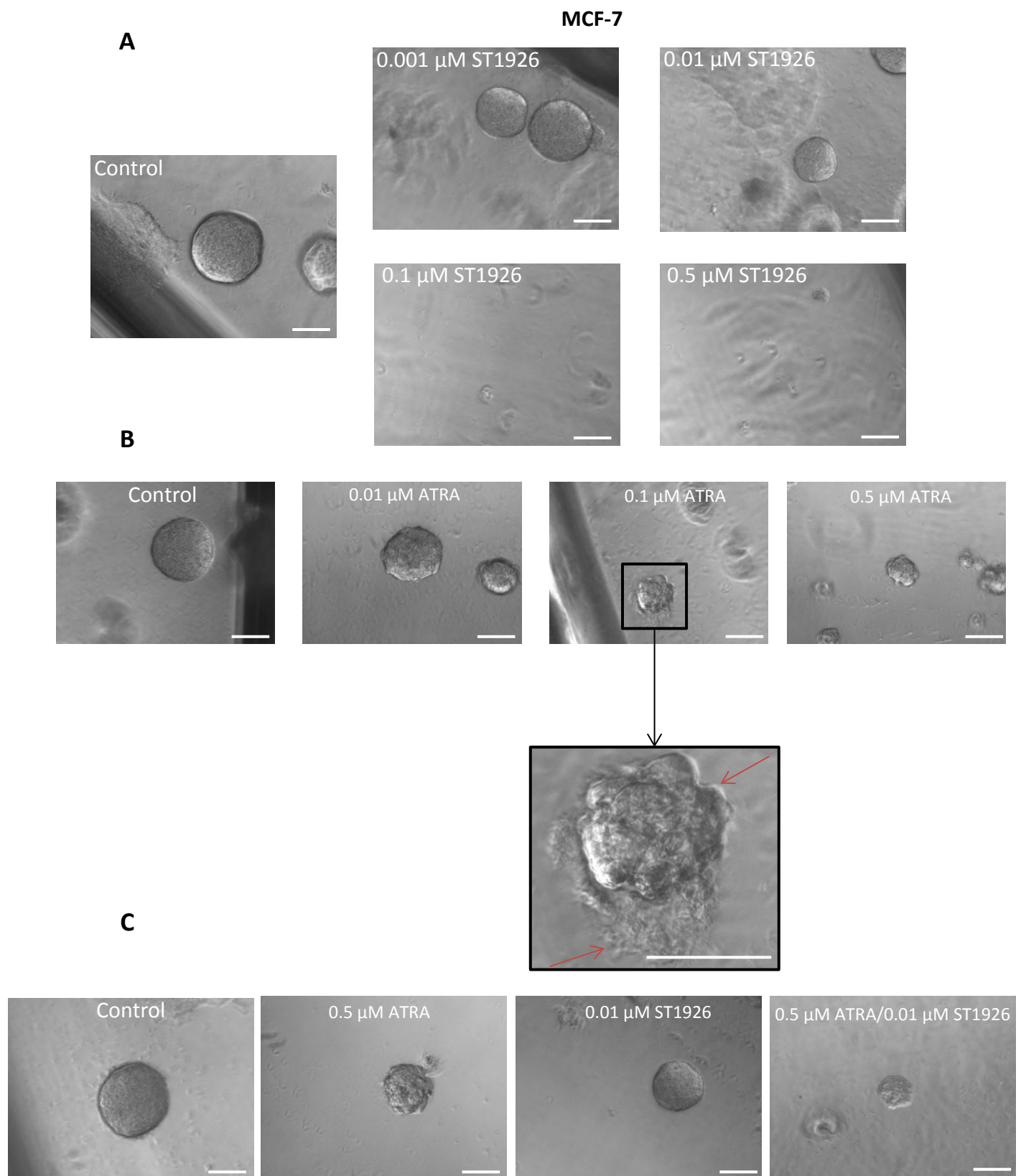


**Figure 40.** Effect of ATRA, ST1926, and their combination on MCF-7 spheres. Representative images of MCF-7 mammospheres treated with the indicated concentrations of ST1926 (A), ATRA (B), or their combination (C). Generated spheres are referred to as G1 (Generation 1) spheres. Phase contrast images were acquired using Zeiss axiovert light microscope (x10). Scale bar represents 100  $\mu\text{m}$ .

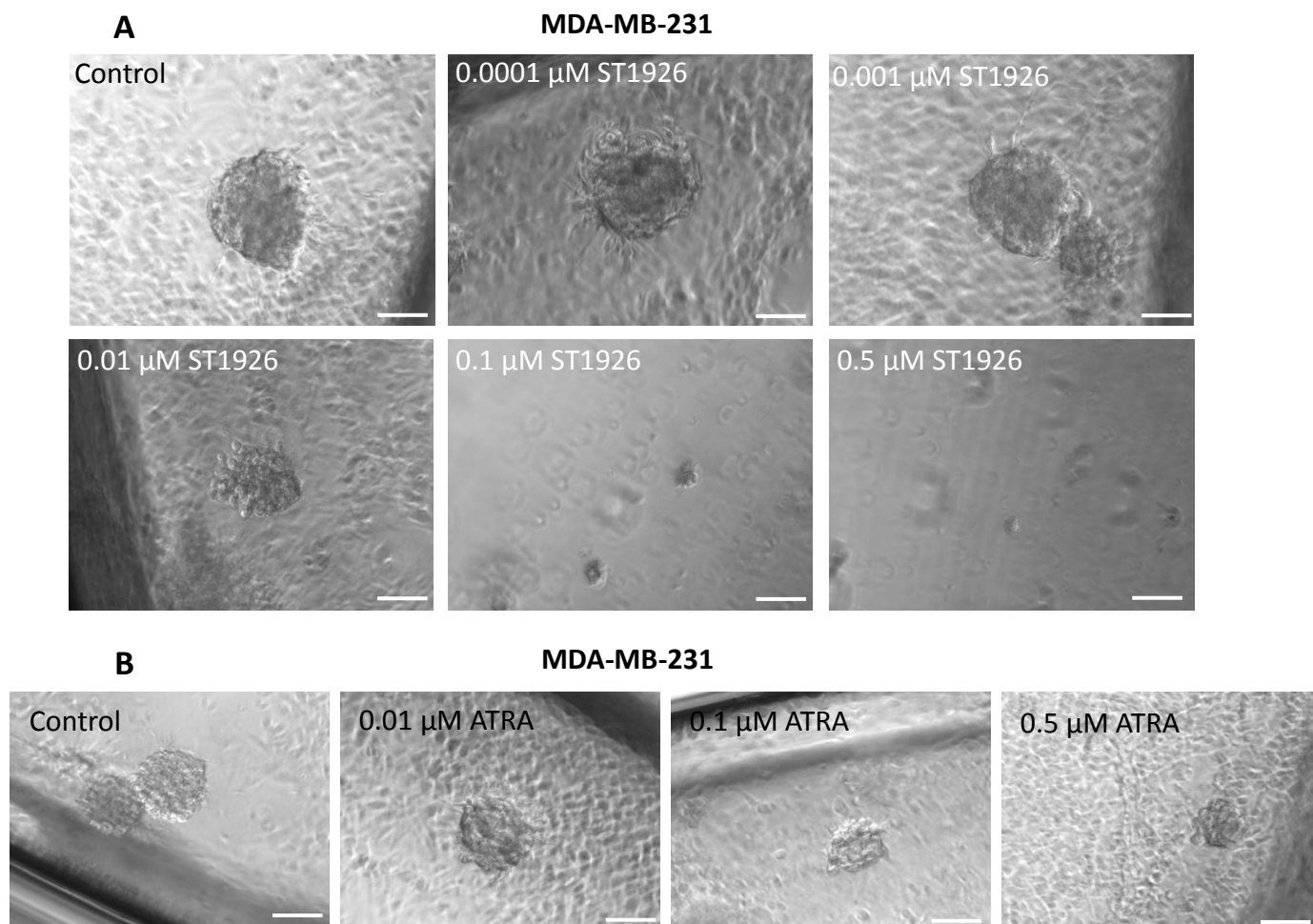


**Figure 41.** Effect of ATRA and ST1926 on MDA-MB-231 spheres. Representative images of MDA-MB-231 mammospheres treated with the indicated concentrations of ST1926 (A) and ATRA (B). Generated spheres are referred to as G1 (Generation 1) spheres. Phase contrast images were acquired using Zeiss axiovert light microscope (x10). Scale bar represents 100  $\mu\text{m}$ .

#### **R. Treatments with ATRA, ST1926, or their combination do not disrupt the lumen and size of HMT-3522 S1 acini in 3D cell culture model**

We have previously shown that ST1926, ATRA, and their combination had minimal effects of the cell growth of ‘normal-like’ MCF-10A and HMT-3522 S1 cells in 2D culture model. To verify these results in a context that mimics the *in vivo* architecture of breast epithelial cells, we aimed at testing the effects of different drug treatments on the lumen of HMT-3522 S1 cells. First, these cells acquired a different morphology when grown on top of an exogenous basement membrane (3D) (Figure 42), and formed acinar structures, with a lumen after omitting EGF from growth media (at day 7). Importantly, all tested concentrations except for 0.5  $\mu$ M ATRA in combination with 0.5  $\mu$ M ST1926, did not have any effect on the lumen of HMT-3522 S1 cells (Figure 43). The percentage of acinar structures with correct lumen under tested conditions was very similar to that of control, with a percentage ranging between 74% and 79%. Treatments with 0.5  $\mu$ M ATRA in combination with 0.5  $\mu$ M ST1926 resulted in 62% of acini with correct lumen morphology, indicating a mild deviation from the control and thus little effect. Representative photographs showing the effect of ATRA, ST1926, and their combination on the lumen-forming ability of HMT-3522 S1 cells are represented in figure 44. To ensure the diameter of acini was not affected, we manually recorded their diameter and compared it to the control ones. The diameters of acini after treatment with 0.5  $\mu$ M ATRA, ST1926 (0.1  $\mu$ M, 0.5  $\mu$ M, 1  $\mu$ M), 0.1  $\mu$ M ST1926/0.5  $\mu$ M ATRA or 0.5  $\mu$ M ST1926/0.5  $\mu$ M ATRA were very similar to the diameter of acini in control cells, indicating lack of treatment cytotoxicity (Figure 45). Although combination treatments with 0.5  $\mu$ M ATRA/0.5  $\mu$ M ST1926 in combination with 0.5  $\mu$ M ST1926 resulted in a relatively increased percentage of acini with incorrect lumen, however, no cytotoxicity was recorded.

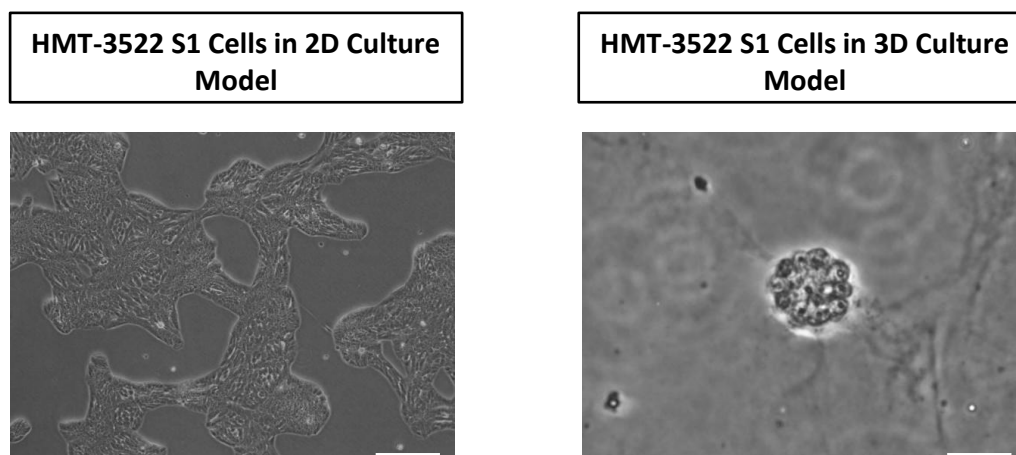


**Figure 42. Morphology of HMT-3522 S1 cells grown in 2D versus 3D cell culture model.** HMT-3522 S1 cells were seeded on Matrigel™ at a density of  $5 \times 10^4$  cells/well in the presence of culture medium containing 5% Matrigel™. Representative phase contrast images were acquired using Zeiss axiovert light microscope (x10). Scale bar represents 100  $\mu$ m.

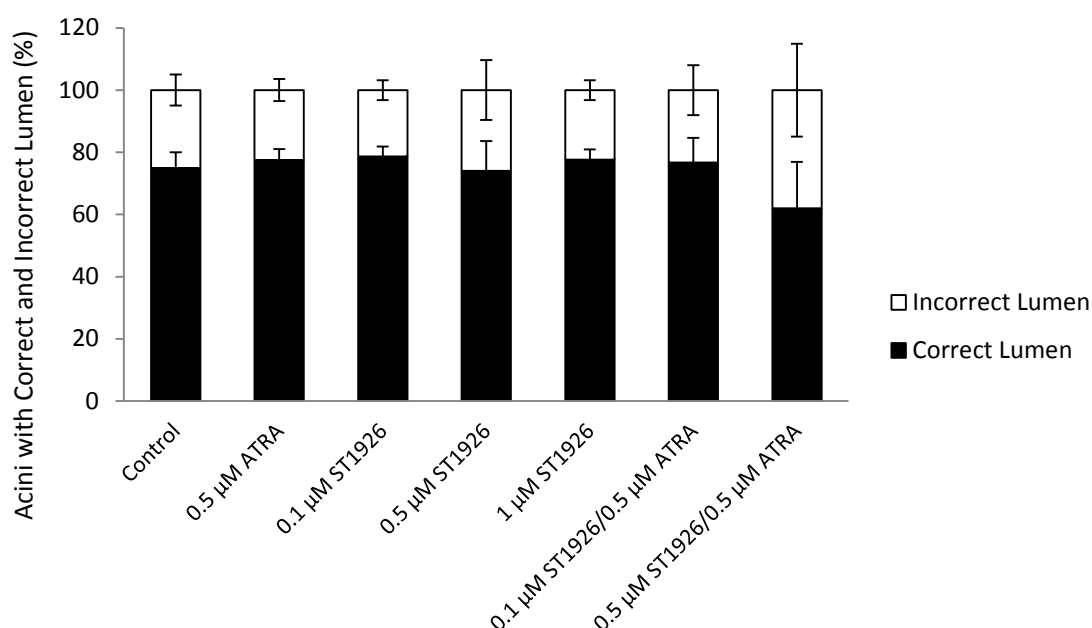


**Figure 43. Effect of ATRA, ST1926, and their combination on the lumen of HMT-3522 S1 cells.** HMT-3522 S1 cells were seeded on Matrigel™ at a density of  $5 \times 10^4$  cells/well in the presence of culture medium containing 5% Matrigel™. Cells were maintained in culture for 7 days and were treated with the indicated concentrations of drugs in EGF-free media to allow acinar completion and differentiation. Nuclei were subsequently stained with Hoechst 33342. A minimum of one hundred acini per condition was analyzed and scored for correct and incorrect lumen formation. Data represent the average of three independent experiments ( $\pm$  SEM).

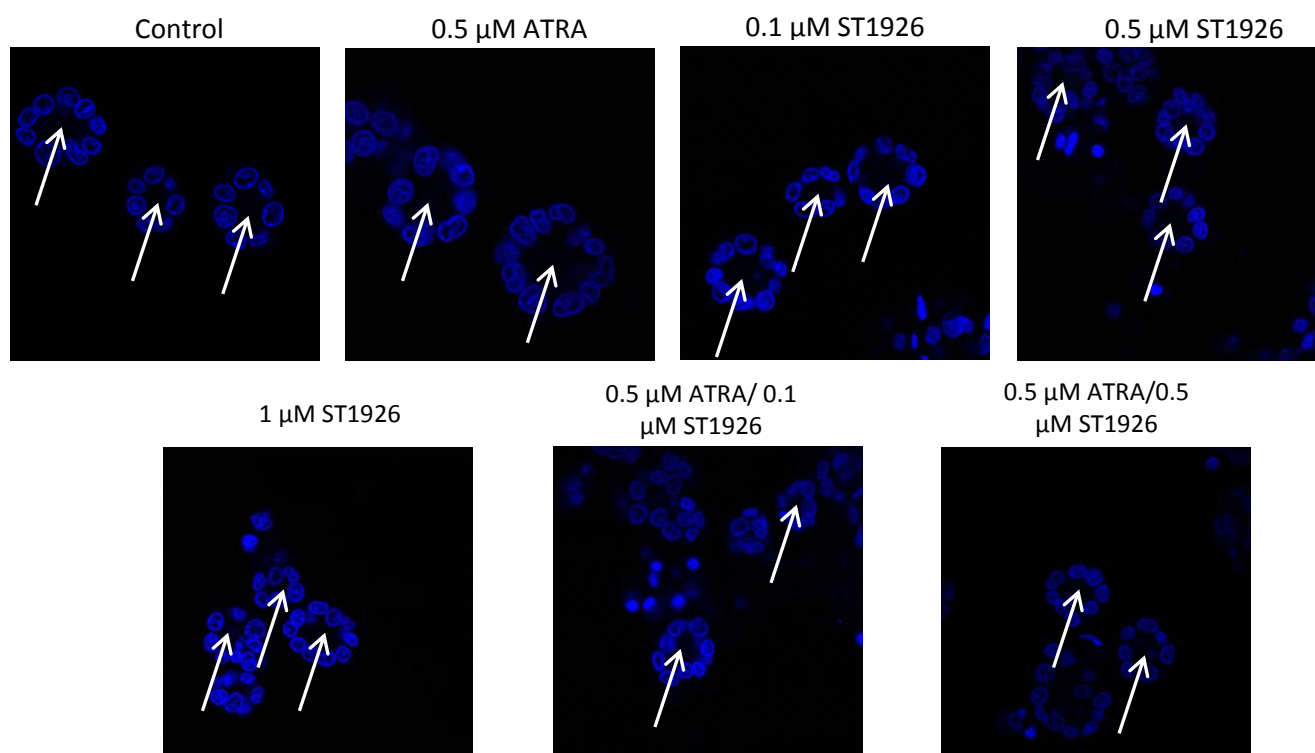


**Figure 44. Representative photographs showing the effect of ATRA, ST1926, and their combination on the lumen of HMT-3522 S1 cells.** HMT-3522 S1 cells were seeded on Matrigel™ at a density of  $5 \times 10^4$  cells/well in the presence of culture medium containing 5% Matrigel™. Cells were maintained in culture for 7 days and were treated with the indicated concentrations of drugs in EGF-free media to allow acinar completion and differentiation. Cells were fixed on day 10 with 4% paraformaldehyde. Nuclei were subsequently stained with Hoechst 33342. The shown photographs are representative of three independent experiments.

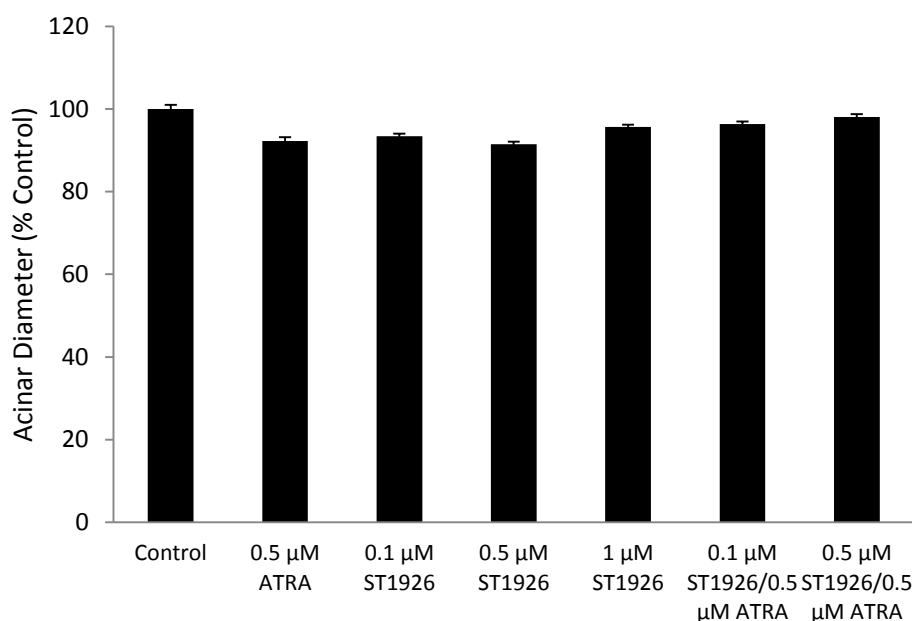


**Figure 45. Effect of ATRA, ST1926, and their combination on the size of HMT-3522 S1 acini.** HMT-3522 S1 cells were seeded on Matrigel<sup>TM</sup> at a density of  $5 \times 10^4$  cells/well in the presence of culture medium containing 5% Matrigel<sup>TM</sup>. Cells were maintained in culture for 7 days and were treated with the indicated concentrations of drugs in EGF-free media to allow acinar completion and differentiation. Cells were fixed on day 10 with 4% paraformaldehyde. Acinar sizes measurements were performed manually on day 10 by recording the diameter of each acinus with respect to the stage micrometer using Zeiss axiovert light microscope. One hundred acini were included in the scoring. The percentage acinar diameter was expressed as percentage growth relative to 0.1% DMSO (control) and treated wells with the indicated concentrations. Data represent the average of three independent experiments ( $\pm$  SEM).



## CHAPTER IV

### DISCUSSION

Survival rates have been improving for most breast cancer patients, however, those for women diagnosed with metastatic triple negative breast cancer remain significantly lower, necessitating the development of effective and safer therapies (Brouckaert 2012; Bayraktar 2013; American Cancer Society 2016). Retinoids, vitamin A and its family of naturally occurring and synthetic analogs, have been extensively studied for their role as chemopreventive and therapeutic agents in different types of tumors, including breast cancer (di Masi 2015). Retinoids are implicated in several physiologically vital processes such as the regulation of cell proliferation, and cell death and differentiation in embryonic development and adult life (Altucci 2001). However, the use of retinoids in clinical trials for solid and hematological malignancies is often hindered by undesirable side effects (Garattini 2014) and resistance to treatment (Garattini 2014; Schenk 2014), and hence, they failed to achieve their primary endpoint. In fact, ATRA and 13-*cis*RA failed phase-II clinical trials, whereas 9-*cis*RA was halted in phase-I clinical trial in patients with breast cancer (Sutton 1997; Garattini 2014).

To overcome retinoid resistance and toxic effects in the clinical setting, synthetic retinoids were developed (Ortiz 2002; Dawson 2001), namely the promising adamantyl compound ST1926 (Cincinelli 2003), which is a CD437 analog (Garattini 2004). ST1926 was shown to be endowed with potent anti-tumor effects in several *in vitro* and *in vivo* cancer models, independently of RAR and *p53* signaling pathways, and to display a favorable pharmacokinetic profile when compared to CD437 (Cincinelli

2003). ST1926 induced tumor growth inhibition in ovarian carcinoma (Zuco 2004; Zuco 2010), neuroblastoma (Di Francesco 2007; Di Francesco 2012), ATL (El Hajj 2014), CML (Nasr 2015), and rhabdomyosarcoma animal models (Basma 2016). In these studies, we investigated the anti-tumor properties of ST1926, ATRA, and combination treatments in 2D human breast cancer models. In addition, we evaluated the influence of the microenvironment, on the response of human normal breast and cancer cells to ATRA, ST1926, and their combination using different 3D cell culture models. Although ST1926 has been previously tested on MCF-7 cells in combination with the epidermal growth factor receptor (EGFR) inhibitor ZD1839 as part of a screening study (Zanchi 2005), this is the first report to elucidate the detailed anti-tumor activities and mechanism of action of ATRA, ST1926, and their combination in 2D and 3D human breast cancer models.

Two well-characterized human breast cancer cell lines, MCF-7 and MDA-MB-231, belonging to the luminal A and triple negative subtype, respectively, were selected to represent breast cancer heterogeneity and mutational signatures. While being resistant to suprapharmacologically achievable ATRA concentrations in 2D models, both cell lines were sensitive to pharmacologically achievable sub- $\mu$ M ST1926 concentrations (Sala 2009; Basma 2016). Furthermore, ST1926-induced growth inhibition in breast cancer cells was independent of *p53* status in accordance with previous studies (Cincinelli 2003; El Hajj 2014). This highlights the promising use of ST1926 in breast tumors with *p53* mutations since they are one of the most frequent genetic alterations occurring in more than 30% of breast carcinomas (Zardavas 2015; Bertheau 2013). In addition, ST1926-induced growth inhibition persisted even upon one hour of drug exposure at sub- $\mu$ M concentrations, suggesting a fast intracellular drug

action and a persistent cell death induction in breast cancer cells after drug removal. Similar results were observed in CML cells (Nasr 2015). Importantly, ST1926 had minimal effects on the growth of the ‘normal-like’ breast epithelial cells, MCF-10A and HMT-3522 S1, at concentrations that induced massive apoptosis in breast cancer cells. Previous studies indicated that ST1926 spares normal resting and activated lymphocytes (El Hajj 2014), and ‘normal-like’ NCM460 colorectal epithelial cells (Abdel-Samad R. unpublished data). Therefore, we decided to use the pharmacologically achievable 0.5  $\mu$ M concentration to investigate ST1926 mechanism of action.

Cell cycle and cell death analysis revealed a prominent S-phase arrest as observed in other types of ST1926-treated cancer cells (Valli 2008; Basma 2016) as well as massive apoptosis induction (El Hajj 2014; Nasr 2015; Basma 2016). Apoptosis was the main cell death mechanism to be reported so far in ST1926 preclinical cancer studies, and it remains to be determined whether other cell death mechanisms are involved.

We then tested for the effects of ST1926 on the DDR, which is translated by the phosphorylation and subsequent activation of several downstream effectors, among which are p53, p21, and  $\gamma$ -H2AX.  $\gamma$ -H2AX has been shown to be a critical determinant of early cellular DNA damage prior to apoptosis (Mah 2010). We showed that ST1926 induced an early upregulation of p53, p21, and  $\gamma$ -H2AX, independently of p53 status, consistent with previous studies showing an early induction of DNA damage by ST1926 in various types of solid and hematological cells (Valli 2008; El Hajj 2014; Nasr 2015; Basma 2016). In addition, recent studies highlighted the critical role of DDR pathways in ST1926-mediated cell death. In fact, ST1926-induced resistance resulted in delayed and reduced DNA damage in neuroblastoma cells (Di Francesco 2015). Also, inhibition

of ATM and ATR, two sensory kinases upstream of the DDR pathway (Zhou 2000), by caffeine led to an attenuated DDR and a decreased phosphorylation of H2AX, CHK2, and p53 with a reduced S-phase arrest in rhabdomyosarcoma cells (Basma 2016). Induction of p21 in p53-mutated or -null cells was also reported where p65 was shown to be involved in enhanced p21 expression by directly binding to the *p21* promoter (Shenglin 2008). Further studies are required to decipher the molecular events that govern the upregulation of p21 by ST1926 independently of p53 and whether p65 is involved in treated breast cancer cells.

The Wnt/ $\beta$ -catenin pathway is one of the fundamental mediators of cell proliferation, cell polarity, and cell fate determination during embryonic development (MacDonald 2009). Furthermore, Wnt signaling regulate homeostasis and mammary gland development (Brennan 2004). Mutations and deregulations in the Wnt/ $\beta$ -catenin pathway and subsequent upregulation of  $\beta$ -catenin response transcription (CRT) promote the development of breast cancer (Jang 2015). Thus, Wnt/ $\beta$ -catenin signaling pathway is an attractive target for breast cancer therapy. Interestingly, ST1926 reduced the expression levels of  $\beta$ -catenin and downstream targets such as cyclin D1 and c-myc. This is the first report regarding the inhibitory effects of ST1926 on the Wnt/ $\beta$ -catenin signaling pathway. Previous studies demonstrated that the degradation of  $\beta$ -catenin is mediated by proteasome- and/or caspase-dependent mechanism (Park 2006; Omori 2011; Rice 2003). Future studies will assess the involvement of caspase and/or proteasome in ST1926-induced  $\beta$ -catenin degradation using the pan-caspase inhibitor z-vad and the proteasome inhibitor PS-341.

Although ATRA has been shown to exhibit its anti-tumor and cytodifferentiating effects primarily through the classical RAR-dependent pathway,

synthetic retinoids, including ST1926, have been shown to mediate their effects mostly through RAR- independent pathways (Cincinelli 2003; Parella 2006). We determined the effects of ST1926 on RAR $\beta$ , RAR $\gamma$ , and RXR $\alpha$  protein expression levels in breast cancer cells. A prominent increase in RAR $\beta$  protein levels while a decrease in RAR $\gamma$  and RXR $\alpha$  were noted upon ST1926 treatment. Similar results were previously obtained whereby ST1926 reduced RAR $\gamma$  and RXR $\alpha$  protein levels in ST1926-treated AML cells (El-Houjeiri MS AUB 2015). However, RAR $\gamma$  transcript levels were shown to be significantly higher in normal primary breast cancer samples when compared to normal mammary tissues (Garattini 2014). RAR $\gamma$  was reported to favor the self-renewal and expansion of hematopoietic stem cells (Purton 2006) and might exert similar effects in breast cancer stem cells (Bosch 2012). Here, we report the repression of RAR $\gamma$ , a gene-signature that is associated with breast tumors (Muscat 2013) by ST1926, which further highlights the promising use of ST1926 in breast cancer treatment.

On the other hand, RAR $\beta$  transcript levels were found to be significantly lower in tumor tissues (Garattini 2014). Current studies reported that the lack of ATRA responsiveness in breast cancer may be linked to aberrant epigenetics, which suppress ATRA-regulated gene expression namely that of RAR $\beta$  2 (Sirchia 2000; Sirchia 2002). ST1926 was found to increase RAR $\beta$  protein levels. In addition, RAR $\alpha$  was found to be a determinant of ATRA sensitivity in ER<sup>+</sup> breast cancer cells (Terao 2011). Thus, it would be of interest to determine the effects of ST1926 on RAR $\alpha$  expression levels in our breast cancer model. Previous studies demonstrated that overexpression of RXR $\alpha$  in ATRA-resistant breast cancer cells enhances the antiproliferative effects of RXR-selective agents, indicating a promising therapeutic use of these rexinoids (Crowe

2004). Although previous studies reported RXR $\alpha$  to be a potential therapeutic target in the treatment of breast cancer (Wan 1998; Crowe 2004), here we showed the repression of RXR $\alpha$  proteins by ST1926 in breast cancer cells.

We showed that our tested breast cancer cells were relatively resistant to ATRA even at suprapharmacological concentrations. However, ST1926-induced upregulation of RAR $\beta$ , a critical determinant of ATRA sensitivity (Connolly 2013), and the synergistic effects of ATRA and ST1926 in neuroblastoma preclinical models (Di Francesco 2011) led us to investigate the effects of ATRA/ST1926 combination treatment on the cell growth and viability of breast cancer cells. Interestingly, sub- $\mu$ M concentrations of ATRA and ST1926 synergized to potently inhibit the proliferation and viability of tested breast cancer cells. ATRA/ST1926 synergistic effects were also reported in neuroblastoma preclinical models (Di Francesco 2011). The cytodifferentiating functions of ATRA, together with the genotoxic properties of ST1926 enhanced the efficiency of treatment in *in vitro* and *in vivo* neuroblastoma models (Di Francesco 2011). It is worth noting that 13-*cis*-RA, and not ATRA, is the established treatment regimen for children with neuroblastoma (Matthay 1999; Matthay 2009).

We found that ATRA/ST1926-induced growth inhibition in the tested breast cancer cells was RAR-independent, as shown by the use of the pan-RAR inverse agonist, BMS493. Recently, ATRA was demonstrated to trigger non-genomic signaling and to activate a series of kinase signaling pathways, and hence bypass the classical retinoic acid nuclear signaling pathway (Schenk 2014). The activation of multiple kinase signaling pathways results in the transcription of multiple target genes and downstream effectors, independently of the nuclear RARs functions (Schenk 2014).

Among the activated kinase signaling pathways by ATRA is the mitogen-activated protein kinase (MAPK) signaling pathway that in turn, activates downstream effectors namely, extracellular signal-regulated kinases (ERKs) and p38 MAPKs (Garattini 2014; Schenk 2014). Because ATRA/ST1926-induced growth inhibition was RAR-independent, we suspect that ATRA is displaying non-genomic RAR effects through the activation of the MAPK signaling pathway. Interestingly, we observed that combination treatments of ATRA and ST1926 induced a massive S-phase arrest in human breast cancer cells. Previous studies showed that ERK and p38 MAPK activation mediates S-phase arrest that was reversed by ERK or p38 MAPK inhibitors (Zhang 2002; Zhu 2004; Guan 2007; Chen 2008). Furthermore, abnormal hyperactivation of ERK leads to massive p21-induced S-phase arrest (Chambard 2006). It is plausible that ATRA is hyperactivating ERK, leading to a subsequent accumulation of cyclin D1 (Chambard 2006), and a p21-induced S-phase arrest. Future studies will determine the involvement of the MAPK signaling pathway in combined ATRA/ST1926-induced growth inhibition in human breast cancer cells by the use of specific ERK and p38 MAPK inhibitors.

Previous studies have shown that ATRA resistance in breast cancer could be overcome by diverting ATRA from peroxisome proliferator-activated receptor  $\beta/\delta$  (PPAR $\beta/\delta$ ) to RAR (Schug 2008). Interestingly, recent studies showed that curcumin sensitizes triple negative breast cancer cells to ATRA through the suppression of FABP5 and PPAR $\beta/\delta$  pathway (Thulasiraman 2014). It would be interesting in future studies to analyze the molecular events involved in ATRA/ST1926 synergistic growth-inhibition in breast cancer cells with different genetic background, and to assess whether combination treatments inhibit FABP5 and PPAR $\beta/\delta$  pathway and restore

ATRA sensitivity in ATRA-resistant breast cancer animal models.

It is well established that 3D cell culture models offer a better screening model to assess the preclinical efficacy of anti-cancer drugs (Lovitt 2014; Edmondson 2014). Testing the anti-tumor activities of molecules on such models may, to a certain extent, predict their potency *in vivo* (Lovitt 2014; Edmondson 2014). We assessed the effects of ATRA and ST1926 on the anchorage-independent growth of breast cancer cells using the soft agar colony formation assay. We demonstrated that nM concentrations of ST1926, that had no effect on the growth of breast cancer cells in 2D cell culture model, reduced the viability of breast cancer colonies in anchorage-independent culture model. Breast cancer cell sensitivity to nM concentrations of ST1926 may be due to the fact that cancer cells grown in 2D culture models were exposed to ST1926 for three days only, as opposed to the soft-agar colony formation assay, where colonies were exposed for eight days. These findings highlight the importance of different 3D culture models in assessing the potency of anti-cancer drugs and in determining the effects of long-term exposure of low drug concentrations on cancer cells.

Furthermore, we showed breast cancer cells were sensitive to  $\mu\text{M}$  ATRA concentrations in anchorage-independent cell culture model. It is of interest to note that ATRA concentrations in patients can range between 0.1  $\mu\text{M}$  and 8  $\mu\text{M}$  following 45 mg/m<sup>2</sup> oral dose (Adamson 1996).

Previous studies demonstrated that drug sensitivity, among other factors, depends on the arrangement of tumor cells. Indeed, tumor cell sensitivity to chemotherapeutic drugs was altered when cells were embedded in lrECM. The organization of cancer cells into a tumor in 3D lrECM culture model was in fact similar to tumors *in vivo*, indicating that anchorage-dependent growth of cancer cells, instead of



a flat monolayer of cells, may in fact mimic the *in vivo* complexity concerning the response to treatments (Lovitt 2014). Furthermore, 3D IrECM culture model enables cell–cell interactions, cell–ECM interactions, and cell populations and structures that resemble the *in vivo* architecture. We showed that treatments with low sub- $\mu$ M concentrations potentially reduced the viability of breast cancer cells using the 3D ‘on-top’ assay. Interestingly, breast cancer cells were more sensitive to sub- $\mu$ M pharmacologically achievable concentrations in anchorage-dependent 3D culture model, when compared to the 2D culture model. Importantly, growing breast cancer cells on top of IrECM did not reduce their sensitivity to drug treatments, although previous studies reported that IrECM 3D culture models might render cancer cells more resistant to anti-cancer drugs (Luca 2013; Imamura 2014; Aljitawi 2014; Edmondson 2014).

Although 3D cell culture model offers numerous advantages, in particular to drug screening, the former model (anchorage-dependent growth) does not depict the effect of all components of the microenvironment. For instance, 3D IrECM culture model takes into consideration only one component of the microenvironment, which is the basement membrane; and excludes all other cellular components, particularly, the stromal cells whose contribution to the cancer niche is positively correlated with tumor growth, metastasis, and treatment resistance (Edmondson 2014). Recent advances led to the development of heterotypic 3D culture models by co-culturing malignant cells with stromal and/or endothelial cells to promote heterotypic interactions for a more valid drug screening (Ghajar 2013). More advanced 3D culture models, such as microengineered organs-on-chip or organotypic 3D models, allow the reconstitution of 3D *in vivo* architecture to answer tissue-specific questions (Huh 2012).

Accumulating evidence suggested that cancer stem cells (CSC) are thought to be responsible for resistance to conventional chemotherapy and tumor relapse (Chen 2013). CSCs can self-renew and generate tumor cells with distinct phenotypes. Targeting the population of CSCs remains essential in achieving complete remission (Pattabiraman 2014). In this study, we demonstrated that nM concentrations of ST1926 decreased mammosphere formation using the 3D sphere formation assay. Furthermore,  $\mu$ M ST1926 concentrations completely abrogated the SFU of breast cancer cells at G1. Given the observed synergy between ST1926 and ATRA in 2D culture models, we aimed to determine the effects of ATRA/ST1926 combination on the sphere-forming ability of MCF-7 cells. Interestingly, combination treatments of nM ST1926 concentrations with  $\mu$ M ATRA concentrations significantly decreased the SFU and displayed drastic morphological changes on treated spheres. In summary, our data indicate that the effect of ATRA, ST1926, and their combination treatments was more pronounced on 3D compared to 2D breast cancer cell models. Additional studies will determine the effects of our drugs on the self-renewal ability of breast cancer cells.

Finally, we aimed at testing the effects of ATRA, ST1926, and their combination on the lumen and acinar size of 'normal-like' HMT-3522 S1 cells in a model that mimics the *in vivo* architecture of breast epithelial cells. Non-neoplastic MCF-10A and HMT-3522 S1 cells form acini when grown in IrECM 3D cell culture model, however, only HMT-3522 S1 cells acquire basoapical polarity (Plachot 2009). Previous studies demonstrated that drug sensitivity of breast cancer cells grown in 3D cell culture model was influenced by basal polarity, and notably the hemidesmosome-directed signaling that was conferring resistance to treatments (Vidi 2014). Given the importance of cell polarity in dictating or predicting drug response, we chose to test the

effects of the drugs on HMT-3522 S1 cells and not MCF-10A cells in 3D cell culture model. We showed that treatments with ATRA, ST1926, and their combination did not disrupt the lumen or affect the diameter of HMT-3522 S1 acini, clearly indicating lack of treatment cytotoxicity and further highlighting the promising use of ATRA, ST1926, and their combination in breast cancer therapy. Additional studies will be conducted to determine the effects of the drugs on the basoapical polarity by staining for integrin  $\alpha$ -6, as a basal polarity marker, and Zo-1, as an apical polarity marker (Plachot 2009).

Even though no major toxicities were encountered when ST1926 was tested in Phase I clinical trial in ovarian cancer patients, however, this synthetic retinoid was found to undergo major glucuronidation by liver enzymes resulting in low plasma concentrations (Sala 2009). Subsequently, ST1926 was halted from being tested in clinical trials. In this study, we report several findings that might overcome ST1926 poor availability and thus, bring ST1926 back to clinical testing. In fact, combination treatments of ATRA and ST1926 at low sub- $\mu$ M concentration were found to sensitize ATRA-resistant breast cancer cells to ATRA. Furthermore, we demonstrated that nM ST1926 concentrations were effective in reducing breast cancer colonies in 3D agar matrix, and in targeting breast cancer stem/progenitor cells in 3D cell culture models. Altogether, these findings are exciting and remain to be confirmed in breast cancer animal models. It is of interest that there has been numerous attempts to synthesize derivatives of ST1926 in the hope to overcome its prominent glucuronidation (Giannini 2012). One of these derivatives is ST5589 that showed growth-inhibitory effects in preclinical models of lymphoma (Bernasconi 2015). However, ST5589 reverted back to its parental drug, ST1926 (Bernasconi 2015). Hence, it remains to be determined if this prodrug will bypass glucuronidation *in vivo*, and thus increase plasma ST1926 half-life.

Alternatively, ongoing efforts from our laboratory generated polymer-stabilized ST1926 nanoparticle formulations that proved to work similarly to the naked drug, when tested on colorectal cancer and AML cells (El-Houjeiri MS AUB 2015, and unpublished data). ST1926 nanoparticle formulation will be evaluated in cancer animal models.

In conclusion, ST1926, ATRA, and their combination treatments were shown to display more potent anti-tumor properties in 3D *versus* 2D human breast cancer models, while sparing normal breast epithelial cells in both culture models. Our results also demonstrate the therapeutic potential of ST1926 in sensitizing breast cancer cells to ATRA. As 3D culture models are more representative of the tumor microenvironment and serve as valid tools in drug discovery, our results highlight the promising use of ATRA/ST1926 combination in metastatic and triple negative breast cancers. *In vivo* survival and efficacy studies should be performed to test for combined ATRA/ST1926 effect in well-established breast cancer animal models.

## REFERENCES

- Adamson, P. C. (1996). All-trans-retinoic acid pharmacology and its impact on the treatment of acute promyelocytic leukemia. *The oncologist*, 1(5), 305-314.
- Aljitawi, O. S., Li, D., Xiao, Y., Zhang, D., Ramachandran, K., Stehno-Bittel, L., ... & Garimella, R. (2014). A novel three-dimensional stromal-based model for in vitro chemotherapy sensitivity testing of leukemia cells. *Leukemia & lymphoma*, 55(2), 378-391.
- Altucci, L., & Gronemeyer, H. (2001). The promise of retinoids to fight against cancer. *Nature Reviews Cancer*, 1(3), 181-193.
- American Cancer Society. Breast Cancer Facts and Figures 2016. Atlanta, Ga: American Cancer Society; 2016.
- Arai, K., Sakamoto, R., Kubota, D., & Kondo, T. (2013). Proteomic approach toward molecular backgrounds of drug resistance of osteosarcoma cells in spheroid culture system. *Proteomics*, 13(15), 2351-2360.
- Basma, H., Ghayad, S. E., Rammal, G., Mancinelli, A., Harajly, M., Ghamloush, F., ... & Pisano, C. (2016). The synthetic retinoid ST1926 as a novel therapeutic agent in rhabdomyosarcoma. *International Journal of Cancer*, 138(6), 1528-1537.
- Bayraktar S, Gluck S: Molecularly targeted therapies for metastatic triple-negative breast cancer. *Breast Cancer Res Treat* 2013, 138(1):21–35.
- Benbrook, D. M., Chambon, P., Rochette-Egly, C., & Asson-Batres, M. A. (2014). History of Retinoic Acid Receptors. In *The Biochemistry of Retinoic Acid Receptors I: Structure, Activation, and Function at the Molecular Level* (pp. 1-20). Springer Netherlands.
- Bernasconi, E., Gaudio, E., Kwee, I., Rinaldi, A., Cascione, L., Tarantelli, C., ... & Giannini, G. (2015). The novel atypical retinoid ST5589 down-regulates Aurora Kinase A and has anti-tumour activity in lymphoma pre-clinical models. *British journal of haematology*, 171(3), 378-386.
- Bertheau, P., Lehmann-Che, J., Varna, M., Dumay, A., Poirot, B., Porcher, R., ... & de Cremoux, P. (2013). p53 in breast cancer subtypes and new insights into response to chemotherapy. *The Breast*, 22, S27-S29.
- Bissell, M. J., & Hines, W. C. (2011). Why don't we get more cancer? A proposed role of the microenvironment in restraining cancer progression. *Nature medicine*, 17(3), 320-329.
- Bosch A, Bertran SP, Lu Y, Garcia A, Jones AM, Dawson MI, et al. Reversal by RARalpha agonist Am 580 of c-Myc-induced imbalance in RARalpha/RARgamma expression during MMTV-Myc tumorigenesis. *Breast Cancer Res* 2012; 14:R121.
- Breitman, T. R., Collins, S. J., & Keene, B. R. (1981). Terminal differentiation of human promyelocytic leukemic cells in primary culture in response to retinoic acid. *Blood*, 57(6), 1000-1004.

- Brennan, K. R., & Brown, A. M. (2004). Wnt proteins in mammary development and cancer. *Journal of mammary gland biology and neoplasia*, 9(2), 119-131.
- Briand, P., Petersen, O. W., & Van Deurs, B. (1987). A new diploid nontumorigenic human breast epithelial cell line isolated and propagated in chemically defined medium. *In vitro cellular & developmental biology*, 23(3), 181-188.
- Briskin, C., & O'Malley, B. (2010). Hormone action in the mammary gland. *Cold Spring Harbor perspectives in biology*, 2(12), a003178.
- Brouckaert O, Wildiers H, Floris G, Neven P: Update on triple-negative breast cancer: prognosis and management strategies. *Int J WomensHealth* 2012, 4:511–520.
- Cailleau, R., Young, R., Olive, M., & Reeves, W. J. (1974). Breast tumor cell lines from pleural effusions. *Journal of the National Cancer Institute*, 53(3), 661-674.
- Cazzaniga, M., Varricchio, C., Montefrancesco, C., Feroce, I., & Guerrieri-Gonzaga, A. (2012). Fenretinide (4-HPR): a preventive chance for women at genetic and familial risk?. *BioMed Research International*, 2012.
- Chambard, J. C., Lefloch, R., Pouyssegur, J., & Lenormand, P. (2007). ERK implication in cell cycle regulation. *Biochimica et Biophysica Acta (BBA)-Molecular Cell Research*, 1773(8), 1299-1310.
- Chen, K., Huang, Y. H., & Chen, J. L. (2013). Understanding and targeting cancer stem cells: therapeutic implications and challenges. *Acta Pharmacologica Sinica*, 34(6), 732-740.
- Chou, T. C. (2010). Drug combination studies and their synergy quantification using the Chou-Talalay method. *Cancer research*, 70(2), 440-446.
- Cincinelli R, Dallavalle S, Merlini L, Penco S, Pisano C, Carminati P, Giannini G, Vesci L, Gaetano C, Illy B, et al. "A novel atypical retinoid endowed with proapoptotic and antitumor activity." *J Med Chem* 46 (2003):909-912.
- Connolly, R. M., Nguyen, N. K., & Sukumar, S. (2013). Molecular pathways: current role and future directions of the retinoic acid pathway in cancer prevention and treatment. *Clinical Cancer Research*, 19(7), 1651-1659.
- Crowe, D. L., & Chandraratna, R. A. (2004). A retinoid X receptor (RXR)-selective retinoid reveals that RXR-alpha is potentially a therapeutic target in breast cancer cell lines, and that it potentiates antiproliferative and apoptotic responses to peroxisome proliferator-activated receptor ligands. *Breast Cancer Res*, 6(5), R546-R555.
- Crown, J., O'shaughnessy, J., & Gullo, G. (2012). Emerging targeted therapies in triple-negative breast cancer. *Annals of oncology*, 23(suppl 6), vi56-vi65.

- Dai, Y., Chen, S., Pei, X. Y., Almenara, J. A., Kramer, L. B., Venditti, C. A., ... & Grant, S. (2008). Interruption of the Ras/MEK/ERK signaling cascade enhances Chk1 inhibitor-induced DNA damage in vitro and in vivo in human multiple myeloma cells. *Blood*, 112(6), 2439-2449.
- Darwiche N, Abou-Lteif G, Bazarbachi A. "Reactive oxygen species mediate N-(4-hydroxyphenyl)retinamide-induced cell death in malignant T cells and are inhibited by the HTLV-I oncoprotein Tax." *Leukemia* 21(2007):261-269.
- Darwiche N, Hatoum A, Dbaiibo G, Kadara H, Nasr R, Abou-Lteif G. "N-(4-hydroxyphenyl)retinamide induces growth arrest and apoptosis in HTLV-1-transformed cells." *Leukemia*, 18(2004): 607-615.
- Darzynkiewicz, Z., Halicka, H. D., Zhao, H., & Podhorecka, M. (2011). Cell synchronization by inhibitors of DNA replication induces replication stress and DNA damage response: analysis by flow cytometry. In *Cell Cycle Synchronization* (pp. 85-96). Humana Press.
- Dawson MI, Zhang X, Hobbs PD, Jong L. "Synthetic retinoids and their usefulness in biology and medicine." In: MA Livera (ed.). *Vitamin A and Retinoids: an Update of Biological Aspects and Clinical Applications*. Birkhauser Verlag: Basel (2001)161–196.
- Di Francesco, A. M., Cusano, G., Franzese, O., Orienti, I., Falconi, M., Vesci, L., & Riccardi, R. (2015). Resistance to the atypical retinoid ST1926 in SK-N-AS cells selected the subline rAS-ST with enhanced sensitivity to ATRA mediated by not conventional mechanisms: DNA damage, G2 accumulation and late telomerase inhibition. *Toxicology in Vitro*, 29(7), 1628-1638.
- Di Francesco, A. M., Meco, D., Torella, A. R., Barone, G., D'Incalci, M., Pisano, C., ... & Riccardi, R. (2007). The novel atypical retinoid ST1926 is active in ATRA resistant neuroblastoma cells acting by a different mechanism. *Biochemical pharmacology*, 73(5), 643-655.
- Di Francesco, A. M., Ubezio, P., Torella, A. R., Meco, D., Pierri, F., Barone, G., ... & Riccardi, R. (2012). Enhanced cell cycle perturbation and apoptosis mediate the synergistic effects of ST1926 and ATRA in neuroblastoma preclinical models. *Investigational new drugs*, 30(4), 1319-1330.
- Di Masi, A., Leboffe, L., De Marinis, E., Pagano, F., Cicconi, L., Rochette-Egly, C., ... & Nervi, C. (2015). Retinoic acid receptors: From molecular mechanisms to cancer therapy. *Molecular aspects of medicine*, 41, 1-115.
- Edmondson, R., Broglie, J. J., Adcock, A. F., & Yang, L. (2014). Three-dimensional cell culture systems and their applications in drug discovery and cell-based biosensors. *Assay and drug development technologies*, 12(4), 207-218.
- El Hajj, H., Khalil, B., Ghandour, B., Nasr, R., Shahine, S., Ghantous, A., ... & Hall, W. W. (2014). Preclinical efficacy of the synthetic retinoid ST1926 for treating adult T-cell leukemia/lymphoma. *Blood*, 124(13), 2072-2080.

- Fadoukhair, Z., Zardavas, D., Chad, M. A., Goulioti, T., Aftimos, P., & Piccart, M. (2015). Evaluation of targeted therapies in advanced breast cancer: the need for large-scale molecular screening and transformative clinical trial designs. *Oncogene*.
- Garattini, E., Bolis, M., Garattini, S. K., Fratelli, M., Centritto, F., Paroni, G., ... & Terao, M. (2014). Retinoids and breast cancer: from basic studies to the clinic and back again. *Cancer treatment reviews*, 40(6), 739-749.
- Garattini, E., Parrella, E., Diomede, L., Kalac, Y., Merlini, L., Simoni, D., ... & Terao, M. (2004). ST1926, a novel and orally active retinoid-related molecule inducing apoptosis in myeloid leukemia cells: modulation of intracellular calcium homeostasis. *Blood*, 103(1), 194-207.
- Ghajar, C. M., Peinado, H., Mori, H., Matei, I. R., Evason, K. J., Brazier, H., ... & Chen, E. I. (2013). The perivascular niche regulates breast tumour dormancy. *Nature cell biology*, 15(7), 807-817.
- Giannini, G., Brunetti, T., Battistuzzi, G., Alloatti, D., Quattrocioni, G., Cima, M. G., ... & Vesci, L. (2012). New retinoid derivatives as back-ups of Adarotene. *Bioorganic & medicinal chemistry*, 20(7), 2405-2415.
- Guille, A., Chaffanet, M., & Birnbaum, D. (2013). Signaling pathway switch in breast cancer. *Cancer cell international*, 13(1), 1.
- Hanahan, D., & Coussens, L. M. (2012). Accessories to the crime: functions of cells recruited to the tumor microenvironment. *Cancer cell*, 21(3), 309-322.
- Hanahan, D., & Weinberg, R. A. (2011). Hallmarks of cancer: the next generation. *cell*, 144(5), 646-674.
- Hennighausen, L., & Robinson, G. W. (2005). Information networks in the mammary gland. *Nature Reviews Molecular Cell Biology*, 6(9), 715-725.
- Huh, D., Matthews, B. D., Mammoto, A., Montoya-Zavala, M., Hsin, H. Y., & Ingber, D. E. (2010). Reconstituting organ-level lung functions on a chip. *Science*, 328(5986), 1662-1668.
- Imamura, Y., Mukohara, T., Shimono, Y., Funakoshi, Y., Chayahara, N., Toyoda, M., ... & Minami, H. (2015). Comparison of 2D-and 3D-culture models as drug-testing platforms in breast cancer. *Oncology reports*, 33(4), 1837-1843 in breast cancer. *Breast Cancer Res* 2002;62:2455–61.
- Inman, J. L., Robertson, C., Mott, J. D., & Bissell, M. J. (2015). Mammary gland development: cell fate specification, stem cells and the microenvironment. *Development*, 142(6), 1028-1042.



- Jang, G. B., Kim, J. Y., Cho, S. D., Park, K. S., Jung, J. Y., Lee, H. Y., ... & Nam, J. S. (2015). Blockade of Wnt/ $\beta$ -catenin signaling suppresses breast cancer metastasis by inhibiting CSC-like phenotype. *Scientific reports*, 5.
- Kadara, H., Schroeder, C. P., Lotan, D., Pisano, C., & Lotan, R. (2006). Induction of GDF-15/NAG-1/MIC-1 in human lung carcinoma cells by retinoid-related molecules and assessment of its role in apoptosis. *Cancer biology & therapy*, 5(5), 518-522.
- Kessenbrock, K., Plaks, V., & Werb, Z. (2010). Matrix metalloproteinases: regulators of the tumor microenvironment. *Cell*, 141(1), 52-67.
- Kim, S. H., J. Turnbull, et al. (2011). "Extracellular matrix and cell signalling: the dynamic cooperation of integrin, proteoglycan and growth factor receptor." *The Journal of Endocrinology* 209(2): 139-151.
- Kola, I., & Landis, J. (2004). Can the pharmaceutical industry reduce attrition rates?. *Nature reviews Drug discovery*, 3(8), 711-716.
- Lee, E. Y., Lee, W. H., Kaetzel, C. S., Parry, G., & Bissell, M. J. (1985). Interaction of mouse mammary epithelial cells with collagen substrata: regulation of casein gene expression and secretion. *Proceedings of the National Academy of Sciences*, 82(5), 1419-1423.
- Lee, E. Y., Lee, W. H., Kaetzel, C. S., Parry, G., & Bissell, M. J. (1985). Interaction of mouse mammary epithelial cells with collagen substrata: regulation of casein gene expression and secretion. *Proceedings of the National Academy of Sciences*, 82(5), 1419-1423.
- Lehmann, B. D., Bauer, J. A., Chen, X., Sanders, M. E., Chakravarthy, A. B., Shyr, Y., & PiTENpol, J. A. (2011). Identification of human triple-negative breast cancer subtypes and preclinical models for selection of targeted therapies. *The Journal of clinical investigation*, 121(7), 2750.
- Levenson, A. S., & Jordan, V. C. (1997). MCF-7: the first hormone-responsive breast cancer cell line. *Cancer research*, 57(15), 3071-3078.
- Lin, E. Y., & Pollard, J. W. (2007). Tumor-associated macrophages press the angiogenic switch in breast cancer. *Cancer Research*, 67(11), 5064-5066.
- Liu CC, Wang H, Wang WD, Zhu MY, Geng QR, Lu Y. Consolidation therapy of arsenic trioxide alternated with chemotherapy achieves remarkable efficacy in newly diagnosed acute promyelocytic leukemia. *Onco Targets Ther*. 2015. 8:3297-3303.
- Lovitt, C. J., Shelper, T. B., & Avery, V. M. (2014). Advanced cell culture techniques for cancer drug discovery. *Biology*, 3(2), 345-367.
- Luca, A. C., Mersch, S., Deenen, R., Schmidt, S., Messner, I., Schäfer, K. L., ... & Krieg, A. (2013). Impact of the 3D microenvironment on phenotype, gene expression, and EGFR inhibition of colorectal cancer cell lines. *PLoS One*, 8(3), e59689.

- Ma, S., Tang, J., Feng, J., Xu, Y., Yu, X., Deng, Q., & Lu, Y. (2008). Induction of p21 by p65 in p53 null cells treated with Doxorubicin. *Biochimica et Biophysica Acta (BBA)-Molecular Cell Research*, 1783(5), 935-940.
- MacDonald, B. T., Tamai, K., & He, X. (2009). Wnt/ $\beta$ -catenin signaling: components, mechanisms, and diseases. *Developmental cell*, 17(1), 9-26.
- Macias, H., & Hinck, L. (2012). Mammary gland development. *Wiley Interdisciplinary Reviews: Developmental Biology*, 1(4), 533-557.
- Mah, L. J., El-Osta, A., & Karagiannis, T. C. (2010).  $\gamma$ H2AX: a sensitive molecular marker of DNA damage and repair. *Leukemia*, 24(4), 679-686.
- Matthay, K. K., Reynolds, C. P., Seeger, R. C., Shimada, H., Adkins, E. S., Haas-Kogan, D., ... & Villablanca, J. G. (2009). Long-term results for children with high-risk neuroblastoma treated on a randomized trial of myeloablative therapy followed by 13-cis-retinoic acid: a children's oncology group study. *Journal of Clinical Oncology*, 27(7), 1007-1013.
- Matthay, K. K., Villablanca, J. G., Seeger, R. C., Stram, D. O., Harris, R. E., Ramsay, N. K., ... & Gerbing, R. B. (1999). Treatment of high-risk neuroblastoma with intensive chemotherapy, radiotherapy, autologous bone marrow transplantation, and 13-cis-retinoic acid. *New England Journal of Medicine*, 341(16), 1165-1173.
- Michalopoulos, G. K., & DeFrances, M. C. (1997). Liver regeneration. *Science*, 276(5309), 60-66.
- Muscat GE, Eriksson NA, Byth K, Loi S, Graham D, Jindal S, et al. Research resource: nuclear receptors as transcriptome: discriminant and prognostic value in breast cancer. *Mol Endocrinol* 2013;27:350–65.
- Nasr, R. R., Hmadi, R. A., El-Eit, R. M., Iskandarani, A. N., Jabbour, M. N., Zaatari, G. S., ... & Darwiche, N. D. (2015). ST1926, an orally active synthetic retinoid, induces apoptosis in chronic myeloid leukemia cells and prolongs survival in a murine model. *International Journal of Cancer*, 137(3), 698-709.
- Nelson, C. H., Buttrick, B. R., & Isoherranen, N. (2013). Therapeutic Potential of the Inhibition of the Retinoic Acid Hydroxylases CYP26A1 and CYP26B1 by Xenobiotics. *Current Topics in Medicinal Chemistry*, 13(12), 1402-1428.
- Nienhuis, H. H., Gaykema, S. B. M., Timmer-Bosscha, H., Jalving, M., Brouwers, A. H., Lub-de Hooge, M. N., ... & Schröder, C. P. (2015). Targeting breast cancer through its microenvironment: current status of preclinical and clinical research in finding relevant targets. *Pharmacology & therapeutics*, 147, 63-79.
- Olivier, M., Eeles, R., Hollstein, M., Khan, M. A., Harris, C. C., & Hainaut, P. (2002). The IARC TP53 database: new online mutation analysis and recommendations to users. *Human mutation*, 19(6), 607-614.

- Omori, E., Matsumoto, K., & Ninomiya-Tsuji, J. (2011). Non-canonical  $\beta$ -catenin degradation mediates reactive oxygen species-induced epidermal cell death. *Oncogene*, 30(30), 3336-3344.
- Ortiz MA, Bayon Y, Lopez-Hernandez FJ, Piedrafito FJ. "Retinoids in combination therapies for the treatment of cancer: mechanisms and perspectives." *Drug Resist Updates* 5 (2002): 162-175.
- Park, S., Gwak, J., Cho, M., Song, T., Won, J., Kim, D. E., ... & Oh, S. (2006). Hexachlorophene inhibits Wnt/ $\beta$ -catenin pathway by promoting Siah-mediated  $\beta$ -catenin degradation. *Molecular pharmacology*, 70(3), 960-966.
- Parrella, E., Gianni, M., Fratelli, M., Barzago, M. M., Raska, I., Diomede, L., ... & Dallavalle, S. (2006). Antitumor activity of the retinoid-related molecules (E)-3-(4'-hydroxy-3'-adamantylbiphenyl-4-yl) acrylic acid (ST1926) and 6-[3-(1-adamantyl)-4-hydroxyphenyl]-2-naphthalene carboxylic acid (CD437) in F9 teratocarcinoma: role of retinoic acid receptor  $\gamma$  and retinoid-independent pathways. *Molecular pharmacology*, 70(3), 909-924.
- Patocs, A., Zhang, L., Xu, Y., Weber, F., Caldes, T., Mutter, G. L., ... & Eng, C. (2007). Breast-cancer stromal cells with TP53 mutations and nodal metastases. *New England Journal of Medicine*, 357(25), 2543-2551.
- Pattabiraman, D. R., & Weinberg, R. A. (2014). Tackling the cancer stem cells—what challenges do they pose?. *Nature reviews Drug discovery*, 13(7), 497-512.
- Perou, C. M., Sørli, T., Eisen, M. B., van de Rijn, M., Jeffrey, S. S., Rees, C. A., ... & Fluge, Ø. (2000). Molecular portraits of human breast tumours. *Nature*, 406(6797), 747-752.
- Petersen, O. W., Rønnov-Jessen, L., Howlett, A. R., & Bissell, M. J. (1992). Interaction with basement membrane serves to rapidly distinguish growth and differentiation pattern of normal and malignant human breast epithelial cells. *Proceedings of the National Academy of Sciences*, 89(19), 9064-9068.
- Petersen, O. W., Rønnov-Jessen, L., Howlett, A. R., & Bissell, M. J. (1992). Interaction with basement membrane serves to rapidly distinguish growth and differentiation pattern of normal and malignant human breast epithelial cells. *Proceedings of the National Academy of Sciences*, 89(19), 9064-9068.
- Plachot, C., & Lelièvre, S. A. (2004). DNA methylation control of tissue polarity and cellular differentiation in the mammary epithelium. *Experimental cell research*, 298(1), 122-132.
- Polyak, K. (2007). Breast cancer: origins and evolution. *The Journal of clinical investigation*, 117(11), 3155-3163.

- Powell BL, Moser B, Stock W, et al. Arsenic trioxide improves event-free and overall survival for adults with acute promyelocytic leukemia: North American Leukemia Intergroup Study C9710. *Blood*. 2010 Nov 11. 116(19):3751-7.
- Purton, L. E., Dworkin, S., Olsen, G. H., Walkley, C. R., Fabb, S. A., Collins, S. J., & Chambon, P. (2006). RAR $\gamma$  is critical for maintaining a balance between hematopoietic stem cell self-renewal and differentiation. *The Journal of experimental medicine*, 203(5), 1283-1293.
- Rhinn, M., & Dollé, P. (2012). Retinoic acid signalling during development. *Development*, 139(5), 843-858.
- Rice, P. L., Kelloff, J., Sullivan, H., Driggers, L. J., Beard, K. S., Kuwada, S., ... & Ahnen, D. J. (2003). Sulindac metabolites induce caspase-and proteasome-dependent degradation of  $\beta$ -catenin protein in human colon cancer cells. *Molecular cancer therapeutics*, 2(9), 885-892.
- Rothschild, E., & Banerjee, D. (2015). Subverting Subversion: A Review on the Breast Cancer Microenvironment and Therapeutic Opportunities. *Breast cancer: basic and clinical research*, 9(Suppl 2), 7.
- Sala, F., Zucchetti, M., Bagnati, R., D'Incalci, M., Pace, S., Capocasa, F., & Marangon, E. (2009). Development and validation of a liquid chromatography–tandem mass spectrometry method for the determination of ST1926, a novel oral antitumor agent, adamantyl retinoid derivative, in plasma of patients in a Phase I study. *Journal of Chromatography B*, 877(27), 3118-3126.
- Schenk, T., Stengel, S., & Zelent, A. (2014). Unlocking the potential of retinoic acid in anticancer therapy. *British journal of cancer*, 111(11), 2039-2045.
- Schnitt, S. J. (2010). Classification and prognosis of invasive breast cancer: from morphology to molecular taxonomy. *Modern Pathology*, 23, S60-S64.
- Schug, T. T., Berry, D. C., Shaw, N. S., Travis, S. N., & Noy, N. (2007). Opposing effects of retinoic acid on cell growth result from alternate activation of two different nuclear receptors. *Cell*, 129(4), 723-733.
- Siegel, R. L., Miller, K. D., & Jemal, A. (2015). Cancer statistics, 2016. *CA: A cancer journal for clinicians*.
- Sirchia, S. M., Ren, M., Pili, R., Sironi, E., Somenzi, G., Ghidoni, R., ... & Sacchi, N. (2002). Endogenous reactivation of the RAR $\beta$ 2 tumor suppressor gene epigenetically silenced in breast cancer. *Cancer research*, 62(9), 2455-2461.
- Sirchia, S. M., Ferguson, A. T., Sironi, E., Subramanyan, S., Orlandi, R., Sukumar, S., & Sacchi, N. (2000). Evidence of epigenetic changes affecting the chromatin state of the retinoic acid receptor beta2 promoter in breast cancer cells. *Oncogene*, 19(12), 1556-1563.

- Smalley, M., & Ashworth, A. (2003). Stem cells and breast cancer: a field in transit. *Nature Reviews Cancer*, 3(11), 832-844.
- Smith, B. A., Shelton, D. N., Kieffer, C., Milash, B., Usary, J., Perou, C. M., ... & Welm, B. E. (2013). Targeting the PyMT oncogene to diverse mammary cell populations enhances tumor heterogeneity and generates rare breast cancer subtypes. *Genes & cancer*, 1947601913475359.
- Soule, H. D., Maloney, T. M., Wolman, S. R., Peterson, W. D., Brenz, R., McGrath, C. M., ... & Brooks, S. C. (1990). Isolation and characterization of a spontaneously immortalized human breast epithelial cell line, MCF-10. *Cancer research*, 50(18), 6075-6086.
- Soule, H. D., Vazquez, J., Long, A., Albert, S., & Brennan, M. (1973). A human cell line from a pleural effusion derived from a breast carcinoma. *Journal of the National Cancer Institute*, 51(5), 1409-1416.
- Sporn MB, Dunlop NM, Newton DL, Smith JM. Prevention of chemical carcinogenesis by vitamin A and its synthetic analogs (retinoids) *Federation Proceedings*. 1976;35(6):1332–1338.
- Stage, I., II, I., & Operable, I. I. I. C. Breast Cancer Treatment (PDQ®).
- Sutton LM, Warmuth MA, Petros WP, Winer EP. Pharmacokinetics and clinical impact of all-trans retinoic acid in metastatic breast cancer: a phase II trial. *Cancer Chemother Pharmacol* 1997;40:335–41.
- Terao, M., Fratelli, M., Kurosaki, M., Zanetti, A., Guarnaccia, V., Paroni, G., ... & Garattini, E. (2011). Induction of miR-21 by Retinoic Acid in Estrogen Receptor-positive Breast Carcinoma Cells BIOLOGICAL CORRELATES AND MOLECULAR TARGETS. *Journal of Biological Chemistry*, 286(5), 4027-4042.
- Thulasiraman, P., McAndrews, D. J., & Mohiudddin, I. Q. (2014). Curcumin restores sensitivity to retinoic acid in triple negative breast cancer cells. *BMC cancer*, 14(1), 724.
- Troester, M. A., Herschkowitz, J. I., Oh, D. S., He, X., Hoadley, K. A., Barbier, C. S., & Perou, C. M. (2006). Gene expression patterns associated with p53 status in breast cancer. *BMC cancer*, 6(1), 276.
- Turinetto, V., & Giachino, C. (2015). Multiple facets of histone variant H2AX: a DNA double-strand-break marker with several biological functions. *Nucleic acids research*, gkv061.
- Valli, C., Paroni, G., Di Francesco, A. M., Riccardi, R., Tavecchio, M., Erba, E., ... & Antocchia, A. (2008). Atypical retinoids ST1926 and CD437 are S-phase-specific agents causing DNA double-strand breaks: significance for the cytotoxic and antiproliferative activity. *Molecular cancer therapeutics*, 7(9), 2941-2954.

- Vidi, P. A., Bissell, M. J., & Lelièvre, S. A. (2013). Three-dimensional culture of human breast epithelial cells: the how and the why. *Epithelial Cell Culture Protocols: Second Edition*, 193-219.
- Vinay, D. S., Ryan, E. P., Pawelec, G., Talib, W. H., Stagg, J., Elkord, E., ... & Signori, E. (2015, December). Immune evasion in cancer: Mechanistic basis and therapeutic strategies. In *Seminars in cancer biology* (Vol. 35, pp. S185-S198). Academic Press.
- Wan, H., Dawson, M. I., Hong, W. K., & Lotan, R. (1998). Overexpressed activated retinoid X receptors can mediate growth inhibitory effects of retinoids in human carcinoma cells. *Journal of Biological Chemistry*, 273(41), 26915-26922.
- Wang, D., Wang, H., Guo, Y., Ning, W., Katkuri, S., Wahli, W., ... & DuBois, R. N. (2006). Crosstalk between peroxisome proliferator-activated receptor  $\delta$  and VEGF stimulates cancer progression. *Proceedings of the National Academy of Sciences*, 103(50), 19069-19074.
- Watson, C. J., & Khaled, W. T. (2008). Mammary development in the embryo and adult: a journey of morphogenesis and commitment. *Development*, 135(6), 995-1003.
- Weigelt, B., Ghajar, C. M., & Bissell, M. J. (2014). The need for complex 3D culture models to unravel novel pathways and identify accurate biomarkers in breast cancer. *Advanced drug delivery reviews*, 69, 42-51.
- Zardavas, D., Irrthum, A., Swanton, C., & Piccart, M. (2015). Clinical management of breast cancer heterogeneity. *Nature reviews Clinical oncology*, 12(7), 381-394.
- Zhang, W., & Liu, H. T. (2002). MAPK signal pathways in the regulation of cell proliferation in mammalian cells. *Cell research*, 12(1), 9-18.
- Zhao H, Piwnica-Worms H. ATR-mediated checkpoint pathways regulate phosphorylation and activation of human Chk1. *Mol Cell Biol*. 2001;21:4129–4139.
- Zhu, H., Zhang, L., Wu, S., Teraishi, F., Davis, J. J., Jacob, D., & Fang, B. (2004). Induction of S-phase arrest and p21 overexpression by a small molecule 2 [[3-(2, 3-dichlorophenoxy) propyl] amino] ethanol in correlation with activation of ERK. *Oncogene*, 23(29).
- Zuco, V., Benedetti, V., De Cesare, M., & Zunino, F. (2010). Sensitization of ovarian carcinoma cells to the atypical retinoid ST1926 by the histone deacetylase inhibitor, RC307: enhanced DNA damage response. *International Journal of Cancer*, 126(5), 1246-1255.
- Zuco, V., Zanchi, C., Cassinelli, G., Lanzi, C., Supino, R., Pisano, C., ... & Zunino, F. (2004). Induction of apoptosis and stress response in ovarian carcinoma cell lines treated with ST1926, an atypical retinoid. *Cell Death & Differentiation*, 11(3), 280-289.

